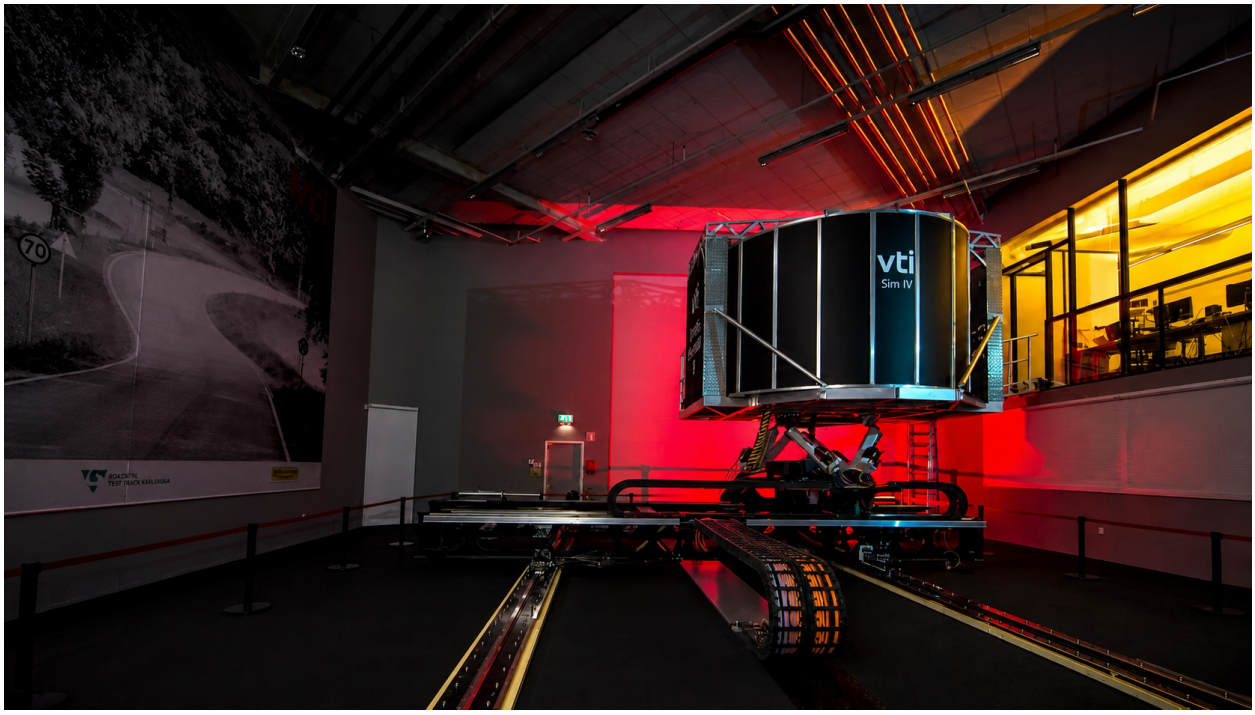
CHALMERS
UNIVERSITY OF TECHNOLOGY




# Modeling and Implementation of Rack-Electric Power Assisted Steering System for driving simulator

Master's thesis in Mobility Engineering

RAMKUMAR HULEPPA MUNAVALLI
ROHAN KUMAAR VASUDEVAN

DEPARTMENT OF MECHANICS AND MARITIME SCIENCES

CHALMERS UNIVERSITY OF TECHNOLOGY
Gothenburg, Sweden 2026
www.chalmers.se

MASTER'S THESIS IN MOBILITY ENGINEERING

# Modelling and Implementation of Rack- Electric Power Assisted Steering System for driving simulator

RAMKUMAR HULEPPA MUNAVALLI
ROHAN KUMAAR VASUDEVAN




CHALMERS
UNIVERSITY OF TECHNOLOGY

DEPARTMENT OF MECHANICS AND MARITIME SCIENCES
*Division of Vehicle Engineering and Autonomous System*
Chalmers University of Technology
Gothenburg, Sweden 2026

Modelling and implementation of Rack- Electric Power Assisted Steering System for driving simulator
RAMKUMAR HULEPPA MUNAVALLI
ROHAN KUMAAR VASUDEVAN

© RAMKUMAR HULEPPA MUNAVALLI , ROHAN KUMAAR VASUDEVAN, 2026.

Supervisor: Smit Saparia, VTI
Examiner: Fredrik Bruzelius, Vehicle Engineering and Autonomous Systems

Master's Thesis 2026
Department of Mechanics and Maritime Sciences
Division of Vehicle Engineering and Autonomous System
Chalmers University of Technology
SE-412 96 Gothenburg
Telephone +46 31 772 1000

Cover: View of SIM IV, the driving simulator used for this Master's thesis activity, located at VTI office at Gothenburg, Sweden 2026.

Typeset in LaTeX
Gothenburg, Sweden 2026

Modeling and Implementation of Rack - Electric Power Assisted Steering System for driving simulator
RAMKUMAR HULEPPA MUNAVALLI
ROHAN KUMAAR VASUDEVAN
Department of Mechanics and maritime Engineering
Division of Vehicle Engineering and Autonomous System
Chalmers University of Technology

# Abstract

Driving simulators play an important role in improving driver safety and supporting the development and testing of driver-assistance systems. Their usefulness depends on the ability of the vehicle model to reproduce the behavior of a real vehicle. Since vehicle response is governed by the mathematical model with interconnected subsystems (Powertrain, steering, etc), modeling each is necessary.

This thesis focuses on the development of an electric power-assisted steering (EPAS) model. The developed steering subsystem was integrated into the vehicle model containing an electric powertrain. During vehicle testing, access to controller area network (CAN) signals was restricted, preventing direct logging of steering-related signals. Consequently, the steering-wheel angle was estimated from two inertial measurement unit (IMU) setup in the vehicle and subsequently used as an input to the steering model.

The vehicle model was evaluated through objective and subjective validation. First, the simulated response with experimental inputs was compared with vehicle response using the ISO/TS 18571 objective rating method. The results showed that the developed model captured the main response trends but did not achieve perfect agreement with the experimental data. This was expected, as several vehicle subsystems outside the steering model were retained from the existing baseline vehicle model and were not re-parameterised for the electric vehicle (used for vehicle tests).

Second, the vehicle model was integrated in the driving simulator andevaluated through a subjective study involving test participants. The developed electric vehicle model with EPAS was compared with a baseline model equipped with hydraulic power-assisted steering (HPAS). Since the HPAS model was used as a reference during EPAS model tuning, the subjective ratings did not show large differences between the two steering systems. The participants did not report a clear or consistent perceived difference between the models. The subjective feedback nevertheless provided valuable input for identifying areas for further refinement of the steering model. The developed model provides a basis for representing electric-vehicle steering architecture.

**Keywords:** Electric vehicle model, Driving simulator / SIM IV, Rack assisted electric power steering, Controller, Angle Estimation, Boost curve, Vehicle test, Steering Functions, Subjective Assessments, HPAS, EPAS.

# Acknowledgements

This thesis marks the completion of an important chapter of our journey at Chalmers University of Technology, and there are many people who have contributed to making this work possible.

First and foremost, I would like to express my sincere gratitude to my thesis partner and dear friend, Rohan Kumaar Vasudevan. We first had the opportunity to work together during the Automotive Engineering Project, where we spent an entire semester working closely on the project. That experience helped us develop a friendship and a good understanding of each other's way of working. What started as a project collaboration eventually led us to decide to work together on our Master's thesis. The challenges, discussions and countless technical decisions throughout this thesis have made the experience even more meaningful. I am truly grateful for his support, teamwork, and friendship throughout this journey.

I would like to express my sincere gratitude to my supervisor at VTI, Smit Saparia, for his continuous academic guidance, valuable feedback, and support throughout the thesis. His technical discussions and constructive suggestions helped us stay focused and move the project forward.

I would also like to thank Anders Ödblom, Research Director of Vehicle Systems and Driving Simulation, Maytheewat Aramrattana, Senior Researcher of Vehicle Systems and Driving Simulation, Mattias Hjort, Research Leader of Vehicle Systems and Driving Simulation, and Abhijeet Behera, Researcher of Vehicle Systems and Driving Simulation, at VTI for their valuable support, technical discussions, and contributions during the project. Their knowledge and willingness to share their experience greatly supported the development and experimental activities of this thesis.

A special thanks goes to Daniel Poveda Pi from the Chalmers REVERE Lab for his tremendous support during the experimental work. His technical expertise, practical guidance, and hands-on assistance with the experimental setup were extremely valuable. His support helped us overcome several practical challenges and successfully carry out the vehicle and simulator experiments.

I would also like to express my sincere gratitude to our supervisor and examiner, Fredrik Bruzelius, for his valuable academic guidance, critical feedback, and constructive comments throughout the thesis. His experience and perspective helped us improve both the technical quality and presentation of the work.

Finally, I would like to thank VTI, Chalmers University of Technology, family and friends who contributed directly or indirectly to this thesis. The support, knowledge, and encouragement received throughout this project have made this Master's journey a memorable and rewarding experience.

Ramkumar Huleppa Munavalli Gothenburg, 2026

# Acknowledgements

If I had to summarise this entire thesis journey in one line, it would be: **"One hell of a journey"**. When we initially got the opportunity to work on this thesis, we were excited and thrilled to take it on. However, as people say, life is full of uncertainties, and there was never a straight route to solving the issues we encountered. Some days were fun, some were boring, and many days were mentally demanding. But I believe that this has been the most important takeaway from this thesis for me: Life is a Challenge.

This thesis marks the completion of one of the most important milestones in my life: I will officially be a master's graduate :)

Firstly, I want to thank my thesis partner, Ramkumar Huleppa Munavalli. Our journey started with taking courses together. Later, we got the chance to be teammates in a project course, where we developed a good synergy and work ethic. This eventually led us to becoming partners in this thesis. Even on days when things were difficult and emotionally demanding, we always found a way to come through. More than anything, Ram is like an older brother to me, and this is a relationship I hope to carry forward forever.

I would also like to thank my supervisor at VTI, Smit Saparia, for his guidance throughout the thesis. He made sure that we never went off track, always pointed us in the right direction, helped me develop a pragmatic perspective on things (I was too optimistic). He ensured that our conversations never became unnecessarily formal and was always open to discussions and suggestions. You could walk into his office with questions at any time without prior notice if it was Smit.

I would also like to extend my sincere gratitude to our supervisor and examiner, Fredrik Bruzelius. Thank you for trusting us and giving us this opportunity. Thank you for the weekly meetings; this thesis would not have taken shape without your support and guidance. I will always look forward to an opportunity to work with you again and learn more from your experience.

A special thanks to Daniel Poveda Pi from the Chalmers REVERE Lab for his assistance with the vehicle tests. He listened to all our problems and helped us throughout the process. Taking time out of his schedule to help us meant a great deal, and we are always grateful for your support and for the opportunity to have worked with you.

Finally, I would like to thank the researchers at VTI—Anders Ödblom, Maytheewat Aramrattana, Mattias Hjort, and Abhijeet Behera—as well as all other colleagues, my friends and family, and everyone who contributed directly or indirectly to this thesis.

Rohan Kumaar Vasudevan Gothenburg, 2026

# List of Acronyms

Below is the list of acronyms that have been used throughout this thesis listed in alphabetical order:

| | |
|---|---|
| VTI | Swedish road and Transport Research Institute |
| SIM IV | Simulator IV |
| CAN | Controller Area Network |
| OBD | On-Board Dignostics |
| DOF | Degree of Freedom |
| COG | Centre Of Gravity |
| R-EPAS | Rack-Electric Power Assisted Steering |
| C-EPS | Column-Electric Power Assisted Steering |
| HPS | Hydraulic Assisted Power Steering |
| IMU | Inertial Measurement Unit |
| GNSS | Global Navigation Satellite System |
| PI | Proportional Integral |
| PD | Proportional Derivative |
| SWA | Steering Wheel Angle |
| SWT | Steering Wheel Torque |
| EPAS | Electric Power Assisted Steering |
| ADAS | Advanced Driver Assistance System |
| DIL | Driver-in-the-Loop |
| CEVT | China Euro Vehicle Technology AB |

# Nomenclature

Below is the nomenclature of indices, sets, parameters, and variables that have been used throughout this thesis.

## Parameters and Variables

| | |
|---|---|
| $a_S^s$ | Measured small-IMU acceleration vector |
| $a_S^{s,c}$ | Center-corrected IMU acceleration |
| $a_{off}$ | Estimated offset acceleration |
| $a_{RT}^{s_0}$ | Projected acceleration onto steering frame |
| $b_g$ | Stationary gyroscope bias |
| $C_{tb}$ | Torsion bar damping |
| $c_{eff}$ (or $c$) | Equivalent damping coefficient (local plant) |
| $e(k)$ | Phase discrepancy |
| $e(t)$ | Tracking error |
| $enable_{AR}$ | Active return function swich logic |
| $F_{tb}$ | Rack force from the torsion bar |
| $F_{road}$ | Opposing road reaction force / Tie rod force |
| $F_{motor}$ | Rack force from assist motor |
| $F_{fric,r}$ | Friction force on the rack |
| $F_{AD}$ | Active damping force |
| $F_{AR}$ | Active return restoring force |
| $g$ | Acceleration due to gravity |
| $i_{tb}$ (or $1/r_{tb}$) | Transmission ratio at the torsion bar pinion side |
| $i_{mot}$ (or $1/r_{mot}$) | Transmission ratio at the motor pinion side |
| $i_m$ | Assist motor current |
| $\dot{i}_m$ | Rate of change of current |
| $J_m$ | Motor rotational inertia |

| | |
|---|---|
| $J_{sw}$ | Steering wheel rotational inertia |
| $K$ | Torque eccentricity coefficient |
| $K(k)$ | Gain of Complementary Filter |
| $K_{tb}$ | Torsion bar stiffness |
| $K_t$ | Motor torque coefficient |
| $K_e$ | Motor back-EMF coefficient |
| $K_p, K_i, K_d$ | PID controller gains (proportional, integral, derivative) |
| $k_{eff}$ (or $k$) | Equivalent stiffness (local plant) |
| $k_{v1}$ | Coefficient of the quadratic function for $k_v$ |
| $k_{v2}$ | Coefficient of the quadratic function for $k_v$ |
| $k_{v3}$ | Coefficient of the quadratic function for $k_v$ |
| $k_{d0}$ | Coefficient of the damping gain function $k_d$ |
| $k_{dv}$ | Coefficient of the damping gain function $k_d$ |
| $k_v$ | Speed-dependent curve coefficient for assist torque |
| $k_a$ | Assist torque mapping scaling factor |
| $k_g$ | Overall mapping gain for assist torque |
| $k_d$ | Active damping speed-dependent gain |
| $k_{AR}, d_{AR}$ | Active return speed-dependent gain functions |
| $k_{tb}, k_{BA}, k_{road}, k_{AD}$ | Scaling factors for reference rack acceleration |
| $L_m$ | Motor inductance |
| $m_R$ | Physical rack mass |
| $m_{eff}$ (or $m$) | Equivalent rack mass (including reflected motor inertia) |
| $m_{desired}$ | Desired equivalent rack mass (virtual rack model) |
| $m_x$ | Acceleration in x-direction measured by MuSe |
| $m_y$ | Acceleration in y-direction measured by MuSe |
| $M_{tb}$ | Torsion bar torque |
| $M_{tb,th}$ | Torsion bar torque threshold value |
| $M_{mot}$ | Net motor torque command |
| $M_{\text{active return}}$ | Active return torque function |
| $M_{AR}$ | Request torque for Active return function |
| $M_{FF}$ | Feedforward torque command |
| $M_Z$ | Tire aligning torque |
| $n_{st}$ | Steering ratio |
| $R_m$ | Motor circuit resistance |

| | |
|---|---|
| $R_v^{s0}$ | Rotation matrix to move from vehicle frame to steering frame |
| $R_{s0}^v$ | Rotation matrix to move from steering frame to vehicle frame |
| $r_{tb}$ | Torsion bar pinion effective radius |
| $r_m$ (or $r_{mot}$) | Motor transmission effective radius |
| $r_p$ | Effective radius of pinion attached to torsion bar |
| $r_x$ | Acceleration in x-direction measured by RT3000 |
| $r_y$ | Acceleration in y-direction measured by RT3000 |
| $SAL$ | Steering arm length (effective leverage for tire force) |
| $SG_{ratio}$ | Steering gear ratio factor |
| $T_{net}$ | Net steering column torque |
| $T_{driver}$ | Estimated driver torque |
| $T_{ecc}$ | Torque eccentricity |
| $T_{fbk}$ | Feedback torque to sensodrive motor |
| $T_{BA}$ | Base assist torque (boost curve output) |
| $T_f$ | LuGre friction torque |
| $T_s, T_c$ | Stribeck and Coulomb friction torque thresholds |
| $v$ | Friction block input (Angular rate or velocity) |
| $V_m$ | Motor control voltage |
| $v_x$ | Vehicle longitudinal speed |
| $v_s$ | Stribeck velocity threshold |
| $w_{acc}$ | Time-varying confidence weight for angle observer |
| $x_{s0}^v$ | Rotation vector in x-direction to move from steering frame to vehicle frame |
| $y_{s0}^v$ | Rotation vector in y-direction to move from steering frame to vehicle frame |
| $y_r$ | Rack displacement |
| $y_{r,th}$ | Threshold rack displacement for Active return function |
| $\dot{y}_r, \ddot{y}_r$ | Rack velocity and acceleration |
| $y_{ref}, \dot{y}_{ref}, \ddot{y}_{ref}$ | Reference rack displacement, velocity, and acceleration |
| $z$ | LuGre friction average bristle deflection state |
| $z_{s0}^v$ | Rotation vector in z-direction to move from steering frame to vehicle frame |
| $\alpha, \alpha_v, \alpha_x$ | Feedforward scaling terms |
| $\alpha_{pole}$ | Additional negative real pole |
| $\alpha$ | Steering wheel angular acceleration |

| | |
|---|---|
| $\delta$ | Steering wheel inclination angle |
| $\Delta t$ | Discrete time step |
| $\zeta$ | Desired closed-loop damping ratio |
| $\theta_{sw}$ (or $\theta_{SW}$) | Steering wheel angle |
| $\dot{\theta}_g$ | Vehicle motion compensated steering rate |
| $\theta_a$ | Angle estimate from accelerometer |
| $\dot{\theta}_{sw}$ (or $\omega_{sw}$) | Steering wheel angular velocity |
| $\theta_{pred}$ | Predicted steering angle (IMU observer) |
| $\theta_{est}$ | Estimated steering angle |
| $\tau$ | Time constant of Complementary filter |
| $\tau_{tb}$ | Twist of the torsion bar |
| $\dot{\tau}_{tb}$ | Rate of twist of the torsion bar |
| $\rho_s$ | Position vector of the small IMU relative to the steering wheel center |
| $\sigma_0, \sigma_1, \sigma_2$ | LuGre friction coefficients (stiffness, damping, viscous) |
| $\omega$ | Steering wheel angular velocity |
| $\omega_{s,z}$ | Angular velocity along z axis used for integration |
| $\dot{\omega}_{sw}$ | Angular acceleration of steering wheel |
| $\omega_{RT}^{s0}$ | Angular rate transformed from IMU frame to steering frame |
| $\omega_{RT}^{v}$ | Angular rate transformed from IMU frame to vehicle frame |
| $\omega_{RT,z}^{s0}$ | Angular rate along z axis tranformed to steering frame |
| $\omega_n$ | Desired closed-loop natural frequency |

# Coordinate Frames and Transformations

**Frames**

| | | |
|---|---|---|
| $X_v$,$X_y$,$X_z$ | Vehicle coordinate notation | [-] |
| $x$,$y$,$z$ | Steering zero coordinate notation | [-] |
| $X$,$Y$,$Z$ | RT3000 sensor coordinate notation | [-] |

**Transformations** *(Note: Superscripts denote the target frame, subscripts denote the original frame)*

| | | |
|---|---|---|
| $X_A^B$ | Translation in the X-axis moving from frame $A$ to frame $B$ (e.g., $X_{s0}^v$ is from steering zero to vehicle frame) | [m] |
| $Y_A^B$ | Translation in the Y-axis moving from frame $A$ to frame $B$ | [m] |

| | | |
|---|---|---|
| $Z_A^B$ | Translation in the Z-axis moving from frame $A$ to frame $B$ | [m] |
| $R_A^B$ | Rotation matrix transforming coordinates from frame $A$ to frame $B$ | [-] |
| $\omega_A^B$ | Angular velocity of frame $A$ expressed in frame $B$ | [deg/s] |
| $a_A^B$ | Acceleration of frame $A$ expressed in frame $B$ | [m/s$^2$] |

# Contents

**List of Acronyms** **ix**

**Nomenclature** **xi**

**List of Figures** **xxiii**

**List of Tables** **xxvii**

**1 Introduction** **1**
1.1 Driving Simulator . . . 2
1.2 Project definition . . . 4
1.3 Motivation . . . 5
1.4 Model Characteristics . . . 5
1.5 Model limitations . . . 6
1.6 Disclosure of AI assistance in thesis . . . 6

**2 Background** **9**
2.1 Existing Vehicle models at vti . . . 10
2.1.1 Simulink® SimCar 14-DOF model . . . 10
2.2 Steering System Architecture . . . 12
2.2.1 Rack . . . 13
2.2.2 Servo motor . . . 14
2.2.3 Torsion Bar . . . 15
2.2.4 Mechanical Analysis . . . 16
2.2.5 Steering system controller . . . 18
2.2.5.1 Steering feel . . . 19
2.2.5.2 Road feel . . . 19
2.2.5.3 Implementation . . . 19

**3 Methodology** **21**
3.1 Modelling . . . 21
3.1.1 Model Interface . . . 22
3.1.2 Model Components . . . 23
3.1.2.1 Steering wheel and column block . . . 23
3.1.2.2 Torsion bar block . . . 24
3.1.2.3 Rack and motor block . . . 24
3.1.2.4 Friction block . . . 26

3.1.3 Steering Functions and Controller design . . . 27
3.1.3.1 Motor Assist function . . . 27
3.1.3.2 Reference model . . . 29
3.1.3.3 Active Damping . . . 29
3.1.3.4 Feedback Control . . . 30
3.1.3.5 Feedforward control . . . 33
3.1.3.6 Active Return . . . 34
3.2 Simulation . . . 36
3.2.1 Simulation environment . . . 36
3.3 Steering wheel angle estimation . . . 37
3.3.1 Theory . . . 38
3.3.2 Method of Steering Wheel Angle Estimation . . . 40
3.3.2.1 Coordinate Frame Definition and Rotation . . . 41
3.3.2.2 Compensation of Vehicle-Body Motion . . . 43
3.3.2.3 Kinematic Offset Compensation . . . 43
3.3.2.4 Accelerometer-Based Angle Observation . . . 44
3.3.2.5 Confidence-Weighted Complementary Filter . . . 44
3.3.3 CAD model & 3-D printing of mountings . . . 45

**4 Experiments** **49**
4.1 Vehicle General Data & Experiments Data . . . 49
4.1.1 Vehicle Data . . . 50
4.1.2 Experiments Data . . . 50
4.2 Experimental Equipment & Testing Track . . . 51
4.2.1 Experimental Vehicle . . . 51
4.2.2 IMU(Inertial measurement unit) . . . 53
4.2.3 OBD - II Cable . . . 55
4.2.4 Test Track . . . 56
4.3 Vehicle Tests . . . 57
4.3.1 Design of Experiments . . . 57
4.3.2 Selection of Tests . . . 58

**5 Postprocessing and Model Refinement** **63**
5.1 Postprocessing of Test Data . . . 63
5.1.1 Filtering of IMU and OBD Data . . . 63
5.1.2 Data Synchronization and Acceleration Translation . . . 66
5.2 Model refinement using old steering model . . . 69
5.2.1 Tuning with HPAS model . . . 70

**6 Results** **73**
6.1 Model response to Experimental input . . . 73
6.1.1 Slalom . . . 73
6.1.2 Double Lane Change . . . 77
6.1.3 Steer and Release . . . 79
6.2 Validation of Steering wheel angle estimate . . . 80
6.2.1 Experiment in SIM IV . . . 81
6.2.2 Validation and Tradeoffs . . . 84

6.3 Subjective Assessments . . . 85
6.3.1 Experiment Design . . . 85
6.3.2 Participants rating and feedback . . . 86
6.3.2.1 Driver Background and Experience . . . 86
6.3.2.2 Subjective comparison of steering systems . . . 87
6.3.2.3 Distribution of Subjective Evaluation Outcome . . . 92

**7 Conclusion** **93**
7.1 Summary & Project Outcomes . . . 93
7.2 Limitations . . . 94
7.3 Future Work . . . 95

**Bibliography** **97**

**A Appendix 1** **I**
A.1 Angle Estimation Results . . . I
A.1.1 Double Lane Change . . . I
A.1.1.1 Speed - 20 Km/hr . . . I
A.1.1.2 Speed - 40 Km/hr . . . II
A.1.1.3 Speed - 60 Km/hr . . . II
A.1.1.4 Speed - 80 Km/hr . . . III
A.1.2 Single Lane Change . . . III
A.1.2.1 Speed - 20 Km/hr . . . III
A.1.2.2 Speed - 40 Km/hr . . . IV
A.1.2.3 Speed - 60 Km/hr . . . IV
A.1.2.4 Speed - 80 Km/hr . . . V
A.1.3 Sine Sweep (90 degs) . . . V
A.1.3.1 Speed - 20 Km/hr . . . V
A.1.3.2 Speed - 40 Km/hr . . . VI
A.1.3.3 Speed - 60 Km/hr . . . VI
A.1.4 Slalom . . . VII
A.1.4.1 Speed - 40 Km/hr . . . VII
A.1.4.2 Speed - 60 Km/hr . . . VII
A.1.4.3 Speed - 80 Km/hr . . . VIII
A.1.5 Steer and Release (180 Degs) . . . VIII
A.1.5.1 Speed - 10 Km/hr . . . VIII
A.1.5.2 Speed - 20 Km/hr . . . IX
A.1.5.3 Speed - 40 Km/hr . . . IX
A.1.6 Steady state circle . . . X
A.1.6.1 Steering wheel angle input - 90 Degs . . . X
A.1.6.2 Steering wheel angle input - 180 Degs . . . X
A.1.7 Step Steer . . . XI
A.1.7.1 Speed - 20 Km/hr . . . XI
A.1.7.2 Speed - 40 Km/hr . . . XI
A.1.7.3 Speed - 60 Km/hr . . . XII

**B Appendix 2** **XIII**

B.1 Model Response to Experimental Input . . . . . XIII
B.1.1 Double Lane Change . . . . . XIII
B.1.1.1 Speed - 20 km/h . . . . . XIII
B.1.1.1.1 Lateral Response Comparison (Model vs. Vehicle) . . . . . XIII
B.1.1.1.2 Steering Response (HPAS vs. EPAS) . . . . XIV
B.1.1.2 Speed - 60 Km/hr . . . . . XIV
B.1.1.2.1 Lateral Response Comparison (Model vs. Vehicle) . . . . . XIV
B.1.1.2.2 Steering Response (HPAS vs. EPAS) . . . . XV
B.1.1.3 Speed - 80 Km/hr . . . . . XV
B.1.1.3.1 Lateral Response Comparison (Model vs. Vehicle) . . . . . XV
B.1.1.3.2 Steering Response (HPAS vs. EPAS) . . . . XVI
B.1.2 Single Lane Change . . . . . XVI
B.1.2.1 Speed - 20 Km/hr . . . . . XVI
B.1.2.2 Speed - 40 Km/hr . . . . . XVI
B.1.2.2.1 Lateral Response Comparison (Model vs. Vehicle) . . . . . XVI
B.1.2.2.2 Steering Response (HPAS vs. EPAS) . . . . XVII
B.1.2.3 Speed - 60 Km/hr . . . . . XVII
B.1.2.3.1 Lateral Response Comparison (Model vs. Vehicle) . . . . . XVII
B.1.2.3.2 Steering Response (HPAS vs. EPAS) . . . . XVIII
B.1.2.4 Speed - 80 Km/hr . . . . . XVIII
B.1.3 Sine Sweep (90 degs) . . . . . XIX
B.1.3.1 Speed - 20 Km/hr . . . . . XIX
B.1.3.1.1 Lateral Response Comparison (Model vs. Vehicle) . . . . . XIX
B.1.3.1.2 Steering Response (HPAS vs. EPAS) . . . . XIX
B.1.3.2 Speed - 40 Km/hr . . . . . XX
B.1.3.2.1 Lateral Response Comparison (Model vs. Vehicle) . . . . . XX
B.1.3.2.2 Steering Response (HPAS vs. EPAS) . . . . XX
B.1.3.3 Speed - 60 Km/hr . . . . . XXI
B.1.3.3.1 Lateral Response Comparison (Model vs. Vehicle) . . . . . XXI
B.1.3.3.2 Steering Response (HPAS vs. EPAS) . . . . XXI
B.1.4 Slalom . . . . . XXII
B.1.4.1 Speed - 60 Km/hr . . . . . XXII
B.1.4.1.1 Lateral Response Comparison (Model vs. Vehicle) . . . . . XXII
B.1.4.1.2 Steering Response (HPAS vs. EPAS) . . . . XXII
B.1.4.2 Speed - 80 Km/hr . . . . . XXIII
B.1.5 Steer and Release (180 Degs) . . . . . XXIII
B.1.6 Steady state circle . . . . . XXIII

B.1.6.1 Steering wheel angle input - 90 Degs . . . . . XXIII
B.1.6.1.1 Lateral Response Comparison (Model vs. Vehicle) . . . . . XXIII
B.1.6.1.2 Steering Response (HPAS vs. EPAS) . . . . XXIV
B.1.6.2 Steering wheel angle input - 180 Degs . . . . . XXIV
B.1.6.2.1 Lateral Response Comparison (Model vs. Vehicle) . . . . . XXIV
B.1.6.2.2 Steering Response (HPAS vs. EPAS) . . . . XXV
B.1.7 Step Steer . . . . . XXV
B.1.7.1 Speed - 20 Km/hr . . . . . XXV
B.1.7.1.1 Lateral Response Comparison (Model vs. Vehicle) . . . . . XXV
B.1.7.1.2 Steering Response (HPAS vs. EPAS) . . . . XXVI
B.1.7.2 Speed - 40 Km/hr . . . . . XXVI
B.1.7.2.1 Lateral Response Comparison (Model vs. Vehicle) . . . . . XXVI
B.1.7.2.2 Steering Response (HPAS vs. EPAS) . . . . XXVII
B.1.7.3 Speed - 60 Km/hr . . . . . XXVII

# List of Figures


1.1 Main subsytems of the Driving simulator . . . . . 2
1.2 Cabin and graphic system of simulator . . . . . 3
1.3 Motion platform . . . . . 4

2.1 Sturcture of Simulink Simcar14DOF model . . . . . 10
2.2 New powertrain Subsystem of Simcar14DOF . . . . . 11
2.3 New Brake Subsystem of Simcar14DOF . . . . . 11
2.4 Schematic of two pinion R-EPAS system [AI Generated] . . . . . 12
2.5 A cross-section of the steering rack suspended by the yoke and pinion [15] . . . . . 14
2.6 The torsion bar in a schematic image [15] . . . . . 16
2.7 The rack with the main forces [15] . . . . . 16
2.8 Illustration of the torques on the steering column [15] . . . . . 17
2.9 Torques and forces on the servo motor transmission [15] . . . . . 17
2.10 A top view of the suspension linkage and tire, showing levers and acting points of forces [15] . . . . . 18

3.1 Schematic of Vehicle model and cabin control file running in different PCs and signal flow . . . . . 22
3.2 Block diagram of model components . . . . . 23
3.3 Bristle contact interface between two surfaces. Bristles on the lower part are shown as rigid for simplicity . . . . . 26
3.4 Steering control functions inside the controller block . . . . . 27
3.5 Assist Torque Map . . . . . 28
3.6 Plot of Damping force . . . . . 30
3.7 Flow chart of the R-EPAS sub systems . . . . . 36
3.8 Schematic of the axes marked in an IMU . . . . . 38
3.9 Schematic of accelerometers and gyroscopes in an IMU . . . . . 39
3.10 Schematic of IMUs mounted on the vehicle . . . . . 39
3.11 Orthogonal axes of IMU's marked. . . . . 41
3.12 Coordinate frames of the IMUs and the vehicle . . . . . 42
3.13 Schematic of coordinate frame translation and rotation onto steering wheel frame . . . . . 43
3.14 Angle Estimate for a step steer maneuver (90 Degs) . . . . . 45
3.15 CAD model of the antenna mountings. . . . . 46
3.16 CAD model of IMU mounting bracket (Exploded view) . . . . . 46
3.17 3-D Printed brackets mounted on the Vehicle . . . . . 47

4.1 Volvo EC40 in REVERE Lab . . . 52
4.2 OxTS RT3000 . . . 54
4.3 Muse wireless & Miniature IMU . . . 55
4.4 OBD-II Cable . . . 56
4.5 Aerial view of Stora Holm Trafikövningsplats . . . 57
4.6 Schematic of Double lane change . . . 58
4.7 Schematic of Sinusoidal Sweep (Low Freq to High Freq) . . . 59
4.8 Schematic of Straight line drive with no driver intervention . . . 59
4.9 Schematic of Step Steer (note the trajectory wont be exact) . . . 60
4.10 Schematic of U-turn . . . 60
4.11 Schematic of Steady state circle (Constant angle) . . . 61
4.12 Schematic of Steer (180 degs) and release . . . 61
4.13 Schematic of Single lane change . . . 62
4.14 Schematic of Slalom . . . 62
4.15 Schematic of Parking maneuver . . . 62

5.1 Raw Gyro signal from Muse before filtering . . . 64
5.2 Filtered Gyro signal logged Muse . . . 64
5.3 Raw Gyro signal from RT3000 before filtering . . . 64
5.4 Filtered Gyro signal logged in RT3000 . . . 64
5.5 Raw Accelerometer signal from Muse before filtering . . . 65
5.6 Filtered Accelerometer signal logged in Muse . . . 65
5.7 Raw Accelerometer signal from RT3000 before filtering . . . 65
5.8 Filtered Accelerometer signal logged in RT3000 . . . 66
5.9 Time synced acceleration signals . . . 67
5.10 Time syned OBD II and RT3000 Longitudinal velocity signal . . . 68
5.11 Plot of Lateral acceleration measured by sensor and Lateral acceleration translated to vehicle CoG . . . 69
5.12 Plot of SWT Vs SWA of both HPAS and EPAS after tuning for Sine Sweep maneuver performed at 20 Km/hr . . . 70

6.1 Yaw rate (Vehicle Vs Model response) . . . 74
6.2 Lateral acceleration (Vehicle Vs Model response) . . . 74
6.3 Feedback torque profile as a function of time . . . 76
6.4 Feedback torque (SWT) Vs Steering wheel angle (SWA) input . . . 76
6.5 Yaw rate (Vehicle Vs Model response) . . . 77
6.6 Lateral acceleration (Vehicle Vs Model response) . . . 77
6.7 Feedback torque profile as a function of time . . . 78
6.8 Feedback torque (SWT) Vs Steering wheel angle (SWA) input . . . 78
6.9 Steering wheel angle estimate for Steer and release maneuver performed at 20 Km/hr . . . 79
6.10 Single return event identified from both vehicle and simualtor logs . . . 79
6.11 Return profile of steering wheel angle after tuning the model . . . 80
6.12 Angular velocity profile during the return event after tuning . . . 80
6.13 Plot of steering wheel angle from angle estimate and simulator after initial startup delay sync . . . 82
6.14 Initial impulse event used for sync . . . 82

6.15 Final impulse event to show hardware clock drift . . . . . 83
6.16 Steering wheel angle profiles after time correlation . . . . . 83
6.17 Chart of participants age . . . . . 86
6.18 Pie chart showing driving experience of participants . . . . . 87
6.19 Chart showing participants experience with driving simulator . . . . . 87
6.20 Straight-line response & Steering friction . . . . . 88
6.21 Road surface info & On-center behavior . . . . . 89
6.22 Steering response & Steering effort . . . . . 90
6.23 Return to center behavior, Steering rhythm & flow and Initial resistance (high inertia effect) . . . . . 90
6.24 Steering feedback & Overshoot (steering moving without input) . . . 91
6.25 Distribution of Subjective Evaluation Outcome . . . . . 92

A.1 Angle estimate for DLC maneuver performed at 20 Km/hr . . . . . I
A.2 Angle estimate for DLC maneuver performed at 40 Km/hr . . . . . II
A.3 Angle estimate for DLC maneuver performed at 60 Km/hr . . . . . II
A.4 Angle estimate for DLC maneuver performed at 80 Km/hr . . . . . III
A.5 Angle estimate for SLC maneuver performed at 20 Km/hr . . . . . III
A.6 Angle estimate for SLC maneuver performed at 40 Km/hr . . . . . IV
A.7 Angle estimate for SLC maneuver performed at 60 Km/hr . . . . . IV
A.8 Angle estimate for SLC maneuver performed at 80 Km/hr . . . . . V
A.9 Angle estimate for Sine Sweep (90 degs) maneuver performed at 20 Km/hr . . . . . V
A.10 Angle estimate for Sine Sweep (90 degs) maneuver performed at 40 Km/hr . . . . . VI
A.11 Angle estimate for Sine Sweep (90 degs) maneuver performed at 60 Km/hr . . . . . VI
A.12 Angle estimate for Slalom maneuver performed at 40 Km/hr . . . . . VII
A.13 Angle estimate for Slalom maneuver performed at 60 Km/hr . . . . . VII
A.14 Angle estimate for Slalom maneuver performed at 80 Km/hr . . . . . VIII
A.15 Angle estimate for Steer and Release (180 degs) maneuver performed at 10 Km/hr . . . . . VIII
A.16 Angle estimate for Steer and Release (180 degs) maneuver performed at 20 Km/hr . . . . . IX
A.17 Angle estimate for Steer and Release (180 degs) maneuver performed at 40 Km/hr . . . . . IX
A.18 Angle estimate for Steady state circle (90 degs fixed steering angle, speed ramped) maneuver . . . . . X
A.19 Angle estimate for Steady state circle (180 degs fixed steering angle, speed ramped) maneuver . . . . . X
A.20 Angle estimate for Step Steer maneuver performed at 20 Km/hr . . . XI
A.21 Angle estimate for Step Steer maneuver performed at 40 Km/hr . . . XI
A.22 Angle estimate for Step Steer maneuver performed at 60 Km/hr . . . XII

B.1 Yaw rate: Vehicle Vs Model response. . . . . XIII
B.2 Lateral acceleration: Vehicle Vs Model response. . . . . XIII
B.3 SWT Vs SWA for the Double lane change maneuver . . . . . XIV

B.4 Yaw rate: Vehicle Vs Model response. . . . . XIV
B.5 Lateral acceleration: Vehicle Vs Model response. . . . . XIV
B.6 SWT Vs SWA for the Double lane change maneuver . . . . . XV
B.7 Yaw rate: Vehicle Vs Model response. . . . . XV
B.8 Lateral acceleration: Vehicle Vs Model response. . . . . XV
B.9 SWT Vs SWA for the Double lane change maneuver . . . . . XVI
B.10 Yaw rate: Vehicle Vs Model response. . . . . XVI
B.11 Lateral acceleration: Vehicle Vs Model response. . . . . XVII
B.12 SWT Vs SWA . . . . . XVII
B.13 Yaw rate: Vehicle Vs Model response. . . . . XVII
B.14 Lateral acceleration: Vehicle Vs Model response. . . . . XVIII
B.15 SWT Vs SWA . . . . . XVIII
B.16 Yaw rate: Vehicle Vs Model response. . . . . XIX
B.17 Lateral acceleration: Vehicle Vs Model response. . . . . XIX
B.18 SWT Vs SWA . . . . . XIX
B.19 Yaw rate: Vehicle Vs Model response. . . . . XX
B.20 Lateral acceleration: Vehicle Vs Model response. . . . . XX
B.21 SWT Vs SWA . . . . . XX
B.22 Yaw rate: Vehicle Vs Model response. . . . . XXI
B.23 Lateral acceleration: Vehicle Vs Model response. . . . . XXI
B.24 SWT Vs SWA . . . . . XXI
B.25 Yaw rate: Vehicle Vs Model response. . . . . XXII
B.26 Lateral acceleration: Vehicle Vs Model response. . . . . XXII
B.27 SWT Vs SWA . . . . . XXII
B.28 Yaw rate: Vehicle Vs Model response. . . . . XXIII
B.29 Lateral acceleration: Vehicle Vs Model response. . . . . XXIII
B.30 SWT Vs SWA . . . . . XXIV
B.31 Yaw rate: Vehicle Vs Model response. . . . . XXIV
B.32 Lateral acceleration: Vehicle Vs Model response. . . . . XXIV
B.33 SWT Vs SWA . . . . . XXV
B.34 Yaw rate: Vehicle Vs Model response. . . . . XXV
B.35 Lateral acceleration: Vehicle Vs Model response. . . . . XXV
B.36 SWT Vs SWA . . . . . XXVI
B.37 Yaw rate: Vehicle Vs Model response. . . . . XXVI
B.38 Lateral acceleration: Vehicle Vs Model response. . . . . XXVI
B.39 SWT Vs SWA . . . . . XXVII

# List of Tables

4.1 Vehicle Data Requirements . . . . . 50
4.2 Experimental Data Requirements . . . . . 51
4.3 Electric drive motor specification . . . . . 53
4.4 Vehicle dimension . . . . . 53
4.5 Tire Sizes . . . . . 53

6.1 ISO scores to analyze correspondence of model and vehicle response . 75
6.2 ISO scores to analyze correspondence of model and vehicle response . 77

# 1
# Introduction

This thesis presents the work carried out to implement Electric Power Assisted Steering(EPAS) in a Electric vehicle model architecture for use in driving simulator. The model is implemented in MATLAB/Simulink and integrated into Simulator (SIM IV), an advanced driving simulator at the Swedish road and Transport Research Institute(VTI) in Göteborg [5]. SIM IV is a high-fidelity simulator platform designed to replicate realistic driving conditions, enabling detailed analysis of vehicle behavior and driver interaction.

As a leading research institute, VTI conducts studies across multiple domains within the automotive field, including passive safety, infrastructure maintenance, environmental impact(air quality and noise) and traffic simulation. With over four decades of experience in driving simulator, VTI has established itself as a key authority in both development of simulator technologies and the execution of experimental studies.

Driving simulator play a crucial role in understanding driver behavior under controlled and repeatable conditions [24] [25]. They are widely used to evaluate driver responses to advanced driver assistance system (ADAS), such as lane-keeping support and stability control, as well as to study the effects of external factors like fatigie, alcohol and drug influence.Since the primary objective of such simulations is to analyze human behavior, it is essential that the virtual driving experience closely matches real-world conditions, ensuring reliable and meaning results.

The current electric vehicle model implemented in the simulator consists of a hydraulic power assisted steering (HPAS) system and a combustion engine powertrain. While this approach provides a simplified representation of steering assistance, it does not fully capture the characteristics of modern steering systems used in contemporary electric vehicles like the motor dynamics and controller functions. In particular, hydraulic systems lack the ability to accurately model energy-efficient operation, variable assist behavior, and advanced control strategies, which are present in current steering systems and will be critical for realistic simulation of model in the simulator after integration.

To address these limitations, this work focuses on the development and integration of a Rack- Electric Power Assisted Steering (R-EPAS) system model. The reason for choosing this steering architecture despite other options stated in [8] and [16] is its presence in modern commercial vehicles and reference research work which

Compared to hydraulic power steering, EPAS offers several advantages [19] [16], including improved energy efficiency due to on-demand assistance, reduced mechanical complexity, and greater flexibility in control design. The rack-assisted configuration enables more direct control of the steering rack force, allowing precise tuning of steering feel and responsiveness across different driving conditions.

Furthermore, EPAS significantly enhances vehicle safety. By enabling advanced control features such as torque overlay, active return control, and integration with driver assistance systems, EPAS can support functions like lane keeping, collision avoidance, and stability enhancement. These features can be built on top of the baseline model that is to be developed, which isnt possible in the existing model. Unlike hydraulic systems, EPAS can adapt in real time to vehicle speed, road conditions, and driver inputs, providing consistent and predictable steering feedback. This adaptability not only improves driving comfort but also contributes to safer vehicle operation by assisting the driver in critical situations.

## 1.1 Driving Simulator

The driving simulator includes a Motion Platform designed to reproduce the physical sensations experienced by the driver during vehicle operation. VTI's driving simulator can be divided into 5 main subsystems as shown in fig 1.1. [13]

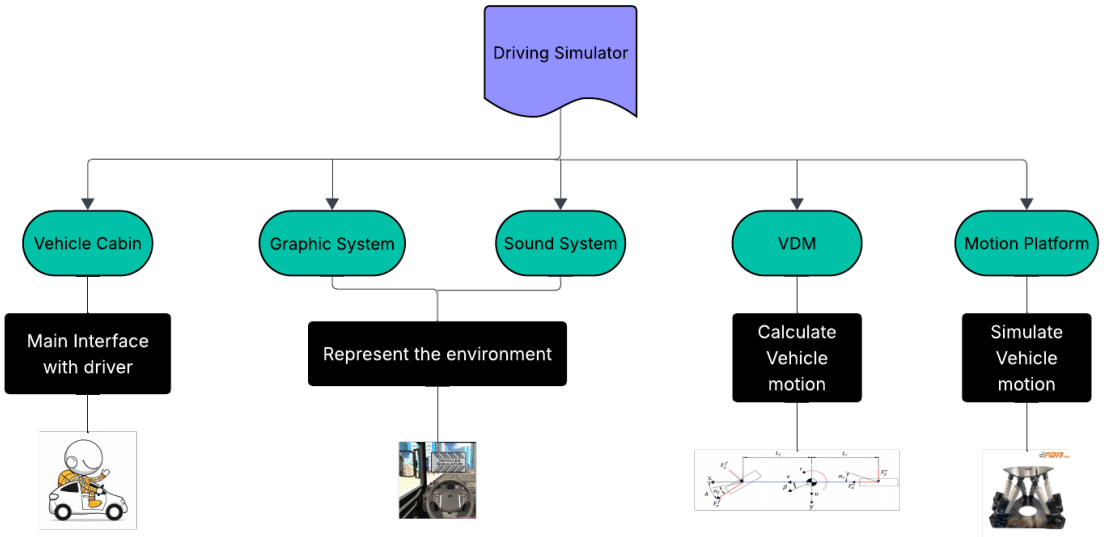



**Figure 1.1:** Main subsytems of the Driving simulator

The first subsystem of the simulator, the vehicle cabin, serves as the primary interface between the driver and the simulation environment. In Sim IV, the cabin is based on a modified Volvo XC60 body, which has been adapted and instrumented to suit simulator requirements, as illustrated in Figure 1.2. In addition, a Volvo truck cabin is also available which has its own dedicated vehicle model.




**Figure 1.2:** Cabin and graphic system of simulator

The second subsystem, the graphic system, provides the visual environment to the driver. It consists of a 180° projection screen that surrounds the vehicle cabin, covering the entire field of view. The visual scene is generated using multiple projectors to ensure an immersive experience. Furthermore, conventional rear-view mirrors have been replaced with LCD displays that simulate the rear environment. Figure 1.2 shows both the arrangement of the surrounding screen and the implementation of the side mirror display.

Another essential subsystem for environmental representation is the sound system, which includes multiple speakers integrated within the cabin.

Although all subsystems contribute to the overall simulation fidelity, the motion of the vehicle cabin is a key factor in achieving a realistic driving experience. In Sim IV, the cabin is mounted on a motion platform that replicates the physical sensations associated with the dynamics of the real vehicle. This platform, shown in Figure 1.3, where in the XY Sled is capable of moving the vehicle cabin in both longitudinal and lateral directions to simulate corresponding accelerations. Additionally, the hexapod can generate rotational and translational motions in X, Y, and Z directions. With these capabilities, the system can reproduce lateral accelerations of up to 0.6g.

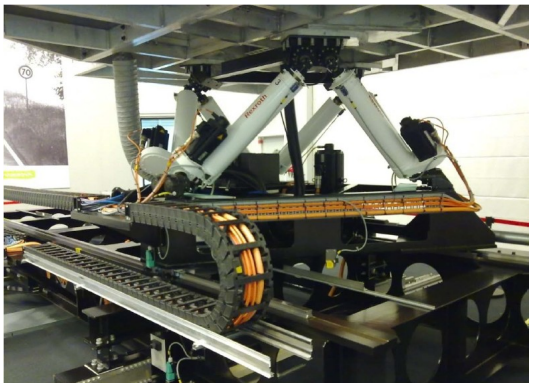


**Figure 1.3:** Motion platform

Finally, the Vehicle Dynamics Model (VDM) is a critical component of the simulator. Since the platform physically reproduces vehicle motion, it is necessary to compute the expected behaviour of a real vehicle under given conditions. This is the role of the VDM, which models the physics of vehicle motion based on inputs related to the vehicle, driver, and environment. It is important to distinguish the VDM from motion cueing algorithms. While the VDM focuses on accurately predicting vehicle dynamics, motion cueing algorithms are responsible for controlling the motion platform to ensure that the driver perceives realistic motion within the simulator.

## 1.2 Project definition

The primary objective of this thesis is to develop and validate the Rack-Electric Power Assisted Steering(R-EPAS) system within the Driver-in-the-Loop (DIL) simulation framework,with the aim of improving steering feel assessment in a driving simulator environment. The work focuses on integrating a physically representative steering system model into an existing vehicle dynamics model to accurately capture the interaction between the driver, steering system, and vehicle response.

A key goal is to design and implement a control-oriented EPAS model that includes rack dynamics, assist torque generation, friction characteristics, and motor behaviour. This model is intended to enable realistic reproduction of steering feedback, including on-center feel, assist variation with speed, and road feedback transmission to the driver.

Furthermore, the thesis aims to investigate and develop control strategies for the EPAS system that can be tuned later after the exprimental and vehicle test data within a Driver-in-the-Loop setup. This allows evaluation of how different assist characteristics and control parameters influence driver perception, steering comfort, and vehicle handling.

Finally, the developed model is validated through simulator-based experiments,

where driver feedback and system response are analysed to assess the realism and effectiveness of the steering feel. The outcome of this work contributes to enhancing simulator fidelity and provides a framework for the development and evaluation of advanced steering systems in a virtual environment.

## 1.3 Motivation

The current Sim IV driving simulator at the Swedish Road and Traffic Research Institute uses a Hydraulic Power Assisted Steering (HPAS) model, which does not fully represent modern vehicle steering systems. In previous thesis work [11], an electric powertrain model was developed based on the Volvo EC40. However, despite using a modern electric vehicle for parameterization, the steering system remained hydraulic, creating a mismatch between the powertrain and steering subsystems in the full vehicle model.

To address this inconsistency of the model not being validated for lateral maneuvers, this work was planned to validate that. But since lateral maneuvers involve contribution from multiple subsystems (Steering, Suspension, Tires), there was a need to go subsystem by subsystem. So, the main goal for the thesis work was on developing a Rack- Electric Power Assisted Steering (R-EPAS) model. R-EPAS, which is used in modern electric vehicles, and having a physuscs based block for each component means that it will be easier build on top (instead of a single boost curve function) of in the future. This makes it more suitable for reproducing realistic steering behavior and adding safety functions (Lane keeping, Lane change, Evasive Steering Assist) in the simulator since the motor block is separate.

By replacing HPS with R-EPAS, the vehicle model that the simulator uses becomes more consistent with modern vehicle architectures and better suited for building other subsystems of the electric vehicle architecture in the future.

## 1.4 Model Characteristics

The developed Rack-Electric Power Assisted Steering (R-EPAS) model must satisfy following characteristics.

- It must accurately represent the steering system dynamics, including steering column, torsion bar, rack-and-pinion mechanism, and electric motor. The model should capture key effects such as rack motion, assist torque generation, and interaction with road forces.
- It must provide a realistic steering feel, particularly around the on-centre region, by incorporating nonlinear assist characteristics, friction effects, and torque feedback to the driver.
- It must include a control-oriented structure, allowing implementation of assist curves, speed-dependent assistance, and torque overlay functions that are representative of modern EPAS systems.

- It must be computationally efficient and suitable for real-time simulation within a Driver-in-the-Loop environment, avoiding numerical instability while maintaining sufficient accuracy.
- The model should support integration with advanced driver assistance systems (ADAS), enabling future studies on functions such as lane keeping, stability control, and driver feedback systems.
- The overall structure should remain as simple as possible, while still achieving the required level of fidelity, to ensure ease of modification, tuning, and implementation in the simulator environment.

## 1.5 Model limitations

The rack-assisted Electric Power Steering (R-EPAS) model developed in this thesis has several limitations, which are outlined below:

- The model is validated under normal driving conditions within the typical operating range of the driving simulator. Therefore, its accuracy is limited when representing highly nonlinear steering behaviour, such as extreme manoeuvres or operation near the physical limits of the steering system.

- The assist torque generation is based on simplified control strategies and defined Boost-assist curves. Advanced control strategies used in production car steering system such as highly complex observer based control strategies are not represented.

- Friction in the steering system, including rack and column friction, is modelled using Lugre friction model approach. Due to time constraints, this couldnt be implemented in the final VM.

- The interaction between the steering system and road surface is simplified. While smooth road feedback is included, high-frequency disturbances and detailed tyre-road interactions affecting steering feel are not fully modelled.

- The entire thesis work mainly focuses on one particular subsystem (Steering), so the other blocks in the vehicle model was untouched and completely replicated from the old model (Suspension, tires).

## 1.6 Disclosure of AI assistance in thesis

AI assistance was crucial for the completion of the thesis work on time due to the workload. Eventhough AI was not used to do the entire thesis work but was used as a helpful partner who aided in correcting grammar and structure of the report, assist with debugging and reviewing the developed angle-estimation algorithm, support the exploration of post-processing methods for the experimental test logs, assist in

the development and checking of procedures used to calculate ISO-based scores for model validation, and provide simplified explanations of relevant technical concepts. AI tools were not used to produce the thesis methodology, experimental results, data analysis, interpretations, conclusions, or final technical content. All AI-generated suggestions, explanations, code-related recommendations, and language revisions were critically reviewed, verified, adapted where necessary, and approved by the authors. The authors take full responsibility for the scientific accuracy, originality, and integrity of the final thesis.

# 2
# Background

Before initiating the modeling phase, it is essential to review previous research work conducted to establish a clear direction and provide a solid theoretical and technical foundation. This chapter first examines existing vehicle model, including those developed in earlier master's thesis and the model currently used at vti. Also, exploration of the previous model development in driving simulators, the fidelity, the approach was essential [26] [21].

The existing electric vehicle model, developed in prior work, focuses primarily on the powertrain and the brake subsystem while not focusing on the steering, suspension and tire subsystems. In addition, the vehicle model currently implemented in Sim IV contains a Hydraulic Power Steering (HPS) system parameterized from an old Volvo S40 vehicle. Therefore, this current steering system model is not well suited for modern electric vehicles, where Electric Power Assisted Steering (EPAS) is standard. This creates a gap between the electric vehicle model and the simulator implementation where the ultimate goal is to transform the existing conventional (ICE) vehicle model to an EV model.

To address this, the literature review focuses on the modelling and control of R-EPAS systems. The reason for choosing a Rack-Assisted Electric Power Steering system is because it more common in current EVs as compared to a Column-Assisted EPS. Even though a column assist architecture is easier to model and abundant literature to refer to like [35] [34], the rack assist architecture was selected due to its current abundance. The research wanted to accomplish a foundational structure which can be calibrated and improved later. Different modelling approaches are analysed to identify a suitable structure that balances physical accuracy with real-time simulation requirements. The model could be built with extreme detials like contact modeling, individual joints and compliance (from bushings, joints, etc) like [22] or could be detialed enough to reproduce the steering dynamics using simple control architecture like [19] [20]

In addition, the review considers control strategies used in modern EPAS systems, including Speed-dependent assist function, Active damping, Reference model and feedback control mechanisms that collectively influence steering feel. These aspects are particularly important for Driver-in-the-Loop (DiL) applications, where realistic steering feedback to the driver is essential since there is no mechanical components but just a feedback motor which replicates the actual steering system's feedback torque.

Overall, this chapter establishes the theoretical and practical basis for developing an R-EPAS model tailored for an electric vehicle. The developed model will later be integrated into the Sim IV simulator to replace the existing HPS system, enabling more realistic steering behaviour and supporting future research on steering feel and advanced driver assistance systems.

## 2.1 Existing Vehicle models at vti

### 2.1.1 Simulink® SimCar 14-DOF model

The Simulink model was built in 2015 to replace the old FORTRAN-based Vehicle Dynamics Model (VDM), which was challenging to modify. Fig 2.1 shows the structure of this Simulink model. It comprises seven subsystems: braking, steering, powertrain, wheels, suspension, axles, and chassis. The model consists of two parts of inputs.
One part of the input is the road information input, which is the road information while the other part is the driver's input, which includes the gas pedal signal, clutch signal, steering wheel angle signal, gear signal, brake signal, and whether the ABS function is on or off. The model outputs are the velocity and acceleration of the vehicle in the XY direction and the state of pitch and roll to reflect the vehicle's dynamic response.

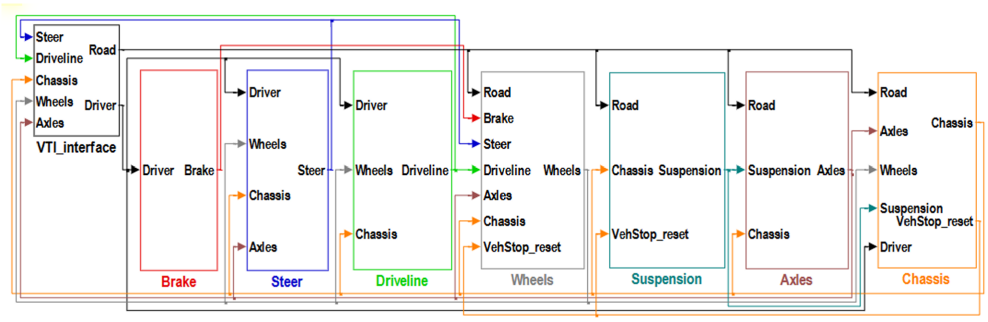



**Figure 2.1:** Sturcture of Simulink Simcar14DOF model

This VDM was built and parameterised to reproduce the response of an ICE vehicle (Volvo S40). The previous master thesis work in 2024 conducted by Zikun Wang and Jinge Jao [11] focused on modifying this 14 DOF VDM to represent an electric vehicle. The main objective of the work was to replace the the old ICE powertrain model is replaced with a dual motor powertrain model, which is equipped with many new features such as fixed and variable torque distribution, regenerative braking, one pedal drive, brake override, and traction control.

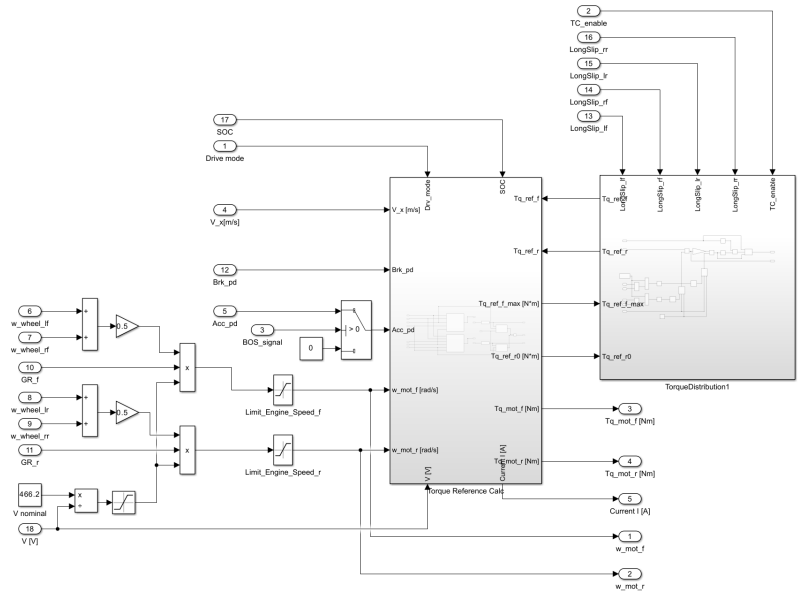



**Figure 2.2:** New powertrain Subsystem of Simcar14DOF

The old brake system was also modified to suit only one input- brake pedal position and suit the energy regeneration feature of the new powertrain model.

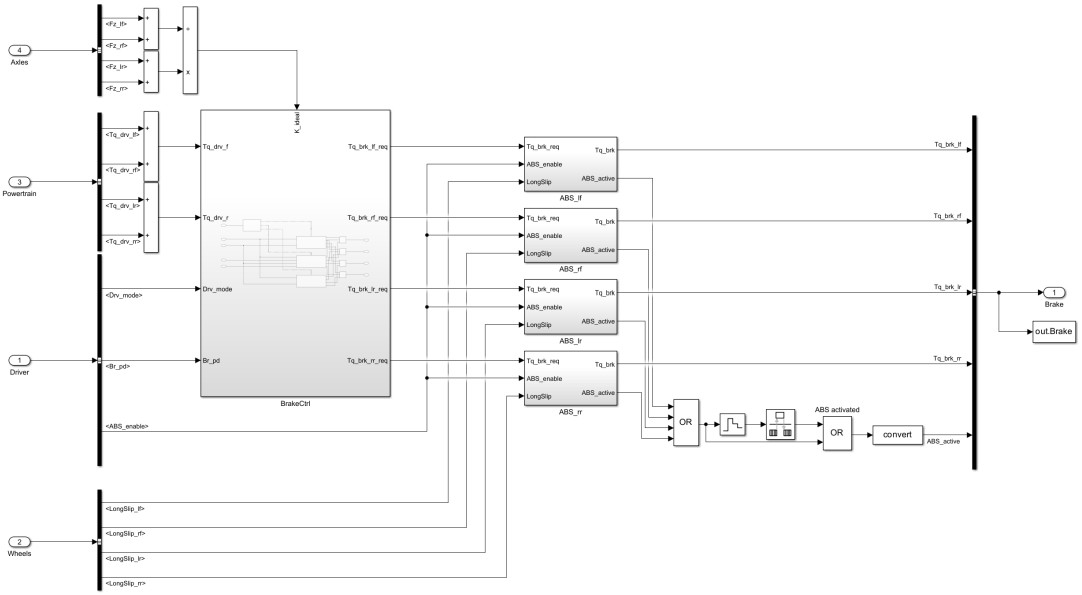



**Figure 2.3:** New Brake Subsystem of Simcar14DOF

The benchmark vehicle used for parameterizing the Vehicle Model (VM) was Volvo EC40 with rear wheel drive powertrain configuration. This was a different powertrain layout compared to the previous thesis work (modeled All wheel drive), so the powertrain model was also modified to suit the available test vehicle and was used during this thesis work for tuning and evaluating the steering response.

The current steering subsystem implemented in the Sim IV driving simulator is based on a Hydraulic Power Steering (HPS) model, which was originally developed by parameterizing the Volvo S40. This steering model represents the existing steering system currently used in the simulator.

Since this thesis mainly focuses on the development and integration of a rack-assisted Electric Power Steering (R-EPAS) system, all other existing subsystems are adopted without modification. Therefore, components such as the wheels, chassis, axles, and suspension systems are not discussed in detail in this report. Readers interested in these subsystems are referred to the Limit Handling report [12] and vehicle model report [18] used during initial development (FORTRAN) for a more comprehensive description of the existing vehicle model.

## 2.2 Steering System Architecture

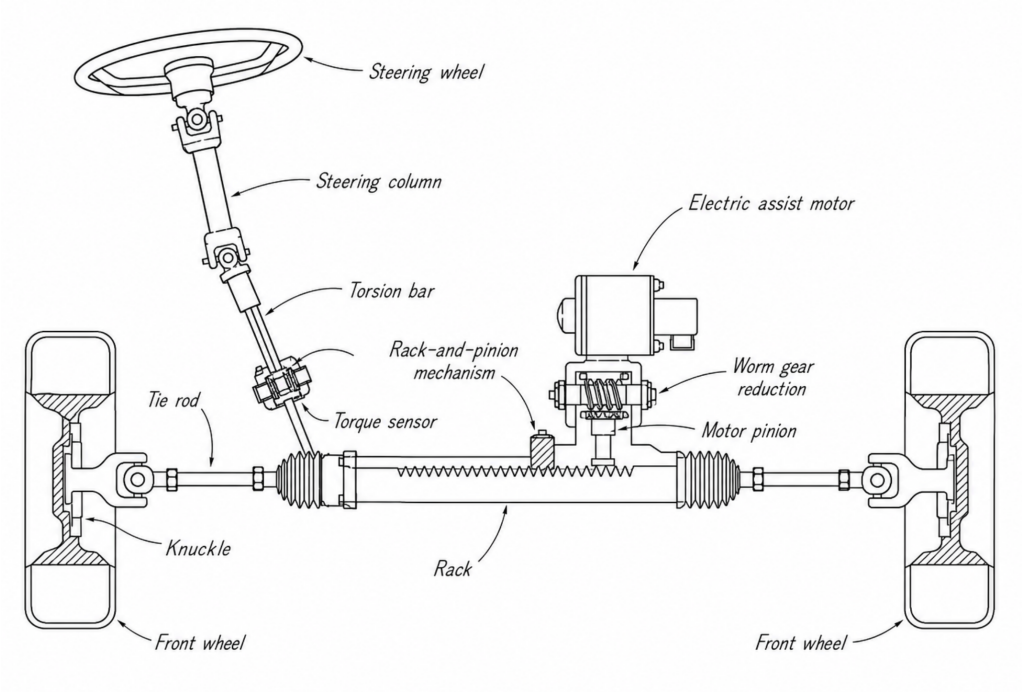



**Figure 2.4:** Schematic of two pinion R-EPAS system [AI Generated]

In an Electric Power Steering (EPAS) system, steering assistance is generated using an electric motor rather than the hydraulic assist mechanism used in conventional Hydraulic Power Assisted Steering (HPAS) systems. In this thesis, a dual-pinion rack-assisted EPAS configuration has been developed and analysed.

The dual-pinion arrangement, shown on fig 2.4 consists of two separate pinions connected to the steering rack: the sensor pinion and the motor pinion. The steering wheel and steering column are connected to the sensor pinion through a torsion bar.

When the driver applies steering torque, the torsion bar twists slightly, allowing the driver input torque to be measured and transferred to the rack as a steering force.

The second pinion, known as the motor pinion, is connected to the electric motor through a worm gear mechanism. This gearing increases the effective torque delivered by the motor to the steering rack. Such torque amplification is necessary because the rack can require very large forces, especially during low-speed manoeuvres or high-load steering conditions. Since steering rack motion generally occurs at relatively low speeds, a higher gear ratio can be used without negatively affecting steering performance. As a result, the motor operates at higher rotational speeds while providing sufficient assist torque to reduce driver effort.

The EPAS system therefore combines mechanical steering components, sensing elements, and electric motor assistance to achieve improved steering feel, reduced driver effort, and enhanced control flexibility. The main components and important concepts related to the developed steering system are discussed in the following sections.

### 2.2.1 Rack

The steering rack is one of the most important components in the dual-pinion EPAS system, as it acts as the central element through which all steering forces are transmitted. The steering column, electric motor, and wheel knuckles are not directly connected to each other; instead, their interactions take place through the rack. Because of this, the rack provides valuable information about the steering system dynamics and plays a key role in the steering control process.

As the rack moves laterally, the tie rods connected to it transfer this motion to the wheels, causing the wheels to steer. Therefore, the displacement, velocity, and force acting on the rack strongly influence the overall steering response and vehicle behaviour.

The rack is supported by two pinions along with their corresponding yoke mechanisms. The yokes are designed to keep the rack in proper contact with the pinions while still allowing smooth linear motion. A spring-loaded preload mechanism is typically used behind the yoke to maintain this contact force. However, the preload level must be carefully adjusted. If the preload is too low, excessive clearance or play can occur between the rack and pinion, leading to reduced steering precision. On the other hand, too much preload increases friction, which can negatively affect steering feel and restrict rack movement.

Due to these factors, the rack and yoke assembly have a significant influence on steering performance, friction characteristics, and driver steering feel in the EPAS system. In Fig 2.5, the rack can be seen in axial view with a yoke and pinion supporting it from either side.

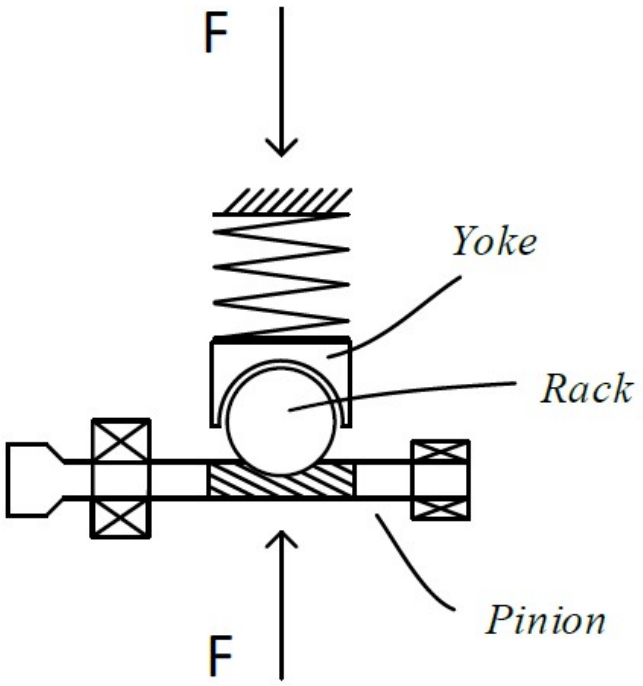



**Figure 2.5:** A cross-section of the steering rack suspended by the yoke and pinion [15]

### 2.2.2 Servo motor

The electric motor used in an EPAS system may be either a DC or an AC machine. One of the most influential motor parameters in steering dynamics is the rotational inertia. In rack-type EPAS systems, the motor is connected to the rack through a transmission with a high gear ratio. Because of this large reduction ratio, the motor itself does not need to produce very high torque directly, allowing the use of a relatively compact motor with lower physical inertia.
Although the motor inertia is physically small, the transmission ratio significantly magnifies its effect at the steering rack. When the rack accelerates, for example due to tyre forces transmitted through the tie rods, the motor must rotate much faster than the rack displacement because of the gear ratio. This results in a much larger effective inertial force acting on the rack side of the system. In other words, the gearing amplifies both the motor torque and the apparent inertia reflected to the rack.
The equivalent rack mass can be expressed as:

$$m_{R,\text{eqv}} = m_R + \left(\frac{J_M}{r_M^2}\right) \tag{2.1}$$

- $m_{R,\text{eqv}}$ = equivalent rack mass
- $m_R$ = physical rack mass
- $J_M$ = motor rotational inertia
- $r_M$ = effective motor radius

where the second term represents the reflected inertia of the motor. In practical EPAS systems, this reflected inertia can correspond to an equivalent mass of approximately 1500 kg, while the actual rack mass itself is only a few kilograms.

This large equivalent inertia introduces a low-pass filtering effect within the steering system. As a consequence, high-frequency force variations travelling through the rack are attenuated before reaching the driver. Rapid changes in tyre grip or small road disturbances therefore become less noticeable in the steering feel. Since the rack is the central element through which all steering forces are transmitted, this filtering effect has a considerable influence on road feedback and cannot be completely eliminated when using an electric motor-assisted steering system.

### 2.2.3 Torsion Bar

The torsion bar is one of the primary sensing elements in the EPAS system Fig 2.6, as it is used to measure the torque applied by the driver relative to the steering rack. The measured torque corresponds to the torque difference between the steering column and the sensor pinion. According to Newton's third law, an equal and opposite reaction torque is always present, meaning that the measured value may also contain feedback forces coming from the steering system and road interaction, not only the direct driver input.

Another factor affecting the measurement is that some torque can be lost between the steering wheel and the torsion bar due to friction, damping, and inertial effects within the steering column assembly.

The torsion bar measures torque by detecting the angular twist along its length. Since the torsion bar stiffness is known and calibrated, the applied torque can be estimated from this deformation. To achieve accurate torque measurement, the torsion bar must be sufficiently compliant so that measurable angular displacement occurs. However, this creates a trade-off, because a stiffer steering feel is generally preferred for improved driver feedback, while a softer torsion bar improves sensing resolution.

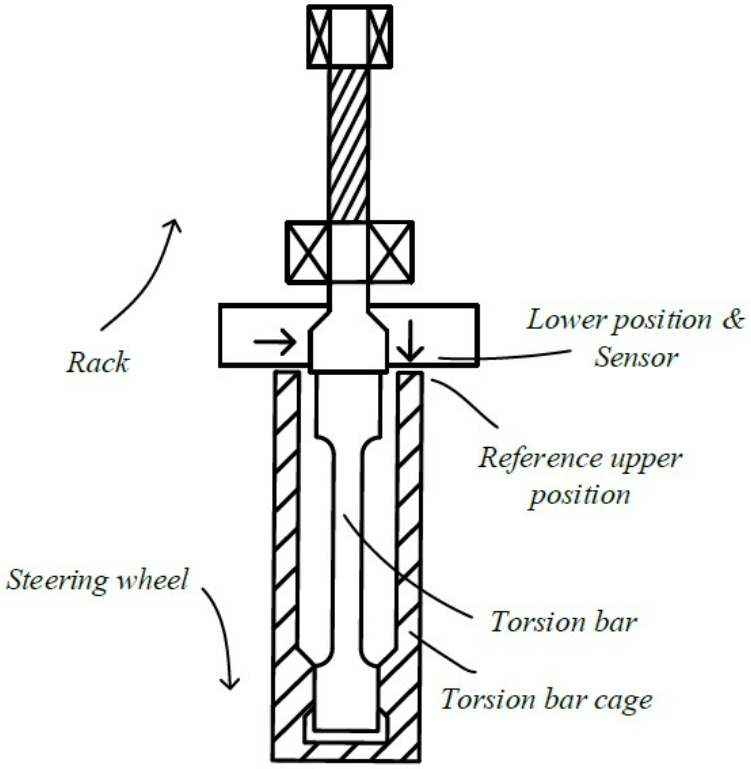



**Figure 2.6:** The torsion bar in a schematic image [15]

### 2.2.4 Mechanical Analysis

In the dual-pinion EPAS system, four main types of forces act on the steering rack at five different locations, as illustrated in Fig 2.7. These forces together determine the steering response, steering feel, and overall system dynamics.

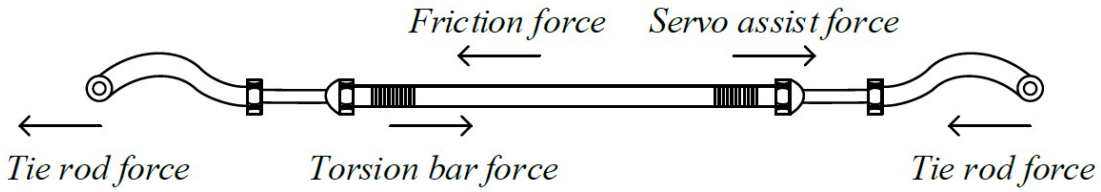



**Figure 2.7:** The rack with the main forces [15]

The first force originates from the torsion bar torque, or equivalently the torque acting at the sensor pinion. This torque is generated through the steering column and is not solely dependent on the driver input. Instead, it is the combined result of driver-applied torque, steering column friction, and inertial effects within the column assembly, as shown in Fig 2.8. Therefore, even when the driver releases the steering wheel, friction and inertia in the steering column can still produce a non-zero torque in the torsion bar depending on the dynamic state of the system.




**Figure 2.8:** Illustration of the torques on the steering column [15]

The second important force acting on the rack is generated by the motor pinion. Compared to the steering column side, the motor side dynamics are more complex due to the presence of additional transmission elements and the motor controller, as shown in Fig 2.9. The worm gear mechanism introduces additional friction, while the high gear ratio significantly affects the dynamics by amplifying the reflected motor inertia acting on the rack.

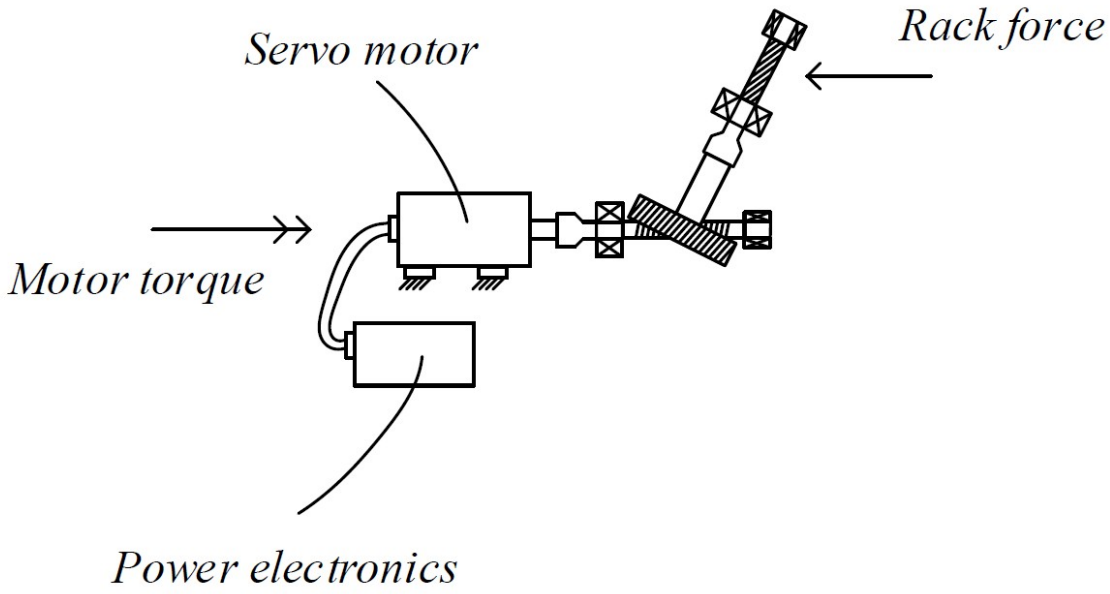



**Figure 2.9:** Torques and forces on the servo motor transmission [15]

The third major force comes from the interaction between the tires and the road surface, illustrated in Fig 2.10. During cornering, tire slip generates lateral tire forces that act on the wheel assembly. Because the wheels are constrained around the King Pin Axis (KPA), these forces create a resisting torque known as the aligning torque. This torque depends on the combined effect of caster trail and pneumatic trail, which together define the lever arm acting on the tie rod force. The resulting tie rod force is transmitted to the steering rack and generally opposes the forces produced by the sensor pinion and motor pinion. However, due to the large reflected inertia in EPAS systems, some of these road feedback forces are mechanically filtered before

reaching the driver, reducing the natural steering feel compared to conventional steering systems.

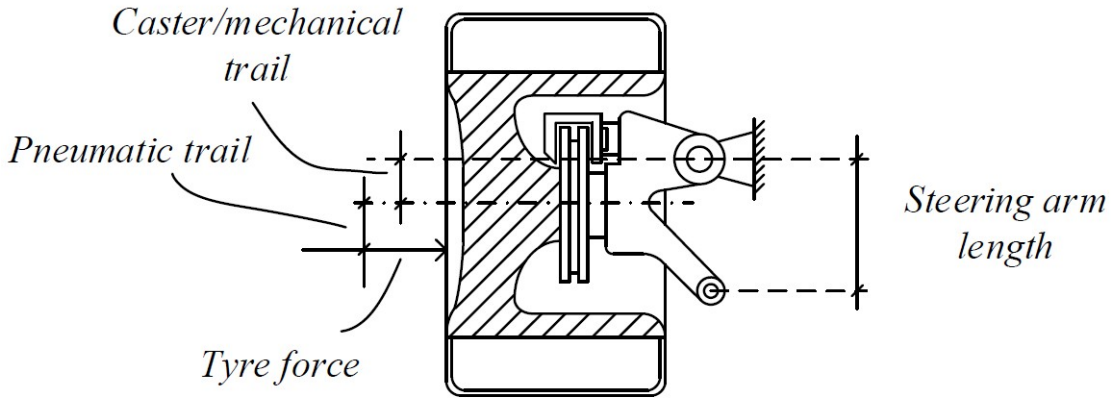



**Figure 2.10:** A top view of the suspension linkage and tire, showing levers and acting points of forces [15]

Friction forces also play an important role in EPAS dynamics. As mentioned earlier, the interaction between the rack and the yoke mechanism generates friction forces that influence both steering stability and steering feel. These friction forces always act opposite to the direction of motion and depend on both displacement and velocity of the moving surfaces. Although friction can help stabilize the steering system, excessive friction negatively affects steering smoothness and responsiveness. In practical EPAS systems, the relative velocities are generally low, meaning that large velocity-dependent friction effects are usually limited.

### 2.2.5 Steering system controller

The electric motor in an EPAS system provides the ability to actively control the steering assist force. This capability is essential for overcoming several challenges associated with electric power steering systems. While the motor itself introduces additional inertia into the steering mechanism, which can negatively affect steering response and road feedback, it also offers the means to compensate for these effects through appropriate control strategies.
By continuously adjusting the assist force based on the steering system state and vehicle operating conditions, the EPAS controller can improve steering stability, responsiveness, and driver comfort. As a result, modern EPAS systems rely heavily on advanced control algorithms to achieve the desired steering characteristics and ensure consistent performance under different driving conditions.
An important objective of these control strategies is to provide a realistic steering feel and road feel to the driver. Steering feel refers to the feedback and resistance perceived by the driver through the steering wheel during steering inputs, while road feel represents the information transmitted from the tyre-road interaction back to the driver. Together, these characteristics form a critical part of the driver's feedback loop, helping the driver assess vehicle behaviour and maintain control.

Without sufficient steering and road feel, the driver's ability to accurately judge vehicle response and road conditions may be reduced, potentially affecting both driving confidence and safety.

#### 2.2.5.1 Steering feel

Steering feel is defined as the relationship between steering wheel torque (SWT) and steering wheel angle (SWA). The most important region is the on-centre area, where the initial torque build-up strongly influences the driver's perception of steering precision and vehicle stability. In modern EPS systems, steering feel is primarily shaped by the boost curve, which determine the amount of motor assistance provided for a given driver input torque. An ideal boost curve should be nonlinear, providing limited assistance around the steering centre to preserve road feedback, followed by a progressive increase in assist torque and a smooth saturation at higher steering torques. Based on this principle, the boost curve developed in this thesis incorporates a dead-zone, nonlinear torque build-up, and saturation characteristics to achieve improved on-centre feel, realistic steering response, and reduced driver effort [31].

#### 2.2.5.2 Road feel

Road feel refers to the steering system's ability to transmit information about road conditions and tyre behaviour back to the driver. It is commonly characterized by the relationship between steering wheel torque (SWT) and vehicle lateral acceleration. Since lateral acceleration is closely related to the lateral forces generated by the tyres, the driver can use the feedback received through the steering wheel, together with the vehicle motion felt through the body, to assess road grip and vehicle stability. As the vehicle approaches its handling limits during cornering, the steering feedback torque should decrease, indicating a reduction in the front tyre's ability to generate additional lateral force. Achieving good road feel often requires a balance with steering feel, as increasing road feedback can improve vehicle responsiveness and initial yaw response, but may negatively affect the desired torque build-up characteristics around the steering centre.

#### 2.2.5.3 Implementation

To achieve the desired steering feel and road feel, significant research has been conducted on the development of reference generation methods for Electric Power Steering systems. Since the driver directly interacts with the steering wheel through two primary variables, steering wheel angle (SWA) and steering wheel torque (SWT), one of these variables is typically used as the controller input while the other is generated as the feedback response. In this way, the controller determines the desired steering behaviour by establishing a relationship between SWA and SWT.

One commonly used approach is based on a virtual rack model. In this method, a virtual steering rack with relatively low inertia is created, and all forces acting on the physical rack are estimated and applied to the virtual system. The actual rack is

then controlled to follow the states of the virtual rack by minimizing the difference between the two systems, a technique known as model-following control. This approach is widely used in automotive steering applications. The virtual rack concept effectively acts as a steering wheel torque reference generator, where the measured steering wheel torque and estimated rack forces are used to determine the desired steering response. By reducing the apparent system inertia, the method improves steering responsiveness and steering feel. However, if not carefully designed, the increased responsiveness can also introduce stability challenges within the steering system.

# 3

# Methodology

## 3.1 Modelling

The R-EPAS model was developed using MATLAB/Simulink, which provides a flexible environment for modelling dynamic systems and implementing control algorithms. When using Simulink, special attention must be given to signal definitions and units, since the software does not automatically verify the physical consistency of the signals. For example, multiplying a force by a distance physically results in a torque, but in Simulink the resulting signal is simply treated as another numerical value unless the user explicitly keeps track of its physical meaning and units.Furthermore, Simulink does not inherently distinguish between different types of physical quantities, such as mechanical forces, torques, or electrical signals. Therefore, maintaining a consistent representation of variables and their units throughout the model is essential to avoid modelling errors.Another important aspect of Simulink is that it is a causal modelling environment, meaning that information flows in a predefined direction through the model components. As a result, the system is represented using Ordinary Differential Equations (ODEs). This differs from modelling languages such as Modelica, which use an acausal approach based on Differential Algebraic Equations (DAEs) and allow physical interfaces to be defined directly without specifying signal causality [2].

The dynamic behaviour of the steering system is governed by the equations of motion, which form the foundation of the mechanical model [16] [15]. According to Newton's second law, the resultant force acting on a mass or rotational inertia produces its corresponding linear or angular acceleration. By integrating the acceleration over time, the velocity is obtained, and a second integration yields the position of the component.These positions are then used to determine the forces generated within the system. For example, the lateral tyre force primarily depends on the steering angle together with the current vehicle states, while the steering rack displacement influences the reaction forces acting on the rack. Similarly, friction forces are largely determined by the relative displacement and motion of the interacting components. In addition, component velocities give rise to damping forces, whereas accelerations are associated with inertial forces. Overall, the system states—namely position, velocity, and acceleration—are used to calculate the various mechanical response forces. These forces are subsequently applied to the equations of motion to determine the accelerations for the next simulation step.

This modeling approach effectively captures the key dynamic characteristics of the EPAS system, including the influence of torsion bar compliance, the effects of reflected motor inertia, and the performance of the steering control strategy following the structure as [15] [32].

### 3.1.1 Model Interface

In the present work, the steering wheel angle from the simulator is used as the input to the torsion-bar block in the vehicle model, while the steering wheel and column dynamics are excluded from that model. This simplification is made because the full vehicle model, including the individual subsystems for powertrain, brakes, steering, wheels, chassis, suspension, and axles, is exported as an FMU and executed in the main compiler software in a separete PC (SIMkernel). The steering wheel and column dynamics are instead represented in a separate Simulink file that runs in another PC (xPC), where the steering wheel angle is computed from the net torque acting on the steering system. This Simulink model includes the sensodrive motor, steering column friction, and damping, and calculates the steering wheel angle and angular velocity from the summed torques. Since these dynamics are already represented in the cabin-control model, they are not duplicated in the vehicle model.

The reason for having separate PCs is mainly computational efficiency, the Vehicle model in SIMkernel runs at 200 Hz and the xPC model runs at 1000 Hz. Therby, the blocks that mainly affect the driver feedback like the feedback torque and the friction are placed in the xPC model. Fig 3.1 shows the signal flow between the PCs.

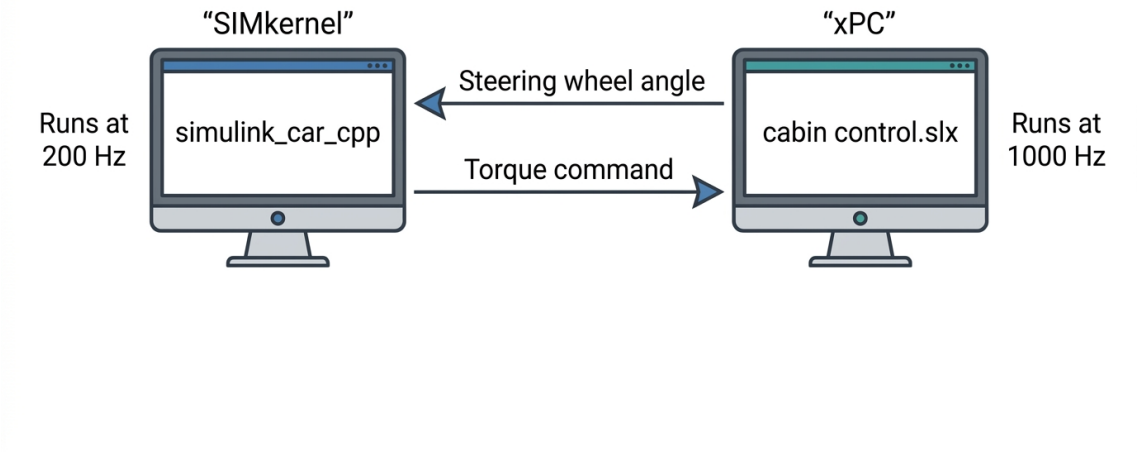



**Figure 3.1:** Schematic of Vehicle model and cabin control file running in different PCs and signal flow

On the rack side, the model still receives the rack force input from the vehicle side

and produces rack displacement as the dynamic response. Vehicle velocity is retained as an additional input to the controller, since assist, damping, and steering wheel return functions are velocity dependent.

### 3.1.2 Model Components

In the following section, the individual components of the steering system model are described together with the equations used to represent their near physical behavior. The Simulink layout of the main components and the controller block is shown in fig 3.2.

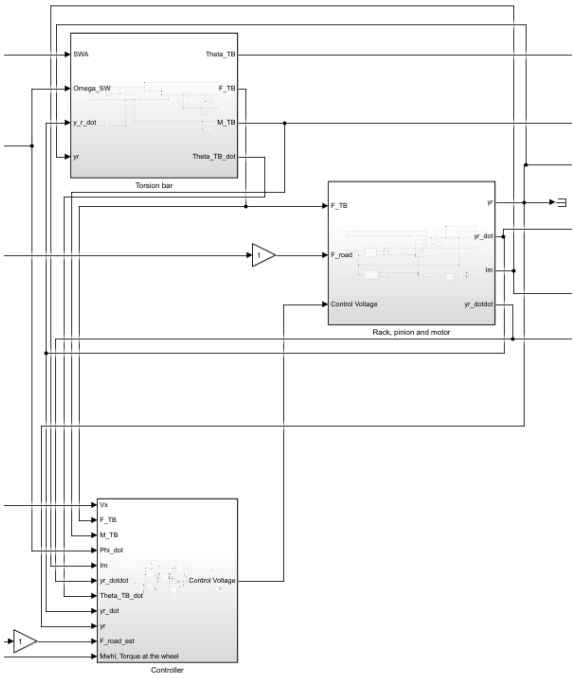



**Figure 3.2:** Block diagram of model components

#### 3.1.2.1 Steering wheel and column block

As mentioned before, the steering column inertia is already modeled in a separate simulink file that runs in the xPC. This block takes three inputs, the steering wheel angular velocity from the sensodrive motor ($\omega_{sw}$), the net model torque ($J.\dot{\omega}$) and an additional term to account for the eccentricity of the steering wheel during rotation ($T_{ecc}$). The driver torque is computed by subtracting the torques from the inertia term ($J.\dot{\omega}$). The feedback term ($T_{fbk}$) is the torsion bar torque coming from the Vehicle model.

$$T_{\text{ecc}} = -K \sin(\theta_{\text{sw}}) \tag{3.1}$$

$$T_{\text{net}} = J_{\text{sw}} \dot{\omega}_{\text{sw}} \tag{3.2}$$

$$T_{\text{net}} = T_{\text{fbk}} + T_{\text{driver}} + T_{\text{ecc}} + T_{\text{friction}} \tag{3.3}$$

The driver torque is estimated from the steering wheel angular velocity but is not used as a direct state in the vehicle steering model. The torque eccentricity is modeled as a sinusoidal function of steering wheel angle. A friction block (LuGre model), using angular velocity as input, is included to calculate the friction torque acting on the steering column, thereby creating a feedback loop within the cabin-side model. This driver torque equation is shown below.

$$T_{\text{driver}} = T_{\text{net}} - T_{\text{fbk}} - T_{\text{ecc}} - T_{\text{friction}} \tag{3.4}$$

#### 3.1.2.2 Torsion bar block

The torsion bar is modeled with the velocity and position at each end of it as inputs ($\theta_{sw}$ & $y_r/r_{tb}$) and the response torque ($M_{tb}$) and force ($F_{tb}$) on the rack as outputs. The steering wheel rotational velocity and position comes directly from the xPC file, and for the rack side it is given as a function of rack displacement and velocity . The steering wheel angular rate minus the rack side velocity gives the rate of twist of the torsion bar as in eq 3.6. Similarly, the twist of the torsion bar was obtained from the difference between the steering wheel angle and the rack side twist (eq 3.5).

$$\tau_{tb} = \theta_{SW} - \frac{y_r}{r_{tb}} \tag{3.5}$$

$$\dot{\tau}_{tb} = \dot{\theta}_{SW} - \frac{\dot{y}_r}{r_{tb}} \tag{3.6}$$

Normally, the torsion bar is modeled as a spring and damper system, where the damping term depends on the rate of change of deformation. The spring force component is the governed by the deformation of the torsion bar. As the torsion bar acts as a sensor which can be used to build the steering functions, the outputs from it will be used in several other blocks of the steering system (especially in the Controller block). The net force generated by the torsion bar is the sum of forces due to the stiffness and damping components (eq 3.15)

$$F_{tb} = \frac{M_{tb}}{r_{tb}} = \frac{K_{tb}\tau_{tb} + C_{tb}\dot{\tau}_{tb}}{r_{tb}} \tag{3.7}$$

#### 3.1.2.3 Rack and motor block

The rack and motor assembly is modeled as a translational inertial system similar to the steering column with the addition of an extra force in the governing equation of motion. This extra force is due to the addition of the motor block which takes voltage from the controller as input.

The inputs for this block are the tie rod (road) forces ($F_{road}$), the rack force from the torsion bar ($F_{tb}$) and the control voltage from the controller ($V_m$) which results

in the motor assist force generated ($F_m$). The rack motion is written as the sum of the two input forces (Torsion bar force, tie rod force), the motor force and the friction force on the rack divided by the equivalent rack mass as in eq 3.8.

$$\ddot{y}_r = \frac{\frac{M_{tb}}{r_{tb}} + F_{road} + F_{motor} - F_{fric,r}}{m_r + \left(\frac{J_m}{r_m^2}\right)} \tag{3.8}$$

$$y_r = \int \dot{y}_r = \int\int \ddot{y}_r \tag{3.9}$$

The term equivalent mass is used since the torsion bar and the motor have their own separate pinions attached to the rack, therefore there will be inertial effect of the motor added. The friction force (eq 3.10) is calculated in the same procedure as for the steering column friction block, here as a function of rack velocity ($\dot{y}_r$).

$$F_{fric,r} = \sigma_{0,rack} z + \sigma_{1,rack} \dot{z} + \sigma_{2,rack} \dot{y}_r \tag{3.10}$$

The assist motor force is modeled as an electric RL circuit which outputs electric current which is then used to compute the motor force while it could have been modeled as a PMSM with its own FOC [38], due to the simplicity and source to motor parameters [15]. The model is given by the sum of voltages coming from; the control voltage, the back EMF and the voltage loss due to circuit resistance. The back EMF is a loss in voltage to the circuit based on the motor velocity, similar to a linear drag loss. The net voltage divided by the motor inductance gives the rate of change in motor current which is integrated to get the current.

$$\dot{i}_m = \frac{V_m - K_e \frac{\dot{y}_r}{r_m} - i_m R_m}{L_m} \tag{3.11}$$

The current at any instant multiplied by the motor torque coefficient gives the torque supplied by the motor.

$$T_m = i_m K_t = \int \dot{i}_m K_t \tag{3.12}$$

This torque is multiplied by the motor effective transmission ratio giving the force on the rack induced by the assist motor.

$$F_{motor} = \frac{T_m}{r_m} \tag{3.13}$$

The net force (sum of all four forces) is divided by the rack equivalent mass to get the rack acceleration which is the output signal which can be integrated to obtain the velocity and displacement. This mass is given by Eq 2.1, derived using the relationship of the gear ratio effect on the motor inertia. The rack velocity is used to determine the motor speed which is used for computing the back EMF during the next time instant in the simulation loop.

The tie rod forces that are generated by the tires are modeled as a function the self aligning torque produced (eq 3.14).

$$F_{road} = -\frac{M_Z}{SAL} \tag{3.14}$$

Here SAL is a scaling term used to convert the moment to translational force acting on the rack, it is written as,

$$SAL = r_{tb}.SG_{ratio} \tag{3.15}$$

#### 3.1.2.4 Friction block

The friction block was developed based on the equations given by [27]. The friction block models the resisting torque generated by the steering system due to contact between moving surfaces. The friction torque used in this model block is based on the LuGre friction model, which describes friction through the deformation of microscopic bristles at the contact interface as in fig 3.3. In this model, the bristles behave like elastic elements with their own stiffness that deform as motion begins, allowing the friction torque to build up gradually instead of switching instantaneously to a constant value (Coulomb friction). This makes the model well suited for capturing both pre-sliding behavior and the transition to pure sliding.

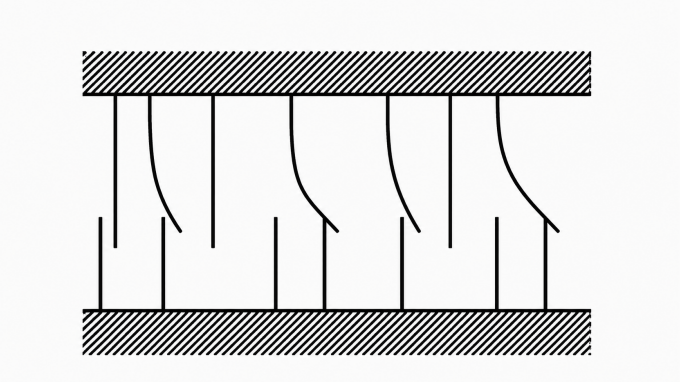


**Figure 3.3:** Bristle contact interface between two surfaces. Bristles on the lower part are shown as rigid for simplicity

The LuGre model uses an internal state ($z$) to represent the average bristle deflection. This state evolves according to the relative velocity and a velocity-dependent function that determines how quickly the bristles deform and how large the friction level becomes. At low speeds, the model reproduces the increase in friction associated with sticking and micro-slip, while at higher speeds it converges toward the sliding friction level. In this way, the model captures the Stribeck effect, static friction, and viscous friction within one continuous formulation.

$$\dot{z} = v - \frac{|v|\sigma_0}{g(v)}z \tag{3.16}$$

$$g(v) = T_c + (T_s - T_c)\, e^{-\left(\frac{v}{v_s}\right)^2} \tag{3.17}$$

The friction force or torque is then computed from the bristle deflection state, its rate of change, and a viscous term (eq 3.18). The elastic part represents the stored deformation in the contact, the damping part accounts for energy dissipation during bristle motion, and the viscous term models speed-dependent energy losses. If the motion reverses direction, the bristle deflection must first unwind (change direction or sign) before the friction torque changes sign.

$$T_f = \sigma_0 z + \sigma_1 \dot{z} + \sigma_2 v \tag{3.18}$$

Since the LuGre friction block includes an internal bristle deflection state that provides memory of past motion, this allows the model to reproduce hysteresis and reversal effects without the need for any logical operations or reference point as mentioned by [27].

### 3.1.3 Steering Functions and Controller design

The steering functions are modeled inside the controller block in fig 3.2. The following figure 3.4 shows the block diagram layout of the individual steering functions and controller implemented in Simulink.

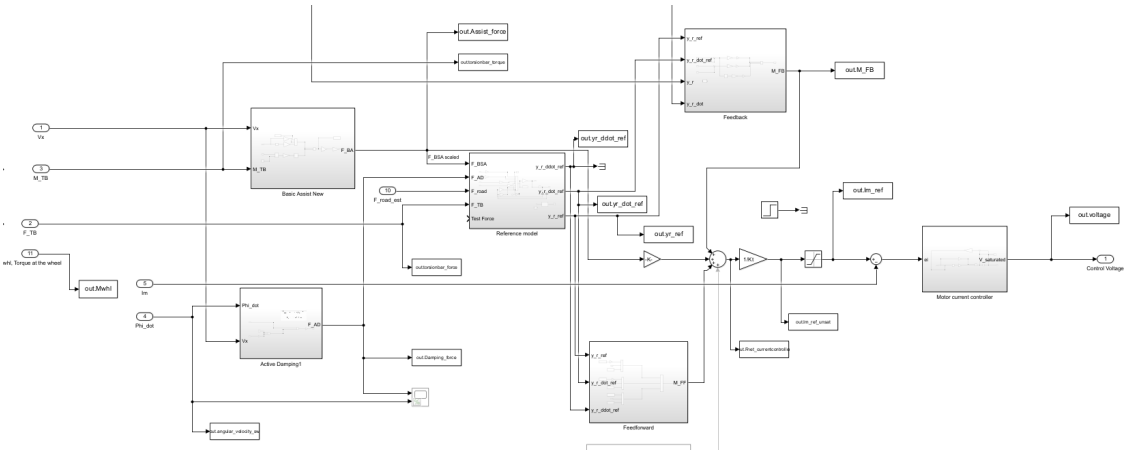



**Figure 3.4:** Steering control functions inside the controller block

#### 3.1.3.1 Motor Assist function

The Motor Assist function is basically a simple replication traditional boost-curve. This means that an assist force is generated as a function of the torsion bar torque which is a result of torsion bar deformation.

The assist force for this steering system is provided directly to the motor and it is also included in some other controller components. While for an HPAS system, the fluid pressure is altered via hydraulic valves and controlled through the steering ECU.

In the automotive industry, the assist force is usually obtained from some kind of lookup table which is speed and torsion bar torque dependent (High assist for low speeds and vice versa). Since there was no access to any form of lookup table, so this project had to rely on developing a assist curve profile from available literature [31] [33]through analytical equations (eq 3.19 & eq 3.20).

It was decided to model the assist torque map as a quadratic equation [31]. The choice of this approach is due to relatively lesser coefficients to tune compared to any complex formulation. The assist block outputs a torque that depends on both the torsion bar torque and the vehicle speed. The curve provides a nonlinear mapping from driver input to steering assistance, such that the level of assist increases with steering effort while remaining dependent on the driving condition. In this way, the steering system produces a speed-sensitive assist behavior that reflects the expected variation in steering feel across the operating range.To better represent the real steering feel, the curve also includes a dead band around zero torsion bar torque, where no assist is generated, and a torque saturation limit, which caps the maximum assist torque at higher inputs. The resulting assist torque (eq 3.19) is then converted into an equivalent force before being introduced into the reference model.

$$T_{BA}(v_x, T_{\text{tb}}) = k_v(v_x)\, k_g\, \tanh\left(\frac{k_a T_{\text{driver}}^3}{2}\right) \tag{3.19}$$

$$k_v(v_x) = k_{v1} v_x^2 + k_{v2} v_x + k_{v3} \tag{3.20}$$

The resulting assist profile generated is shown in the figure below,

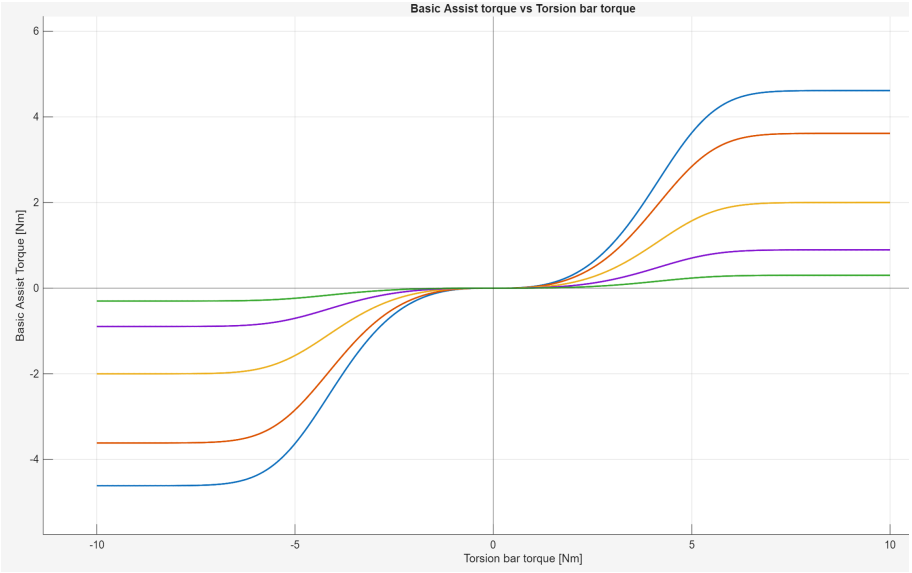



**Figure 3.5:** Assist Torque Map

#### 3.1.3.2 Reference model

As discussed earlier, the motor inertia is enlarged by the motor transmission giving a very high equivalent rack mass of approximately 1500 kg, the system needs a control strategy to compensate for this effect. This has been done by implementing a model follower strategy [15]. The plant (rack and motor) is set to follow the mechanical response of a reference model that has the wanted, apparent forces as inputs [32]. The estimated forces are applied to a fictitious mass that is set to a significantly lower value than the real equivalent mass. This mass value differs between different OEMs which makes them standout relatively and even in the steering modes offered in passenger cars this variable subject to change since its not a physical parameter.

The reference model computes the desired rack acceleration based on the net longitudinal force acting on the steering rack. The forces considered include the mechanical input from the torsion bar, the motor assist force, the opposing road reaction force, and damping force. By combining these contributions and dividing by the desired equivalent rack mass, the model generates the reference rack acceleration (eq 3.21), which is subsequently integrated to obtain the desired rack velocity and position. This mimics a virtual rack, that the real rack should follow.

$$\ddot{y}_{r,\text{ref}} = \frac{k_{tb}\frac{M_{tb}}{r_p} + k_{BA}\frac{M_{BA}}{r_m} - k_{\text{road}}F_{\text{road}} - k_{AD}F_{AD}}{m_{\text{desired}}} \tag{3.21}$$

This effectively lowers the inertia in the system as the real rack, ideally, moves as a light rack. The desired rack mass acts as a tuning parameter for inertia compensation, that is, a lower desired rack mass means a high inertia compensation. Inertia compensation is a term describing the method of lowering the effective inertia of the steering system by amplifying the rack movements using the servo motor power actively.

#### 3.1.3.3 Active Damping

The active damping function is introduced to improve steering stability and suppress unwanted steering oscillations induced by the inertia coming from the motor by generating a damping force proportional to the steering wheel angular velocity. This function is also essential for shaping the desired steering feel; in our case, the feedback torque applied to the sensodrive motor mimics the torsion bar torque. Due to a lack of resources (lookup tables), this function was designed only with respect to the steering wheel angular velocity but not the driver or torsion bar torque. If the torques were used, the function could be tuned to stabilize the system significantly during small driver inputs and to intervene less at higher steering wheel torques, thereby improving steering ability.

Unlike passive damping, the damping coefficient is varied as a function of vehicle speed (eq 3.22), allowing the steering system to provide greater damping at higher speeds while maintaining lighter steering effort at low speeds.

$$k_d(v_x) = k_{d0} + k_{dv} v_x \tag{3.22}$$

For the present work, a linear speed-dependent damping gain was selected due to its simplicity and ease of parameter tuning, which provided a satisfactory damping effect over the operating speed range taking the damping function from the old VM as reference for tuning [12]. The damping force is written as a function of the gain ($k_d$) and steering wheel angular velocity ($\dot{\theta}_{sw}$), see equation below,

$$F_{\mathrm{AD}} = -k_d(v_x)\,\dot{\theta}_{sw} \tag{3.23}$$

The damping force versus the steering wheel angular rate (input) is show in the figure below,

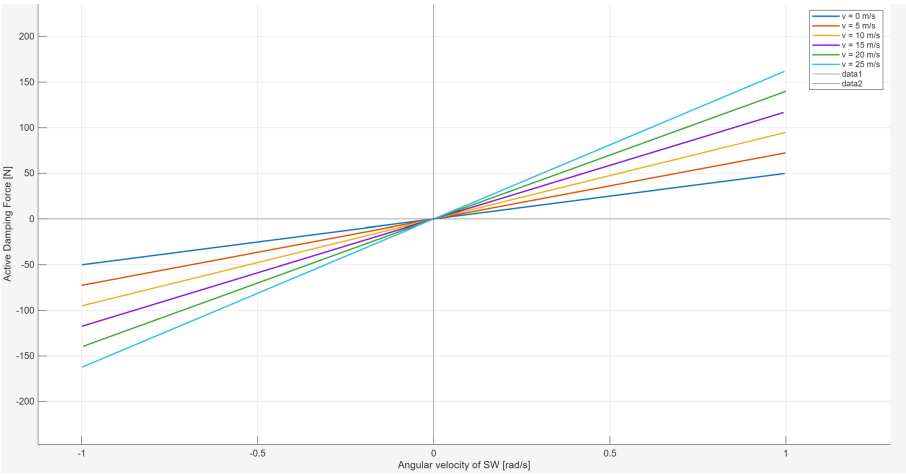



**Figure 3.6:** Plot of Damping force

#### 3.1.3.4 Feedback Control

The steering rack (plant) considered in this work exhibits nonlinear behavior due to effects of friction block, forces from the tires, and torsion bar. Therefore, for controller design, a local equivalent linear model was planned to be used since the main control objective is tracking around a nominal operating region rather than global stabilization of the full nonlinear plant due to time restrictions. The controller design used follows a model-based strategy in which the nonlinear rack dynamics are approximated by a second-order linear system identified from time-domain excitation (force from the motor) isolating effects of other inputs (friction and tire), and the resulting model is then used for analytical PID gain derivation.

The nonlinear steering rack is approximated by a mass–spring–damper model of the form

$$m\ddot{x}(t) + c\dot{x}(t) + kx(t) = \frac{M_{\text{mot}}(t)}{r_m} \tag{3.24}$$

where $x(t)$ is the rack displacement, $m$ is the equivalent mass, $c$ is the equivalent damping coefficient, $k$ is the equivalent stiffness, $M_{\text{mot}}(t)$ is the motor torque, and $r_m$ is the effective motor transmission radius. This structure is appropriate because the dominant local dynamics can be represented by inertia, dissipation, and restoring effects.

The plant parameters m, c, and k are identified from the plant response using step and pulse excitations. Step inputs are useful for exposing the transient and steady-state response, while pulse-like excitations reveal short-time inertial and damping characteristics. The equivalent parameter set was identified from the applied force input and measured rack displacement response by constructing a regression matrix and estimating the mass, damping, and stiffness coefficients using least-squares fitting.

Under zero initial conditions, taking the laplace transform of the identified local plant becomes

$$(ms^2 + cs + k)X(s) = \frac{1}{r_m} M_{\text{mot}}(s) \tag{3.25}$$

The transfer function of the equivalent linear plant is

$$G(s) = \frac{X(s)}{M_{\text{mot}}(s)} = \frac{1}{r_m(ms^2 + cs + k)} \tag{3.26}$$

A parallel-form PID controller is selected due to its simplicity [4]. The controller structure written in the laplace domain is

$$C(s) = \frac{K_d s^2 + K_p s + K_i}{s} \tag{3.27}$$

where $K_p$, $K_i$, and $K_d$ are the proportional, integral, and derivative gains, respectively.

The proportional term shapes the effective stiffness of the closed-loop system, the derivative term adds damping and suppresses oscillations, and the integral term removes steady-state offset.

The tracking error is defined as

$$e(t) = y_{\text{ref}}(t) - y_r(t) \tag{3.28}$$

where $y_{\text{ref}}(t)$ is the rack position reference coming from the reference block. The

corresponding control law in the time domain is

$$M_{\text{mot}}(t) = K_p e(t) + K_i \int_0^t e(\tau)\, d\tau + K_d \frac{de(t)}{dt} \tag{3.29}$$

For a unity-feedback configuration, the closed-loop transfer function is

$$T(s) = \frac{C(s)G(s)}{1 + C(s)G(s)} \tag{3.30}$$

and the closed-loop characteristic equation is

$$1 + C(s)G(s) = 0 \tag{3.31}$$

Substituting the plant and controller expressions into the characteristic equation yields

$$1 + \left(\frac{K_d s^2 + K_p s + K_i}{s}\right)\left(\frac{1}{r_m(ms^2 + cs + k)}\right) = 0 \tag{3.32}$$

After expanding the equation, collecting terms in powers of $s$, and normalizing, the closed-loop characteristic polynomial becomes

$$s^3 + \frac{r_m c + K_d}{r_m m} s^2 + \frac{r_m k + K_p}{r_m m} s + \frac{K_i}{r_m m} = 0 \tag{3.33}$$

To impose the closed-loop dynamics, a third-order target polynomial is defined as the product of a dominant second-order term and an additional real pole:

$$P_d(s) = (s^2 + 2\zeta\omega_n s + \omega_n^2)(s + \alpha) \tag{3.34}$$

where $\zeta$ is the desired damping ratio, $\omega_n$ is the desired natural frequency, and $\alpha$ is the location of the additional real pole.

Expanding the desired polynomial gives

$$P_d(s) = s^3 + (\alpha + 2\zeta\omega_n)s^2 + (\omega_n^2 + 2\zeta\omega_n\alpha)s + \omega_n^2\alpha \tag{3.35}$$

The actual closed-loop polynomial is now matched to the desired polynomial by equating coefficients of equal powers of $s$:

$$\frac{r_m c + K_d}{r_m m} = \alpha + 2\zeta\omega_n \tag{3.36}$$

$$\frac{r_m k + K_p}{r_m m} = \omega_n^2 + 2\zeta\omega_n\alpha \tag{3.37}$$

$$\frac{K_i}{r_m m} = \omega_n^2\alpha \tag{3.38}$$

Solving the above three equations gives the final PID gains for the controller whose output is motor torque $M_{\text{mot}}$ are

$$K_p = r_m \left[m(\omega_n^2 + 2\zeta\omega_n\alpha) - k\right] \tag{3.39}$$

$$K_i = r_m m\omega_n^2\alpha \tag{3.40}$$

$$K_d = r_m \left[m(\alpha + 2\zeta\omega_n) - c\right] \tag{3.41}$$

It should be noted that the controller uses fixed parameters. So, it cant be guaranteed that the controller will perform well over a global operating range. To improve the performance of the controller, these parameters could be given dynamic values (Gain Scheduling) to give a more flexible system behavior regarding responsiveness and stability.

#### 3.1.3.5 Feedforward control

The feedforward term was derived from the identified equivalent rack model in order to improve nominal tracking performance while minimizing the effort of the PID control on compensating for the errors. The feedforward block calculates the torque needed to achieve the reference values, given by the virtual model, with the real rack and sends this torque directly to the torque summation. The purpose of this method is to directly achieve reference translations that is close to the reference value.

Using the identified linear rack model, the equation fo the torque command is written as,

$$m_{eq}\ddot{y}_r + b_{eq}\dot{y}_r + c_{eq}y_r = i_{mot}M_{mot} \tag{3.42}$$

Solving the nominal model for the motor torque (Feedforward torque term) yields an inverse-dynamics feedforward equation of the form

$$M_{FF} = \alpha_{mot}\frac{m_{eq}}{i_{mot}}\ddot{y}_{r,\text{ref}} + \alpha_v\frac{b_{eq}}{i_{mot}}\dot{y}_{r,\text{ref}} + \alpha_x\frac{c_{eq}}{i_{mot}}y_{r,\text{ref}} \tag{3.43}$$

where $\alpha_a$, $\alpha_v$, $\alpha_x$ are the scaling terms (either 1 or 0) which is used to eliminate the contribution of the reference terms and $y_{r,\text{ref}}$, $\dot{y}_{r,\text{ref}}$, and $\ddot{y}_{r,\text{ref}}$ are the reference displacement, reference velocity, and reference acceleration, respectively.

Although the feedforward block was structurally consistent with the identified local model, it was not fully retained in the final implementation. The primary reason is that inversion-based feedforward performance depends strongly on the fidelity of the inverse model [15] and on the availability of reliable reference derivatives, which was the reason for using the scaling terms. Since it was previously explained that the steering rack exhibits nonlinear and operating-point-dependent behavior, and therefore the benefit of nominal inverse compensation was expected to be limited when compared with the effect of the feedback-based design alone.

For this reason, in the final controller implementation, the feedforward torque command including only the reference velocity and displacement was implemented because the acceleration term is prone to induce instability as mentioned in (Reference). The effect of the feedforward block on reducing the effort of the feedback block was not investigated in detail due to time restraints.

#### 3.1.3.6 Active Return

An active return function was introduced to assist the steering system in returning the steering wheel in the simulator toward its centered position when the driver was no longer applying a significant steering torque. The purpose of this function was to improve self-centering behavior which only from the aligning torque from the tires on the knuckle giving the tie rod forces is expected not enough to bring the steering back to center sufficiently, when driving in low speeds. Active return functions largely affect the steering feel and it is therefore important to tune the characteristics of it [15].

When at low steering wheel torques, the function adds a resisting torque bringing the steering wheel back to zero angle. The function is active the driver is effectively not demanding steering torque and when the rack is sufficiently displaced from the center. This prevents the return function from counteracting intentional driver input and making the controller end up in equilibrium off-centre while still providing a controlled self-centering action when the steering wheel is released.

The function contribution is applied conditionally as

$$M_{\text{active return}} = \begin{cases} M_{AR}, & \text{enable}_{AR} = 1 \\ 0, & \text{enable}_{AR} = 0 \end{cases} \tag{3.44}$$

$$\text{enable}_{AR} = (|M_{tb}| < M_{tb,\text{th}}) \ \wedge \ (|y_r| > y_{\text{th}}) \tag{3.45}$$

where $M_{tb}$ is the torsion bar torque (computed in the model), $M_{tb,\text{th}}$ is the predefined torque threshold, $y_r$ is the rack displacement, and $y_{\text{th}}$ is the displacement threshold beyond which active return is allowed to act.

When the active return function is enabled, a return torque should be generated,

$$F_{AR} = -k_{AR}(v_x)\, y_r - d_{AR}(v_x)\, \dot{y}_r \tag{3.46}$$

$$M_{AR} = r_{mot}\, F_{AR} \tag{3.47}$$

where $k_{AR}(v_x)$ and $d_{AR}(v_x)$ are speed-dependent gain functions and $v_x$ denotes vehicle longitudinal speed.

The first term in the force equation acts as a virtual spring, generating a restoring torque proportional to rack displacement. The second term acts as a virtual damper, opposing rack velocity in order to reduce overshoot and suppress oscillatory return behavior.

After implementing the model in the simulator, it was noticed that the effect of the tie-rod forces resulted in good self centering behavior. Due to that, the active return function was removed from the final implementation as it resulted in too fast return which compromised the realism in the simulator. This could have been due to incorrect tuning of the function, this could be improved later in the future so that there will be a function which assists in natural return behavior as a function of speed and driver torque input.

The flow chart diagram of the R-EPAS subsystem is shown in the below fig 3.7

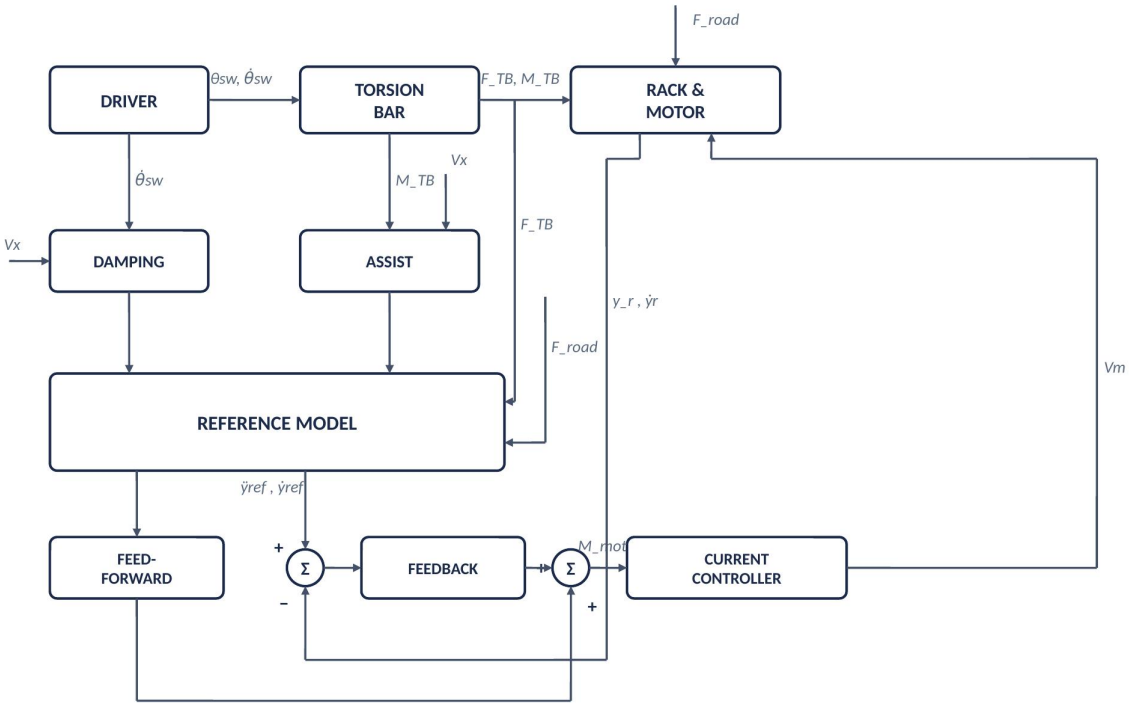



**Figure 3.7:** Flow chart of the R-EPAS sub systems

## 3.2 Simulation

During the development of the R-EPAS model, simulations were carried out continuously to evaluate the behaviour of the system and support the modelling process. These simulations played an essential role in identifying modelling errors, validating subsystem interactions, and debugging the implementation as new components were added. Regular simulation of the intermediate model allowed issues to be detected and corrected at an early stage, making the development process more efficient. To verify the correctness of the developed model, its response was compared with that of an existing benchmark steering model. The differences between the two models were analysed to assess the validity of the implemented steering dynamics and control strategy. Throughout the project, the majority of simulation activities were dedicated to model development, parameter tuning, and troubleshooting rather than final performance evaluation. Only after the steering model reached a satisfactory level of maturity were simulations used to generate the final results and assess the steering characteristics of the developed R-EPAS system.

### 3.2.1 Simulation environment

The developed Rack-Assisted Electric Power Steering (R-EPAS) model was implemented and evaluated entirely in MATLAB/Simulink, which served as the primary simulation environment throughout this thesis. Simulink provides a convenient platform for modelling the steering system dynamics, implementing the control algo-

rithms, and analysing the interaction between the driver input and the steering mechanism. The R-EPAS model was integrated with the existing electric vehicle model. The primary inputs to the model are the steering wheel angle and the accelerator pedal position, which represent the driver's steering and powertrain commands, respectively. The steering wheel angle determines the driver steering demand, while the accelerator pedal input influences the vehicle speed, which is subsequently used by the EPAS controller to generate speed-dependent steering assistance. During the development process, simulations (using simple inputs like Sine wave, Pulse input, etc) were performed repeatedly to verify the mathematical model, tune the controller parameters, and evaluate the steering system behaviour under different operating conditions.

Various steering manoeuvres were simulated after collecting data from vehicle tests to analyse the steering wheel reaction torque, rack displacement, motor assist torque, and overall steering response with refrence to the old steereing model (HPAS). The simulation results were used to refine the model and ensure stable and realistic steering behaviour before performing the final performance evaluation. The model parameters are derived from relevant vehicle data and design documentation and available literature. These include the vehicle mass, centre of gravity location, and overall geometric dimensions, as well as the parameters of the steering model.

## 3.3 Steering wheel angle estimation

One of the main challenges faced during this project was to obtain vehicle data to tune the vehicle model. A major limitation was the lack of access to the vehicle CAN bus, which prevented direct acquisition of steering-related signals. Consequently, the steering input and other signals had to be measured using external sensors, as discussed in Chapter 4.

In theory, the steering subsystem could be driven by either steering torque or steering angle. Measuring torque would have required a custom steering-wheel attachment equipped with a strain gauge, where wheel twist would be converted into an voltage signal (due to strain generated) during steering motion. However, this approach was difficult to realize experimentally and would have required a more complex design for mountings and data acquisition setup was hard to explore. In addition, vehicle insurance restrictions made such a modification impractical.Due to these reasons, measuring vehicle data through externally mounted sensors was necessary [29].

Finally, the steering wheel angle was estimated using MuSe V3 inertial measurement unit (IMU) mounted on the steering wheel [7], while avoiding any interference with the driver or the airbag system. The IMU, together with the RT3000 inertial navigation system [6], was used to estimate the steering wheel angle because the estimation accuracy in current industry grade sensors are high [28].

### 3.3.1 Theory

An inertial measurement unit, or IMU, is an electronic sensor module used to measure the motion and orientation of a body to which it is attached. Generally, an IMU contains three orthogonal accelerometers and gyroscopes, some even have their dedicated internal clock so that the measurements can be sampled and time stamped consistently.

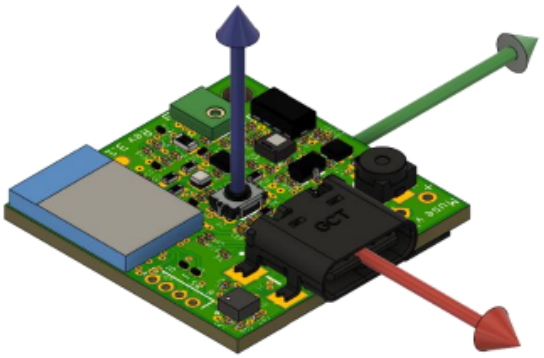


**Figure 3.8:** Schematic of the axes marked in an IMU

The accelerometer measures specific force along its three sensor axes, meaning it responds to both linear acceleration and the effect of gravity. Physically, accelerometers sense the motion of a small internal proof mass, and the resulting displacement or force is converted into an electrical signal that represents acceleration along each axis. The gyroscope measures angular velocity about the three sensor axes, typically by sensing the motion of a vibrating internal mass under Coriolis forces, which allows rotational motion to be inferred. Together, these sensors provide complementary information: the accelerometer is useful for identifying the gravity direction in static or low-dynamic conditions, while the gyroscope captures rapid rotational motion.

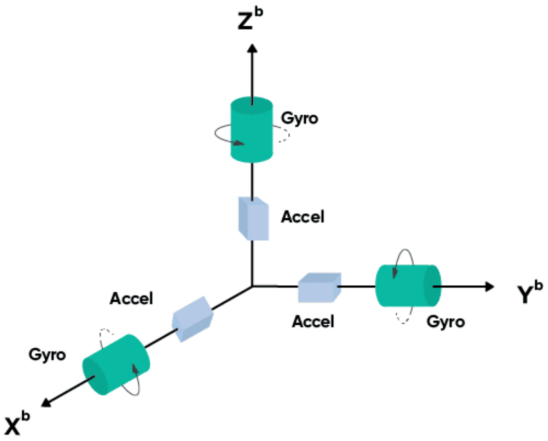



**Figure 3.9:** Schematic of accelerometers and gyroscopes in an IMU

In this work, the most relevant outputs were the accelerometer and gyroscope signals, and the timestamps, because these formed the basis for steering-angle estimation and synchronization between the steering-wheel sensor and the vehicle-mounted RT3000 system.

The steering-angle estimation process in this work was based on inertial measurements from two systems: an IMU mounted on the steering wheel (on the wheel grip) and an RT3000 inertial navigation system mounted on the vehicle body (under the front passenger seat). Under static conditions, the steering-wheel IMU accelerometer is dominated by gravity, which makes it possible to estimate initial inclination angles such as roll and pitch relative to the local level frame. However, accelerometers alone cannot determine yaw, since gravity provides no heading reference. Figure 3.6 shows a illustration on how the sensors were mounted in the vehicle.

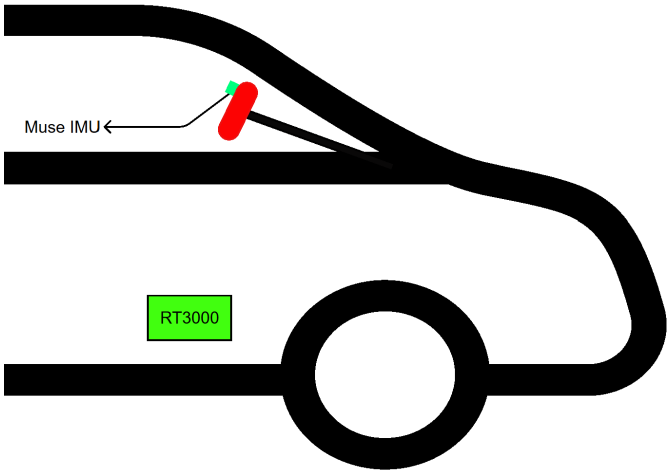



**Figure 3.10:** Schematic of IMUs mounted on the vehicle

The main challenge in this estimation process is the steering-wheel IMU does not measure steering motion in isolation. Because the sensor is rigidly attached to the steering wheel, it is influenced not only by the driver's steering input but also by the motion of the entire vehicle body (during lateral maneuvers), including yaw, pitch and roll. This makes the measured inertial signals (by Muse IMU) a superposition of local steering-wheel motion and global vehicle-body motion. It becomes even more trickier because the steering wheel is mounted at an inclination relative to the vehicle frame, so body rotations do not appear on just one sensor axis but are projected across multiple IMU axes.

To address this, the RT3000 was used as a reference sensor for the vehicle-body dynamics. By expressing the steering-wheel IMU measurements and the RT3000 measurements in consistent coordinate frames, the contribution of vehicle-body motion can be estimated and removed from the steering-wheel IMU signals. This compensation step is central to the method, because it helps isolate the motion that is actually caused by steering-wheel rotation rather than by the vehicle moving as a whole.

A further practical issue is that inertial sensors are imperfect and subject to measurement errors. Accelerometers are affected by bias, misalignment, and noise, while gyroscopes are affected by bias, noise, and bias drift over time. So, the postprocessing step of the raw sensor data is crucial to avoid errors in the estimation procedure.

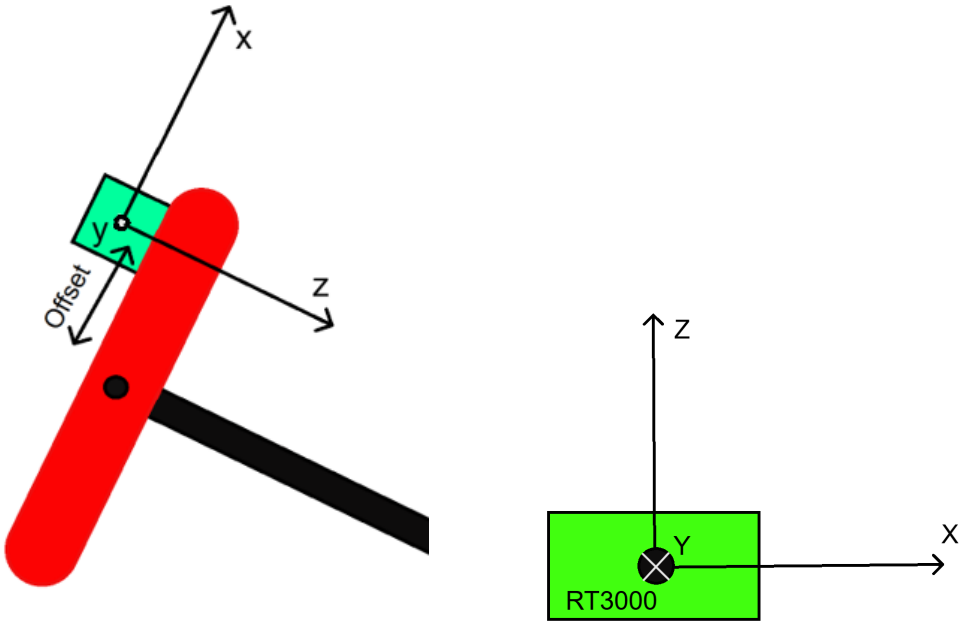
These effects are vital to notice because even a small gyroscope bias (For instance, 1 deg/s over 100 secs results in a angle drift of 100 degs) accumulates into a large angle drift after integration, and accelerometer disturbances during dynamic maneuvers can corrupt gravity-based orientation estimates.

Therefore, accurate steering-angle estimation depends not only on the inertial measurements themselves, but also on synchronization, frame alignment, compensation of vehicle-body motion, and mitigation of sensor errors before the final angle is estimated.

### 3.3.2 Method of Steering Wheel Angle Estimation

As discussed, the steering wheel angle was determined using a setup with two IMUs taking aid from previous research [30] where IMU was used to estimate the angle using Kalman filter architecture. The steering-wheel mounted IMU provided triaxial and angular rate and acceleration measurements in the local sensor frame (x, y, z) inclined onto the steering wheel plane, while the RT3000 provided vehicle-body angular rates and accelerations in its own frame (X, Y, Z) which is aligned with the vehicle reference frame ($X_v$, $Y_v$, $Z_v$). The estimation problem was formulated as a coordinate frame transformation (translation and rotation) and sensor-fusion task, in which the vehicle-body contribution measured by the RT3000 was projected onto the steering-wheel frame and subtracted from the wheel IMU measurements before

the final angle estimation.




**(a)** Axes of Muse IMU **(b)** Axes of RT3000

**Figure 3.11:** Orthogonal axes of IMU's marked.

#### 3.3.2.1 Coordinate Frame Definition and Rotation

The key step in the method is the definition of a zero-steering frame, denoted by $s_0$, whose axes coincide with the small IMU axes when the steering wheel is in the neutral position (Zero angle input). The RT3000 frame was defined such that $+X$ points toward the rear of the vehicle, $+Y$ points to the left, and $+Z$ points upward. Because the steering wheel is mounted with an inclination $\delta$ relative to the vehicle frame, its axes has to be related to the vehicle frame through a rotation matrix [17].

Using the known steering-wheel inclination angle $\delta$, the unit vectors of the zero-steering frame were written in vehicle-frame coordinates as

$$\mathbf{x}_{s_0}^{v} = \begin{bmatrix} \sin\delta \\ 0 \\ \cos\delta \end{bmatrix}, \qquad \mathbf{z}_{s_0}^{v} = \begin{bmatrix} \cos\delta \\ 0 \\ -\sin\delta \end{bmatrix}. \tag{3.48}$$

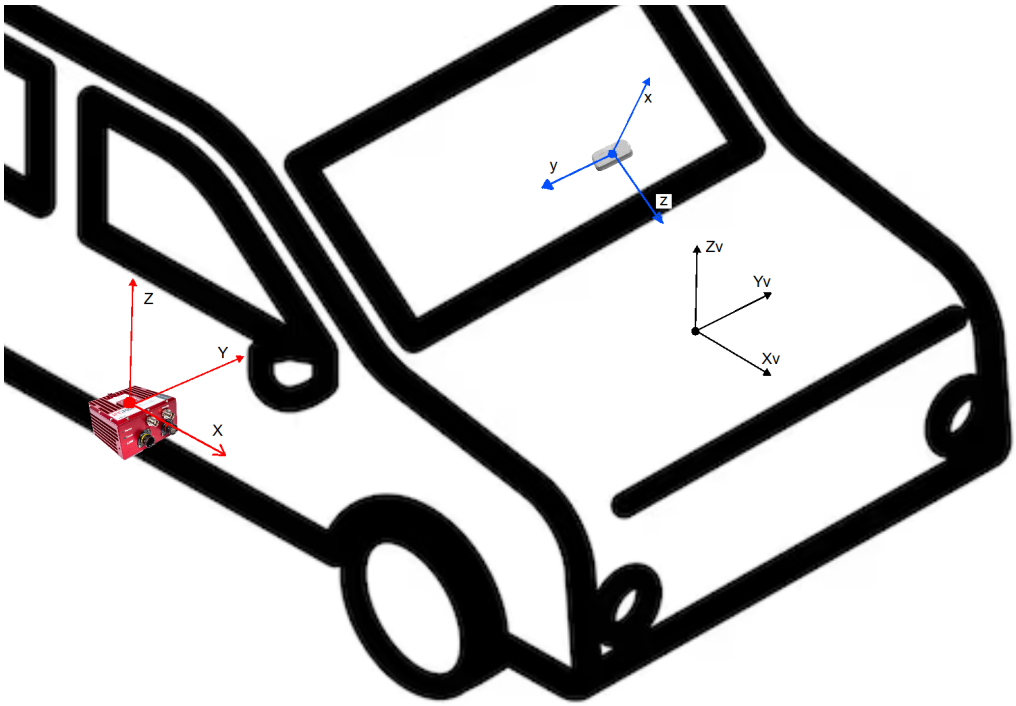



**Figure 3.12:** Coordinate frames of the IMUs and the vehicle

**NOTE :** The terms 'vehicle frame' and 'RT3000 frame' refer to the same physical reference frame, as the sensor is rigidly mounted parallel to the vehicle's principal geometry. However, they employ different coordinate axes; while they share the same longitudinal, lateral, and vertical orientations, their specific axis labels (X, Y, Z) and positive sign conventions differ.

To guarantee a valid, right-handed orthonormal basis and prevent an invalid reflection matrix (sign error in case the IMU was flipped), the third axis was computed via the cross product:

$$\mathbf{y}_{s_0}^{v} = \mathbf{z}_{s_0}^{v} \times \mathbf{x}_{s_0}^{v}. \tag{3.49}$$

The rotation matrix mapping vectors from the steering-wheel zero frame to the vehicle frame was formed by concatenating these vectors:

$$\mathbf{R}_{v}^{s_0} = \left[\mathbf{x}_{s_0}^{v} \quad \mathbf{y}_{s_0}^{v} \quad \mathbf{z}_{s_0}^{v}\right]. \tag{3.50}$$

As $\mathbf{R}_{v}^{s_0}$ is orthogonal, its inverse is simply its transpose. This means we can transform the rotation matrix to represent steering wheel frame to RT3000 frame and vice versa. The matrix used to project vehicle-frame quantities into the steering-wheel frame is therefore:

$$\mathbf{R}_{s_0}^{v} = (\mathbf{R}_{v}^{s_0})^{T}. \tag{3.51}$$

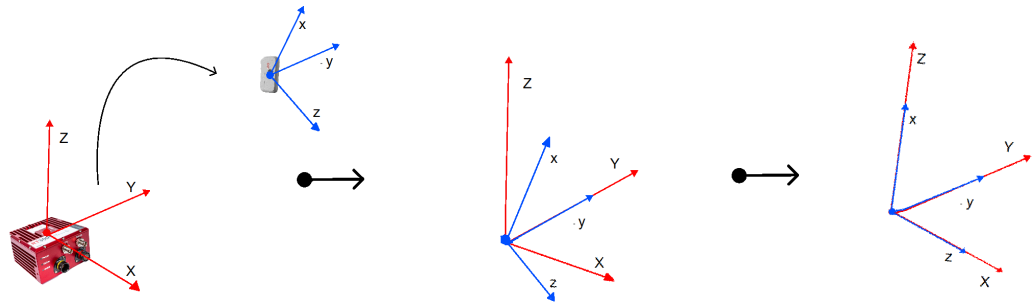



**Figure 3.13:** Schematic of coordinate frame translation and rotation onto steering wheel frame

It is also important to note that the translation of RT3000 measurements to the steering wheel is not discussed. This was because the RT3000 software (NAVsuite) [6] lets you configure the local points where you want the data to be translated (the user just has to input the x, y, z distances from the device to the point of interest). This is essential for the accelerometer data since its subject to change at different locations in the vehicle.

#### 3.3.2.2 Compensation of Vehicle-Body Motion

To isolate the motion of the steering wheel relative to the vehicle, the RT3000 acceleration $\mathbf{a}_{RT}^{v}$ and angular-rate $\boldsymbol{\omega}_{RT}^{v}$ vectors were projected into the zero-steering frame:

$$\mathbf{a}_{RT}^{s_0} = \mathbf{R}_{s_0}^{v}\mathbf{a}_{RT}^{v}, \qquad \boldsymbol{\omega}_{RT}^{s_0} = \mathbf{R}_{s_0}^{v}\boldsymbol{\omega}_{RT}^{v}. \tag{3.52}$$

With both sensing systems expressed in a consistent coordinate frame, the vehicle-body angular rate about the steering axis was subtracted from the bias-corrected steering-wheel IMU rate.

The compensated steering rate is:

$$\dot{\theta}_g(t) = \omega_{S,z}(t) - b_g - \omega_{RT,z}^{s_0}(t). \tag{3.53}$$

Here $\omega_{S,z}$ denotes the selected steering-axis gyroscope signal (axis of rotation) and $b_g$ denotes the estimated stationary gyroscope bias.

#### 3.3.2.3 Kinematic Offset Compensation

The IMU was mounted at a radial offset from the center of the steering column (defined by the vector $\boldsymbol{\rho}_s$). Thereby, rotation of the steering wheel will induce tangential and centripetal accelerations that contaminate the specific force measurement. These rotational accelerations were modeled as:

$$\mathbf{a}_{off} = \boldsymbol{\alpha} \times \boldsymbol{\rho}_s + \boldsymbol{\omega} \times (\boldsymbol{\omega} \times \boldsymbol{\rho}_s) \tag{3.54}$$

where $\boldsymbol{\omega}$ and $\boldsymbol{\alpha}$ are the angular velocity and angular acceleration about the steering axis, respectively. The measured small-IMU acceleration vector $\mathbf{a}_S^s$ was corrected to represent the center of rotation:

$$\mathbf{a}_{S,c}^s = \mathbf{a}_S^s - \mathbf{a}_{off}. \tag{3.55}$$

#### 3.3.2.4 Accelerometer-Based Angle Observation

A low-frequency observation of the steering angle was derived from the relative orientation between the projected RT3000 reference acceleration $\mathbf{a}_{RT}^{s_0}$ and the center-corrected IMU acceleration $\mathbf{a}_{S,c}^s$. Extracting the planar components orthogonal to the steering axis as $\mathbf{r} = [r_x, r_y]^T$ (reference) and $\mathbf{m} = [m_x, m_y]^T$ (measured), the raw geometric angle was computed using the planar dot and cross products:

$$\theta_a = \text{atan2}(r_x m_y - r_y m_x,\ r_x m_x + r_y m_y). \tag{3.56}$$

This signal, zero-referenced to a known initial state, serves as the absolute orientation reference to correct gyroscope drift over time.

#### 3.3.2.5 Confidence-Weighted Complementary Filter

The steering-wheel angle was estimated using a complementary-filter approach that combines low-frequency accelerometer information with high-frequency gyroscope information [39]. The compensated gyroscope signal provides the prediction step:

$$\theta_{pred}(k) = \theta_{est}(k-1) + \dot{\theta}_g(k)\Delta t. \tag{3.57}$$

The discrepancy between the accelerometer observation and the predicted angle generates an innovation term,

$$e(k) = \text{wrap}_{180}(\theta_a(k) - \theta_{pred}(k) \tag{3.58}$$

In standard complementary formulations, the correction gain is fixed. However, the reliability of the accelerometer-based orientation observation is highly transient and degrades during dynamic maneuvers (since the tests mainly consisted of lateral movements).
To address this, the base complementary gain is modulated by a time-varying confidence weight $w_{acc}(k) \in [0, 1]$, computed via a series of continuous soft-gating functions:

$$K(k) = \left(\frac{\Delta t}{\tau_{base} + \Delta t}\right) w_{acc}(k). \tag{3.59}$$

The soft-gating logic reduces $w_{acc}(k)$ toward zero under four specific conditions:

1. **Offset and Rate Limits:** If the estimated offset acceleration ($\mathbf{a}_{off}$) or the absolute steering rate ($\dot{\theta}_g$) exceeds predefined thresholds, indicating severe tangential/centripetal disturbances.
2. **Translational Disturbances:** If the magnitude mismatch between $\mathbf{a}_{S,c}^s$ and $\mathbf{a}_{RT}^{s_0}$ grows large, indicating uncompensated high-frequency vehicle vibrations or road impacts.

3. **Projection Stability:** If the planar magnitude of the reference vector approaches zero (e.g., extreme vehicle pitch), degrading the numerical conditioning of Equation 3.56.
4. **Innovation Outliers:** If the phase discrepancy $e(k)$ grows unphysically large within a single time step, indicating a potential physical shock.

The final estimate is updated by applying the adaptive gain to the innovation:

$$\theta_{est}(k) = \theta_{pred}(k) + K(k)e(k). \tag{3.60}$$

This structure ensures that during steady-state or slow-steering maneuvers, $w_{acc} \approx 1$, allowing the accelerometer to actively correct gyroscope drift. Conversely, during aggressive steering or harsh vehicle dynamics, $w_{acc} \to 0$, protecting the estimate from corrupted specific-force vectors and relying entirely on the transient response of the gyroscopes.

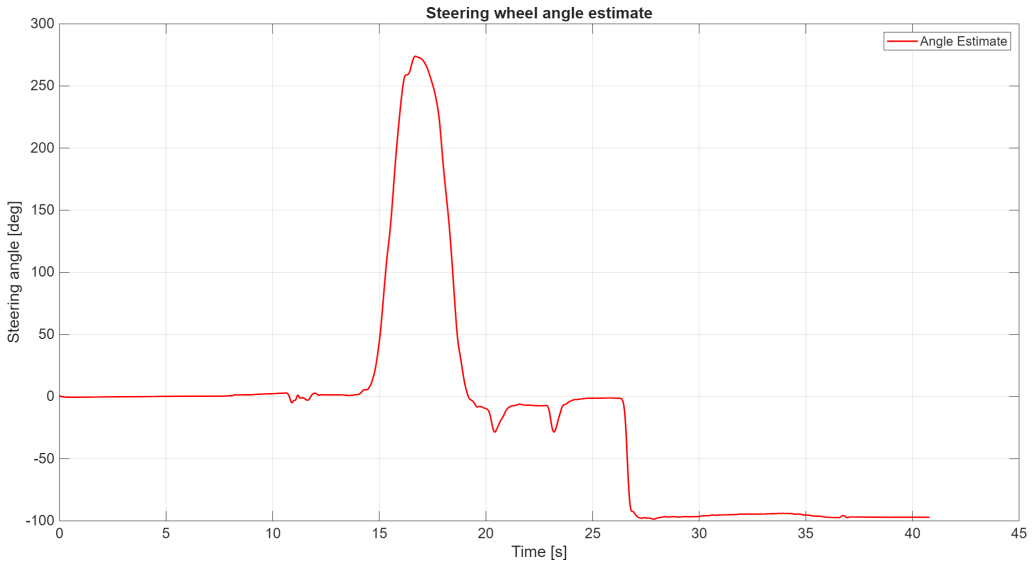


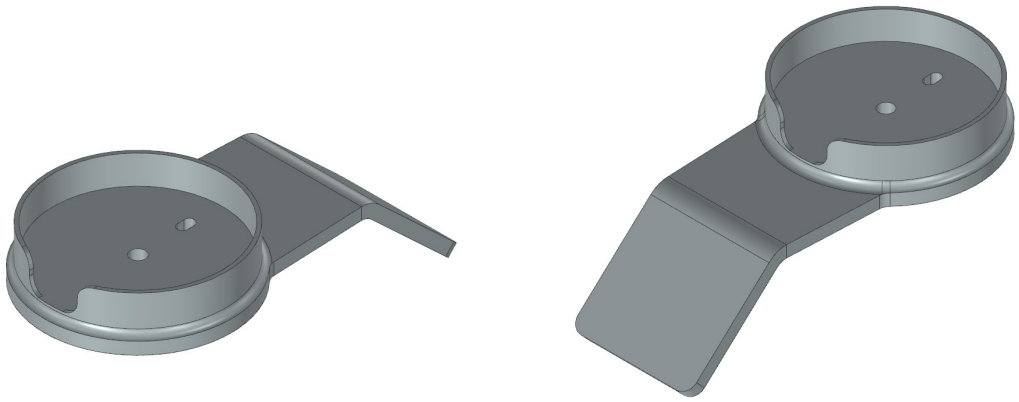

**Figure 3.14:** Angle Estimate for a step steer maneuver (90 Degs)

### 3.3.3 CAD model & 3-D printing of mountings

To facilitate the experimental data collection, custom mounting brackets were designed and 3D printed for both the OxTS RT3000 inertial navigation system and the MUSE wireless IMU from 211e. Since commercially available mounting solutions were not suitable for installation in the specific vehicle, dedicated brackets were designed to ensure secure sensor placement and reliable data acquisition [37].

For the antennas of OxTS RT3000, custom mounting brackets were designed to securely hold them to the roof of the car. The antenna mounts were designed to provide a rigid and stable installation while maintaining the correct antenna orientation and spacing recommended. This ensured reliable satellite reception throughout the experiments and minimized measurement errors caused by antenna movement or vibration during vehicle operation. The brackets were designed to be easily in-

stalled through a Velcro tape and removed without need for any modifications in the vehicle.



**(a)** Left antenna bracket **(b)** Right antenna bracket

**Figure 3.15:** CAD model of the antenna mountings.

To measure the steering wheel rotational motion during the experimental tests, the MUSE IMU was mounted on the steering wheel using a separate custom-designed bracket. A dedicated mounting was designed for the particular steering wheel dimensions and particularly for this application.

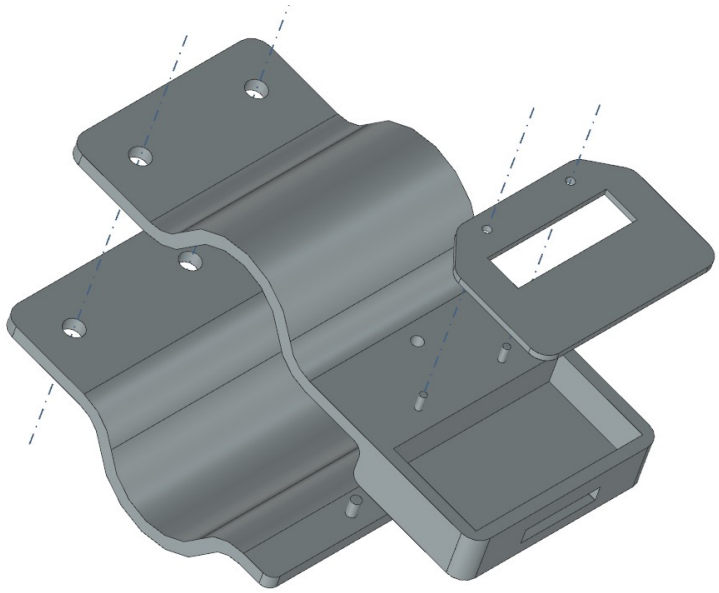


**Figure 3.16:** CAD model of IMU mounting bracket (Exploded view)

The CAD models of both mounting brackets were made taking into account the dimensions of the sensor and antennas, the mounting locations, and the structural requirements. The designs were optimized to provide sufficient stiffness while remaining lightweight so that they would not interfere with vehicle operation. Particular attention was given to ensuring that both the antennas and the IMU remained

firmly secured throughout the experimental tests to avoid measurement inaccuracies caused by sensor movement.

After completing the design, the mounting brackets were manufactured using a 3D printer at the FUSE Lab, Chalmers University of Technology. The use of 3D printing enabled rapid prototyping, allowing the designs to be evaluated and refined through trial runs before the final components were produced.

Figures 3.17a and 3.17b shows the corresponding 3D-printed components installed on the vehicle. custom-designed brackets ensured stable sensor placement throughout the experiments.



**(a)** Image of antenna brackets




**(b)** Image of IMU bracket

**Figure 3.17:** 3-D Printed brackets mounted on the Vehicle

# 4

# Experiments

The previous chapter described the methodology of the Rack-Electric Power Assisted Steering (R-EPAS) system developed in this thesis. To ensure that the proposed steering model represents the behaviour of a electric power steering system and provides a realistic steering feel for Driver-in-the-Loop applications, experimental validation and model tuning were carried out. This chapter presents the procedures used to evaluate and validate the developed R-EPAS model. The validation process consists of two main stages. The first stage involves collecting the necessary steering and vehicle response data from the benchmark vehicle, the Volvo EC40 vehicle is been used to acquire the necessary steering system data. The second stage focuses on tuning and validating the developed R-EPAS model by comparing the simulation results with the measured vehicle data. The experimental data are used to adjust key model parameters, including the steering assist characteristics, boost curve, controller gains, and steering system dynamics.The measured data not only serve as inputs for parameter tuning but also provide a basis for assessing the developed model. By comparing the simulated steering response with the experimental observations, the model is iteratively refined to improve its fidelity. This validation process ensures that the developed R-EPAS model reproduces the steering characteristics of the electric vehicle and is suitable for integration into the Sim IV driving simulator for future steering feel studies and Driver-in-the-Loop research.

## 4.1 Vehicle General Data & Experiments Data

Before tuning and validating the developed R-EPAS model, it was necessary to identify the vehicle parameters and experimental data required for the modelling process.The data used in this thesis can be divided into two categories: vehicle parameter data and experimental steering data. The vehicle parameter data consist of the physical and mechanical properties of the steering system, such as steering ratio, rack geometry, motor characteristics, torsion bar stiffness, electric motor inertia, and other parameters required to construct the mathematical model. The experimental steering data were obtained from the vehicle Volvo EC40, and include measurements of steering wheel angle, vehicle speed and other relevant signals recorded during different steering manoeuvres at different speeds.

### 4.1.1 Vehicle Data

To ensure that the developed R-EPAS model accurately represents the steering behaviour of a modern electric vehicle, it was necessary to obtain the steering system parameters required for model development.These parameters include the rack and electric motor parameters, torsional bar parameters, steering system and controller paramters, inertias, friction coefficients and other mechanical parameters that define the steering system dynamics. The test vehicle considered in this thesis is the Volvo EC40. However, due to the unavailability or access to detailed steering system parameters for the Volvo EC40, it was not possible to directly parameterize the R-EPAS model using EC40 data. Instead, the steering system parameters were adopted from the master's thesis (Functional Modelling and Simulation of an Electric Power Assisted Steering by Albin Gröndahl). The steering system investigated in that work was developed using data from a modern electric vehicle at CEVT (China Euro Vehicle Technology AB), making the parameters representative of a production electric power steering system. These parameters provided a reliable basis for developing the mathematical model. The use of these parameters enabled the development of a R-EPAS model while maintaining compatibility with the existing electric vehicle model. The final steering characteristics were further refined through controller tuning and simulation-based validation to achieve the desired steering feel and steering response.

**Table 4.1:** Vehicle Data Requirements

| No. | Name | Units |
|---|---|---|
| 1 | Vehicle mass | Kg |
| 2 | Vehicle size | m*m*m |
| 3 | Vehicle centre of gravity position | (X,Y,Z) |
| 4 | Track width | m |
| 5 | Wheelbase | m |
| 6 | Wheel radius | m |

### 4.1.2 Experiments Data

The collection of experimental data is an essential step in the development and validation of the proposed R-EPAS model. Experimental measurements provide the reference required to tune the steering model and evaluate whether its dynamic response accurately represents that of a real electric vehicle. Therefore, obtaining reliable and synchronized vehicle data is fundamental to achieving a realistic steering simulation. The collected experimental dataset forms the basis for tuning the controller parameters, validating the steering response, and comparing the behaviour of the developed R-EPAS model with that of the benchmark vehicle. Table 4.2, summarizes the experimental signals used in this study, together with their corresponding units and measurement sources.

**Table 4.2:** Experimental Data Requirements

| No. | Name | Units | Data Source |
|---|---|---|---|
| 1 | Speed $x$ | m/s | IMU Sensor |
| 2 | Speed $y$ | m/s | IMU Sensor |
| 3 | Speed $z$ | m/s | IMU Sensor |
| 4 | Acceleration $x$ | $m/s^2$ | IMU Sensor |
| 5 | Acceleration $y$ | $m/s^2$ | IMU Sensor |
| 6 | Acceleration $z$ | $m/s^2$ | IMU Sensor |
| 7 | Accelerator pedal position | % | OBD-II |
| 8 | Steering wheel angle | ° | IMU Sensor |
| 9 | Testing time | s | IMU / OBD-II |
| 10 | Yaw velocity | °/s | IMU Sensor |
| 11 | Pitch velocity | °/s | IMU Sensor |
| 12 | Roll velocity | °/s | IMU Sensor |
| 13 | Roll angle | ° | IMU Sensor |
| 14 | Pitch angle | ° | IMU Sensor |
| 15 | Yaw angle | ° | IMU Sensor |

## 4.2 Experimental Equipment & Testing Track

The development and validation of the proposed R-EPAS model require reliable experimental data collected under controlled driving conditions. This was achieved using three essential elements: the test vehicle, the data acquisition equipment, and the test track. Together, these components enabled the measurement of the steering and vehicle dynamic signals required for model parameterization, tuning, and validation. The following sections describe the experimental vehicle, the instrumentation used for data acquisition, and the characteristics of the test track in detail.

### 4.2.1 Experimental Vehicle

The selection of the experimental vehicle plays a crucial role in the development and validation of the proposed Rack-Assisted Electric Power Steering (R-EPAS) model. To obtain representative steering characteristics, the test vehicle should closely resemble the vehicle for which the steering model is intended and should accurately represent the behaviour of a modern electric vehicle. Furthermore, the vehicle must be in good operating condition to ensure that the measured steering and vehicle dynamic data are not affected by mechanical faults or abnormal system behaviour.
In this thesis, the Volvo EC40 was selected as the test vehicle, as shown in Fig. 4.1. The EC40 is a fully electric coupe style Crossover vehicle equipped with a production Rack-Assisted Electric Power Steering (R-EPAS) system, making it a suitable

reference for the development and validation of the steering model. In addition, the same vehicle architecture was previously used but with all wheel drive powertrain configuration(C40 Recharge twin) and to parameterize the existing electric vehicle model for the available test vehicle with rear wheel drive powertrain configuration, the powertrain block was modified to suit the motor map and pedal profile of the current vehicle, ensuring consistency between the vehicle dynamics model and the proposed steering system. The main vehicle specifications are presented in Tables 4.3, 4.4, and 4.5.
The experimental data were collected during driving tests at test track using a human driver, meaning all steering inputs and accelerator pedal commands were applied manually. During the experiments, accelerator pedal position were recorded through the vehicle's OBD-II interface, and the steering wheel angle, vehicle speed and inertial measurements were obtained using an IMU. These measurements were subsequently used to tune and validate the developed R-EPAS model.




**Figure 4.1:** Volvo EC40 in REVERE Lab

**Table 4.3:** Electric drive motor specification

| Parameter | Units | Value |
|---|---|---|
| Location in Car | - | Rear |
| Electric Motor Type | - | synchronous motor with permanent magnet |
| Electric Motor Model | - | EAD 3.1 |
| Max. Power Output | kW<br>hp | 185/<br>252 |
| Max. Torque | Nm | 420 |

**Table 4.4:** Vehicle dimension

| Dimension | mm |
|---|---|
| Ground Clearance | 171 |
| Length | 4440 |
| Width | 1873 |
| Height | 1591 |
| Wheelbase | 2702 |
| Front Track width | 1601 |
| Rear Track width | 1608 |
| Width including Folded-Out Door Mirrors | 2034 |
| Width including Folded-In Door Mirrors | 1938 |

**Table 4.5:** Tire Sizes

| Location | Size |
|---|---|
| Front | 235/50 R19, 7.5x19x50, 235/45 R20, 8x20x50.5 |
| Rear | 255/45 R19, 8.5x19x56, 255/40 R20, 9x20x58.5 |

### 4.2.2 IMU(Inertial measurement unit)

The experimental validation of the developed R-EPAS model requires accurate measurement of both the vehicle motion and the steering wheel dynamics. To achieve this, two Inertial Measurement Units (IMUs) were used during the data collection process.

The first sensor is an OxTS RT3000 inertial measurement unit, which was rigidly mounted underneath the front passenger seat to ensure that it accurately captured the vehicle body motion while minimizing measurement errors caused by vibrations or sensor movement, as shown in Fig. 4.2. The RT3000 combines inertial sensors with GNSS technology to provide high-accuracy measurements of the vehicle's longitudinal, lateral, and vertical accelerations, angular velocities, vehicle speed, and orientation. During the experiments, the recorded data were stored and monitored using the OxTS server for subsequent processing and analysis.

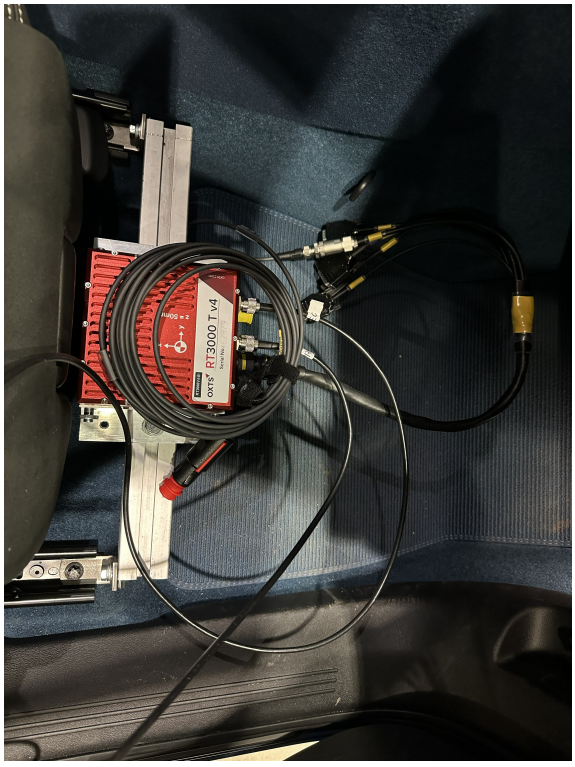



**Figure 4.2:** OxTS RT3000

To measure the steering wheel motion, a second IMU, the MUSE Wireless & Miniature IMU, was mounted directly on the steering wheel, as shown in Fig. 4.3. Mounting the sensor on the steering wheel enabled accurate measurement of the steering wheel angular motion throughout the driving manoeuvres. The steering wheel IMU data were recorded using the MUSA V3 Viewer software and later synchronized with the vehicle measurements obtained from the RT3000.



**Figure 4.3:** Muse wireless & Miniature IMU

### 4.2.3 OBD - II Cable

To accurately acquire the accelerator pedal position signals, this project utilized the On-Board Diagnostics II (OBD-II) interface to establish communication between the vehicle and the data acquisition system. The OBD-II interface is a standardized diagnostic port available on modern vehicles, providing direct access to signals generated by the vehicle's Electronic Control Unit (ECU). By using a compatible OBD-II interface connected to the Volvo EC40, as shown in Fig. 4.4, it was possible to continuously monitor and record accelerator pedal position during the experimental tests.

In this project, OBD Auto Doctor was used as the data logging software to acquire the required accelerator pedal position information. The software enabled real-time recording of accelerator pedal position, which was essential for the development and validation of the Rack-Assisted Electric Power Steering (R-EPAS) model. The recorded data were stored for subsequent synchronization with the measurements obtained from the inertial measurement units (IMUs)

The OBD-II interface provides an efficient and accurate method for vehicle data acquisition since the measurements are obtained directly from the vehicle's ECU. In addition, the OBD-II standard is widely implemented in modern passenger vehicles, allowing the same hardware and software configuration to be used across different vehicle platforms. Another advantage of this approach is that it requires no additional modifications or intrusive sensor installations on the vehicle, thereby

preserving the original vehicle configuration.



**Figure 4.4:** OBD-II Cable

### 4.2.4 Test Track

To obtain reliable and repeatable experimental data for the development and validation of the R-EPAS model, the driving tests were conducted on a controlled test track with suitable road conditions. A well-maintained test environment minimizes the influence of external factors and ensures that the measured steering response is primarily affected by the vehicle dynamics rather than road disturbances.

The experimental tests were carried out at Stora Holm Trafikövningsplats in Gothenburg, Sweden, as shown in Fig. 4.5. The facility consists of well-maintained asphalt roads designed for vehicle testing and driver training, making it an ideal location for collecting steering and vehicle dynamic data. The track provides a safe and controlled environment with sufficient straight sections and open areas to perform a wide variety of steering manoeuvres under consistent road conditions.

To improve the quality and repeatability of the measurements, the experiments were conducted under favourable weather conditions on a dry road surface. The controlled environment of the test track reduced the influence of traffic and other external disturbances, allowing accurate acquisition of steering wheel angle, vehicle speed, and other dynamic signals required for the parameterization and validation of the developed R-EPAS model.



**Figure 4.5:** Aerial view of Stora Holm Trafikövningsplats

## 4.3 Vehicle Tests

In this section, the method of design behind the selected vehicle test procedures used for model evaluation are presented. The objective of these tests is to capture the vehicle's dynamic behavior across a range of driving speeds and maneuver types, for validation of the developed model. The test were inspired from the research work in [9] and [10]

The design of the vehicle tests was not limited to the steering system alone; instead, it was structured to provide data applicable to additional subsystems, such as suspension, as well as active control functions including Electronic Stability Control (ESC) if developed in the future.

This section is divided into two main parts: Design of Experiments, which outlines the strategy and considerations behind the test planning, and Selection of Tests, which elaborates the specific maneuvers and range of speeds chosen for data collection.

### 4.3.1 Design of Experiments

Faced with the practical constraints of available test track, measurement equipment, and testing time, a limited but representative set of vehicle tests was selected for model evaluation. The purpose of the entire section was to capture the vehicle's response over a range of speeds and maneuvers, with emphasis on the steering response and lateral behavior relevant to the EPAS and development of other subsystems.

There was also a need to isolate the tests to extract the effect of an individual steering function (Steer and Release test to eliminate driver intervention and assess the steering wheel return behavior). By planning tests in this manner and across different speeds, it was easier to validate a few steering controller functions.

The test selection was guided by the need to excite the vehicle in a controlled manner while maintaining safe and repeatable test conditions (at least 2 iterations). The selected maneuvers were intended to provide data for both steady-state and transient behavior, enabling assessment of model performance under different operating conditions. In addition, the test plan was designed with future extensibility in mind, so that the same framework could later be used for suspension-related analyses and more.

### 4.3.2 Selection of Tests

A set of ten vehicle maneuvers was selected to provide complementary excitation in both the time and frequency domains for evaluation of the EPAS and vehicle lateral dynamics models. The selected tests were intended to capture the vehicle response under a range of operating conditions, from low-speed maneuverability to higher-speed transient behavior, while remaining feasible within the available experimental resources and safety constraints.

**Double lane change:** — The double lane change is a transient handling maneuver that rapidly excites the steering system through consecutive left-right steering inputs. It was used to evaluate the steering system's ability to provide precise assistance (Speed dependent) and predictable vehicle response during aggressive directional changes (can be used to assess the vehicle stability at high speeds). This test was one of the scenario which was replicated in the driving simulator for subjective assessment conducted later. The test was performed at four different speeds (20, 40, 60, 80 Km/hr) and was repeated twice for each case.

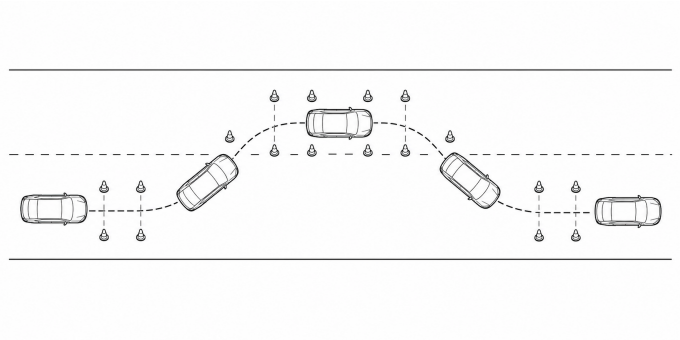


**Figure 4.6:** Schematic of Double lane change

**Sine sweep:** — A sinusoidal steering input with continuously increasing frequency is applied. This maneuver characterizes the frequency response of the steering system. This maneuver can be used to analyze how the vehicle's yaw rate, lateral acceleration, respond to the changing steering frequencies, which is essential for calibrating Electronic Stability Control (ESC) system which mainly relies on vehicle yaw rate. The test was performed at three different speeds (20, 40, 60 Km/hr) and

was repeated twice for each case.

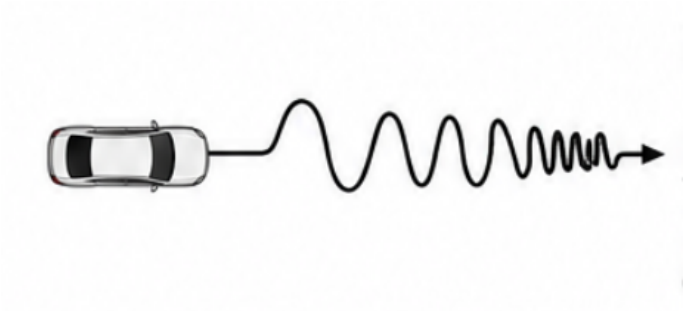


**Figure 4.7:** Schematic of Sinusoidal Sweep (Low Freq to High Freq)

**Straight-line drive without driver intervention:** — The vehicle is accelerated to the predefined speed on a flat, straight road, and the driver releases the steering wheel. It was used to evaluate the vehicle's directional stability, steering system center-point alignment since the driver input is zero ($T_{driver} = 0$). Also, key metrics steering wheel angle offset was logged when the driver intervened for minor corrections. The test was performed at three different speeds (20, 40, 60 Km/hr) and was repeated twice for each case.

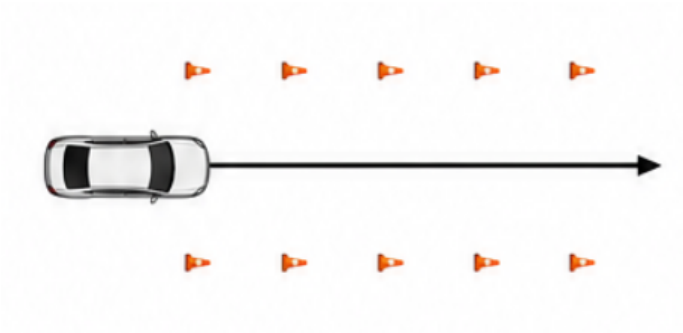


**Figure 4.8:** Schematic of Straight line drive with no driver intervention

**Step steer:** — The driver accelerated the vehicle to a constant speed, and applies a rapid, sudden steering wheel angle (90 degs) and holds it fixed. It was used to evaluate the response of the steering system and vehicle lateral motion under abrupt input conditions. The test was performed at three different speeds (20, 40, 60 Km/hr) and was repeated twice for each case.

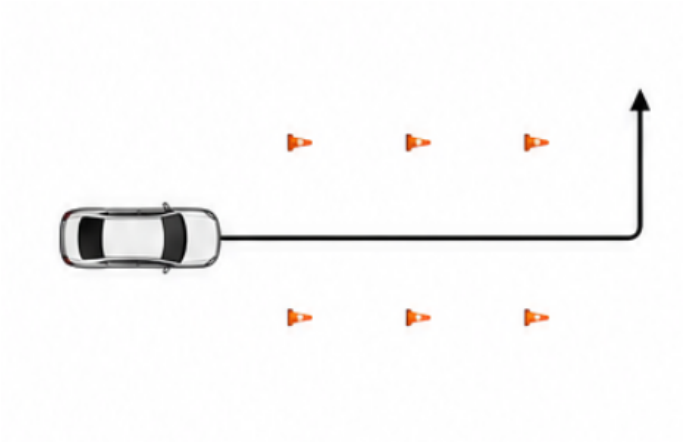


**Figure 4.9:** Schematic of Step Steer (note the trajectory wont be exact)

**U-turn:** — Low-speed maneuverability and high steering-angle behavior were assessed by means of a large-radius turning maneuver by maintaining a constant speed and almost constant steering angle input. This test was used to examine lateral response and steering assist behavior at low-speed. The test was performed at three different speeds (10, 20, 40 Km/hr) and was repeated twice for each case. For the 20 Km/hr case, a separate test case was done to check symmetry (opposite direction steering angle input).

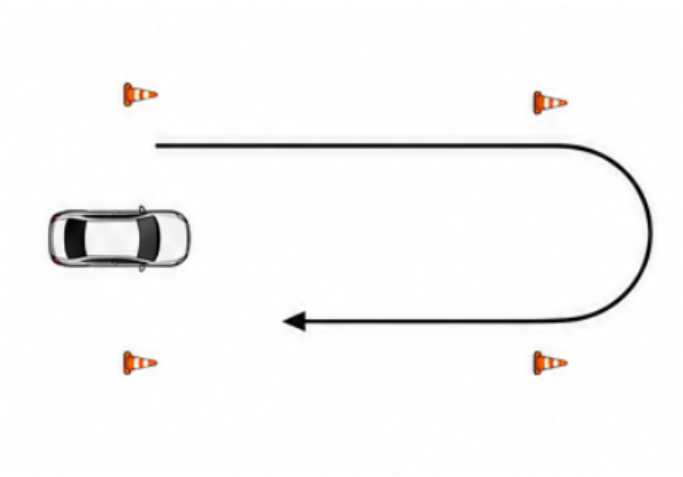


**Figure 4.10:** Schematic of U-turn

**Steady-state circle:** — Steady-state cornering can be performed in three ways (constant speed, constant angle and constant radius). Although the ultimate metric which engineers evaluate is the understeer gradient from all the three approaches, this test was evaluated as a constant angle approach where the driver locks the steering wheel angle (90 & 180 degs in this project) and slowly ramps up the speed. One interesting observation through this test was that the vehicle didn't exceed a speed of 50 Km/hr which is evidence of a safety feature intervention like ESC. The yaw rate and angle, roll rate and angle, yaw and lateral acceleration gain with speed can be analyzed to derive the threshold value and metric used by the stability system

to intervene. The test was performed for two different steering angle inputs (90 and 180 degs) and was repeated twice for each case.

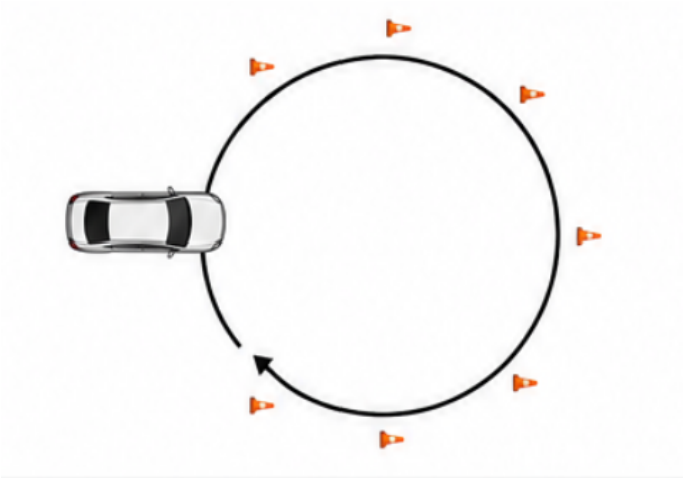


**Figure 4.11:** Schematic of Steady state circle (Constant angle)

**Steer and Release:** — Self-aligning behavior of the steering wheel (steering system to be abstract) were investigated through this test, where the driver steers to a particular angle and releases the wheel ($T_{driver} = 0$) thereby just isolating the steering system and the tires to return the steering wheel to zero angle. This test was used to observe steering return dynamics by recording the steering wheel angle. The test was performed at three different speeds (10, 20, 40 Km/hr), one angle input of 180 degs and was not repeated for iterations.

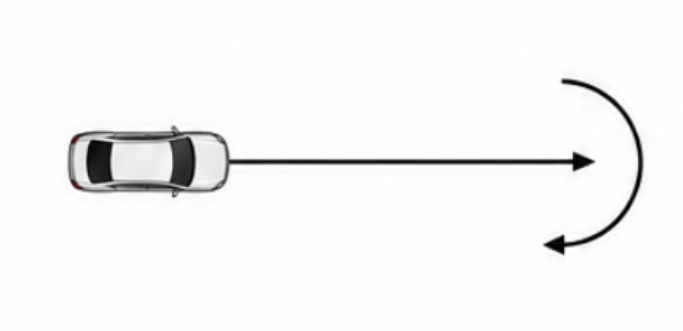


**Figure 4.12:** Schematic of Steer (180 degs) and release

**Single lane change:** — In this test, vehicle changes from one lane to an adjacent parallel lane at a fixed speed. The transient lateral response was evaluated by applying a single evasive steering input. This maneuver was used to assess recovery behavior and lateral response under less aggressive conditions than the double lane change. The test was performed at four different speeds (20, 40, 60, 80 Km/hr) and was not repeated for iterations.

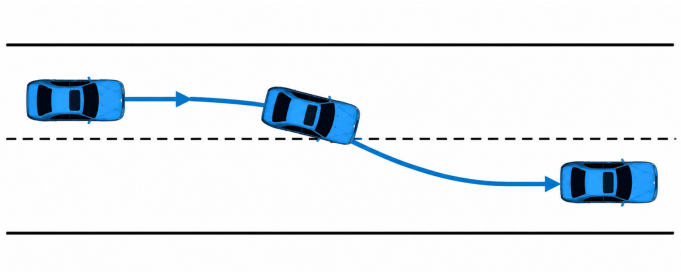


**Figure 4.13:** Schematic of Single lane change

**Slalom:** — Repeated alternating steering inputs were applied in order to assess steering hysteresis and vehicle response to successive direction steering switches. This test was also part of the driving simulator subjective assessment. The test was performed at three different speeds (40, 60, 80 Km/hr) and was not repeated for iterations.

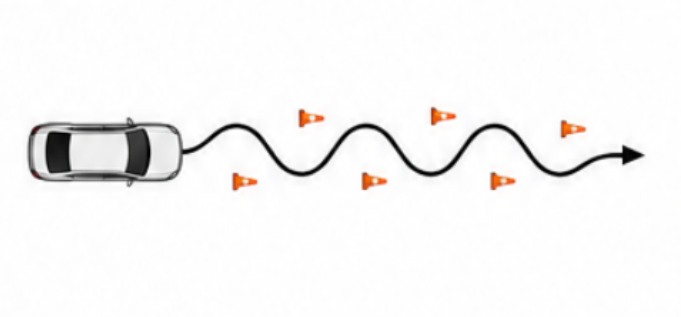


**Figure 4.14:** Schematic of Slalom

**Parking (Switch lane and halt):** — Low-speed steering behavior, where the speeds are very low (10, 20 Km/hr). This test was performed to assess low speed assist behavior for large steering angle inputs. The test was performed at two different speeds (10, 20 Km/hr) and was not repeated for iterations.

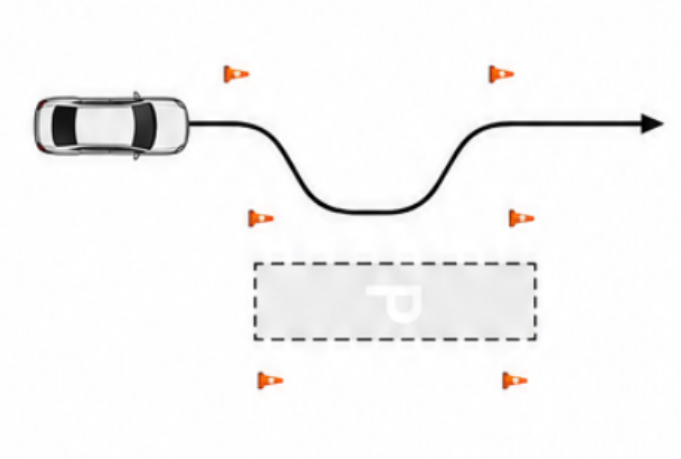


**Figure 4.15:** Schematic of Parking maneuver

# 5

# Postprocessing and Model Refinement

## 5.1 Postprocessing of Test Data

Raw data collected from the vehicle's OBD network and external IMUs (Muse and RT3000) are inherently susceptible to high-frequency measurement noise and asynchronous sampling since they were manually switched on for logging. This means that there is a need for a post-processing step to filter the signal noise and align the datasets both spatially (particularly the lateral acceleration) and temporally (time sync between signals) before using it in the vehicle model for tuning [37].

### 5.1.1 Filtering of IMU and OBD Data

Sensor noise in the raw acceleration and angular velocity signals can adversely affect the stability of the vehicle model and its validation. To mitigate this, a Power Spectral Density (PSD) analysis was first performed on the raw data to identify frequency regions of maximum energy (dB), which helped in fixing the optimal cutoff frequencies for the accelerometer and gyroscope signals.

Low-pass Butterworth filters were implemented, utilizing a 4th-order configuration for angular rates and a 1st-order configuration for accelerations. The Butterworth design ensures that all dynamic frequencies below the cutoff are passed uniformly without artificial amplification or attenuation ripples, preserving the true physical magnitude which was essential while comparing the model response and measured signals.

A 4th-order configuration for filtering was utilized for the angular rates (gyroscope data) to provide a steep roll-off, meaning that it aggressively eliminates high-frequency driveline and road vibrations without harming the inherently smooth measurements, it was expected that the rates captured by gyroscope is smooth without high freq vibration due to the kind of manuevers performed and since they were performed by a human. The following figures shows the raw and filtered gyrocope data from both RT3000 (Fig 5.1 and 5.2) and Muse IMU (Fig 5.3 and 5.4).

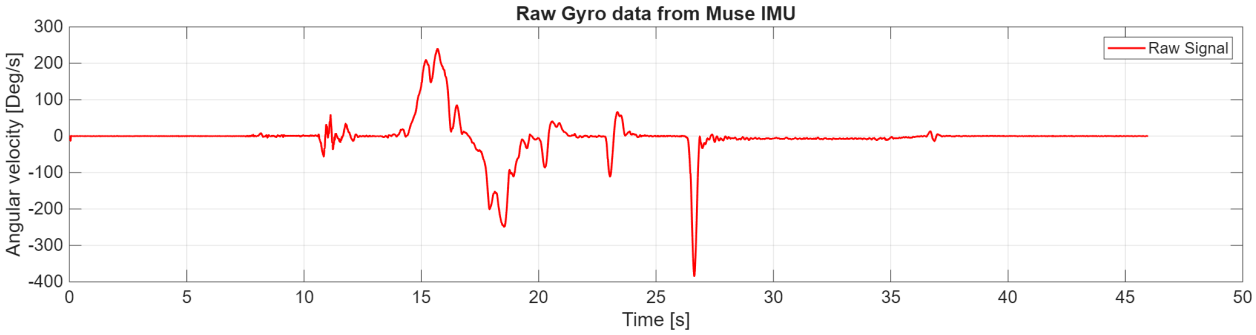



**Figure 5.1:** Raw Gyro signal from Muse before filtering

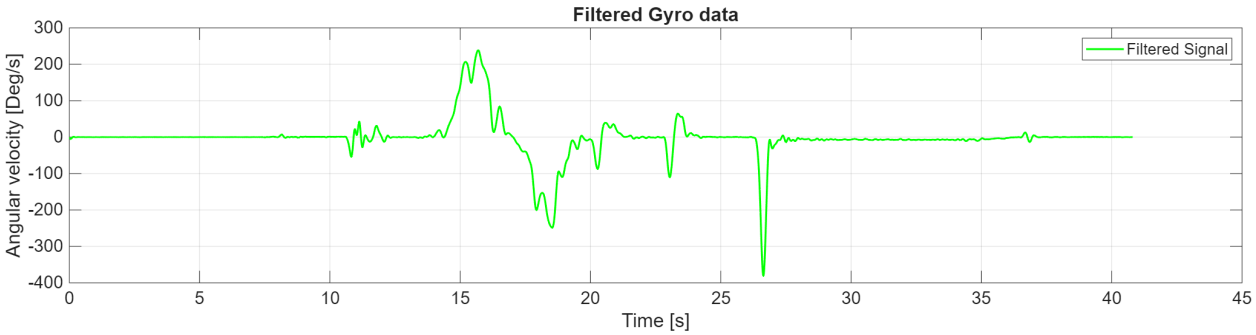



**Figure 5.2:** Filtered Gyro signal logged Muse

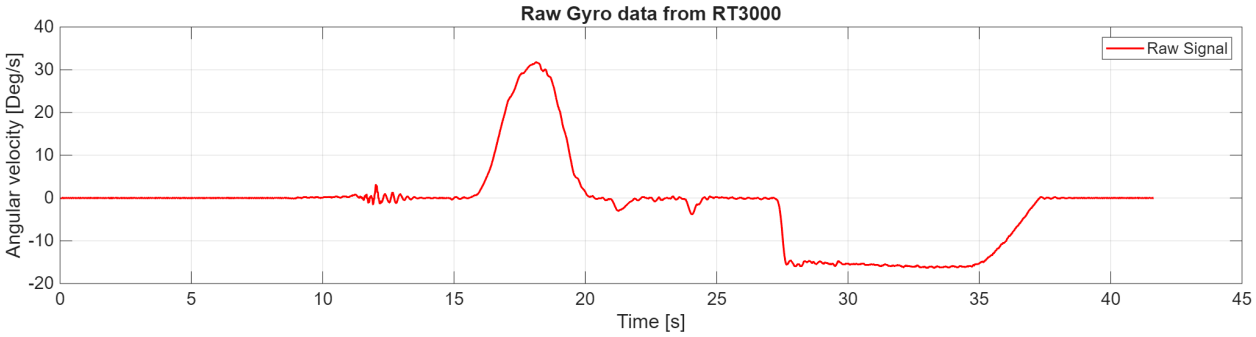



**Figure 5.3:** Raw Gyro signal from RT3000 before filtering

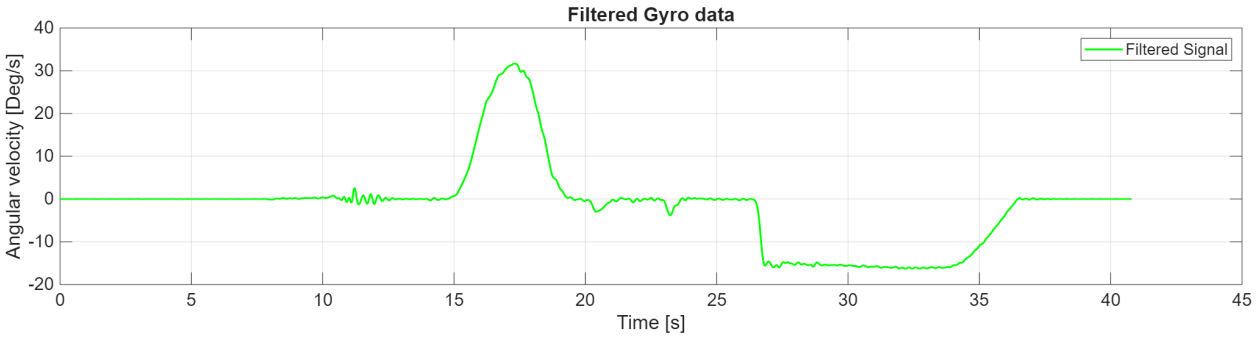



**Figure 5.4:** Filtered Gyro signal logged in RT3000

On the other hand, a 1st-order configuration was utilized for accelerations. Because accelerometers capture sudden, sharp force transients (such as the harsh braking peak used for synchronization), utilizing a higher-order filter could induce overshoot. The 1st-order filter preserves the true temporal shape and amplitude of these sharp transient force peaks. The following figures shows the raw and filtered accelerometer data from both RT3000 (Fig 5.5 and 5.6) and Muse IMU (Fig 5.7 and 5.8).

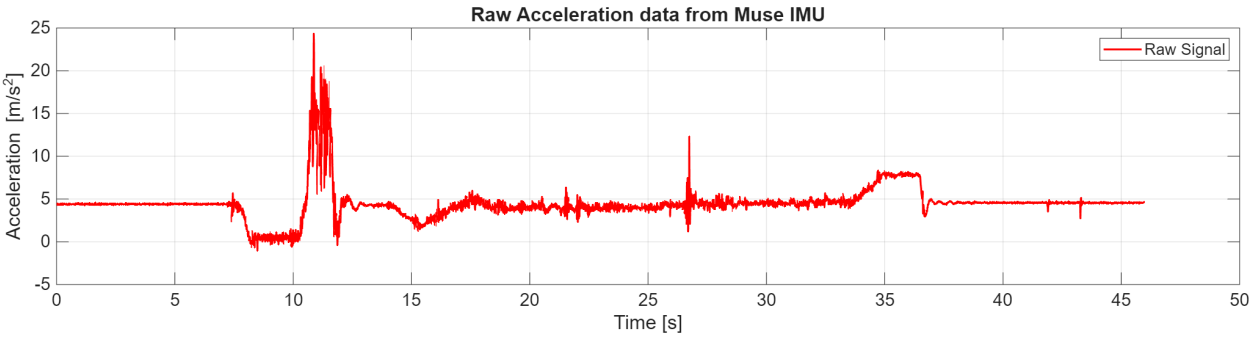



**Figure 5.5:** Raw Accelerometer signal from Muse before filtering

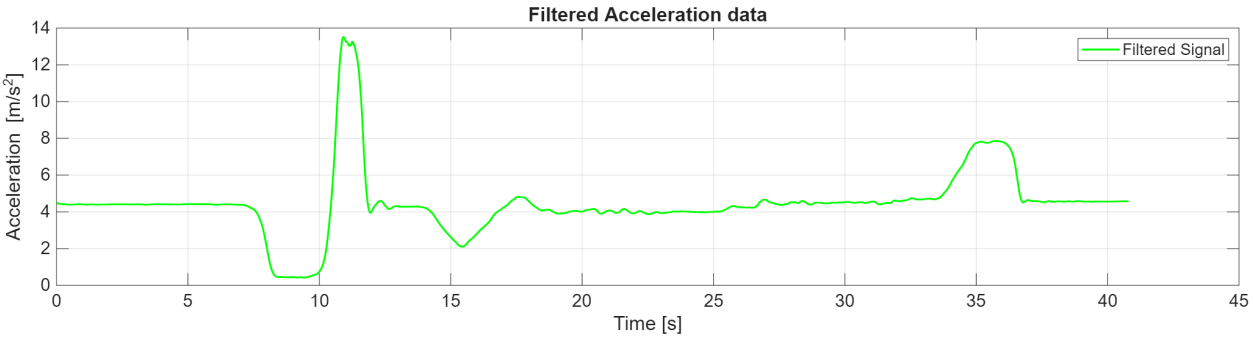



**Figure 5.6:** Filtered Accelerometer signal logged in Muse

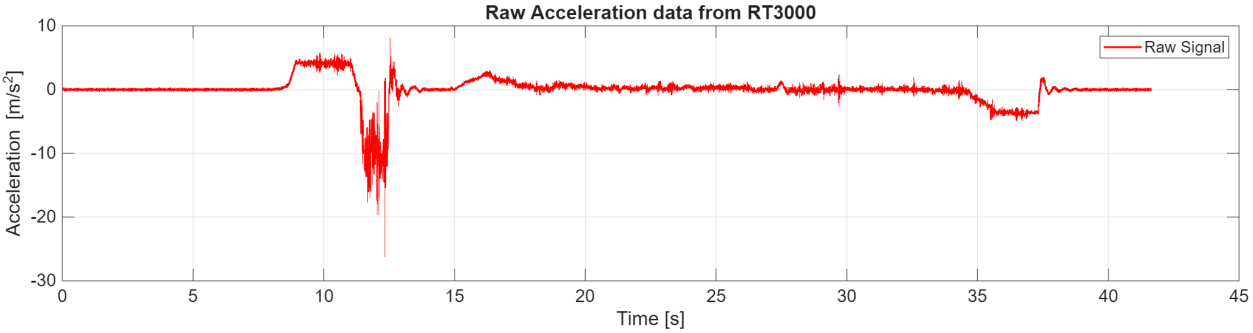



**Figure 5.7:** Raw Accelerometer signal from RT3000 before filtering

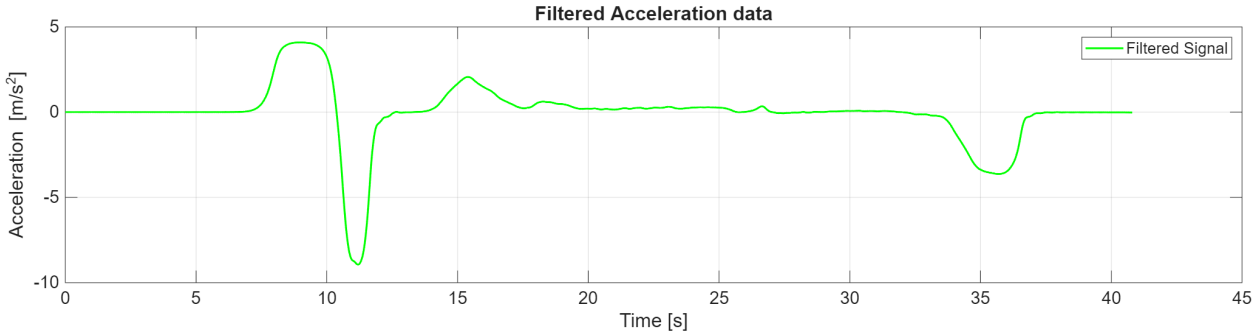



**Figure 5.8:** Filtered Accelerometer signal logged in RT3000

To eliminate phase lag that would otherwise corrupt the temporal alignment between sensors and model response, zero-phase digital filtering was implemented using MATLAB's `filtfilt` function. This filters the data in the forward direction and subsequently filters it in the reverse direction, resulting in a net-zero phase shift.

This is critical for data synchronization, ensuring that transient peaks maintain their exact physical timestamp. This is also vital because while comparing the model variables (Yaw rate and Lateral acceleration) with the sensor measured signals, a phase lag will question the validation.

Furthermore, as an anti-aliasing safeguard, all cutoff frequencies were strictly capped at 45% of the sampling frequency ($0.45 \cdot f_s$) as per the Nyquist rule.

### 5.1.2 Data Synchronization and Acceleration Translation

As the sensors were manually turned on during each test maneuver, it demands the need for time synchronization between the signals logged by the IMUs and OBD II scanner (OBD Auto Doctor).

For this, a harsh braking was deliberately executed at the initiation of each test run since vehicle's OBD system lacks a precise absolute clock, creating a sharp, recognizable dip in the longitudinal acceleration thereby a dip in the longitudinal speed logged by both RT3000, Muse IMU and OBD II scanner (OBD Auto Doctor). This prominent negative peak served as a highly reliable signal flag to calculate the exact time offset and perfectly align the accelerations signals in the longitudinal direction of both the IMUS.

The figure 5.9 shows the accelerations after the time sync is performed to match the negative peak (around 10-15 Secs).

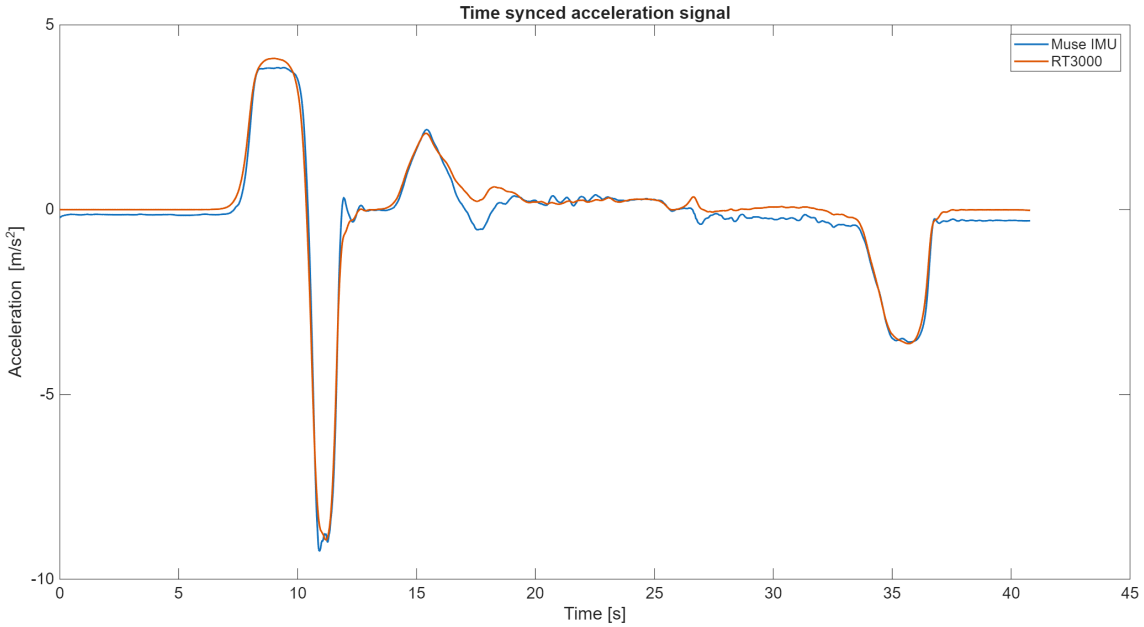



**Figure 5.9:** Time synced acceleration signals

The same prominent braking event was used to align the OBD speed with the RT3000 longitudinal velocity. Figure 5.10 shows the longitudinal speeds after time synchronization.

It can be observed that, even though the signals are aligned in time, amplitude mismatches and stair step like profile in OBD II signal remain due to fundamental differences between the measurement systems. The RT3000 captures continuous, true ground velocity at 100 Hz by fusing GPS and inertial data. In contrast, the OBD system estimates speed from wheel rotation at a much lower frequency (in this case  2 Hz) with significant integer quantization, causing the visible stepped profile.

Furthermore, the OBD signal is subjected to internal ECU low-pass filtering—which dampens its response to rapid acceleration and braking transients — and its amplitude is susceptible to dynamic wheel slip and static tire-radius assumptions. Ultimately, the RT3000 represents a high-fidelity ground truth data, and the remaining magnitude deviations simply reflect the inherent resolution and processing limitations of standard vehicle bus data. Also, during interpolation of the low freq OBD II data onto high freq RT3000 dataset, the speed holds its previous value, creating those flat steps.

After the previous steps, all the sensor dataset are in sync for use in the model and for angle estimation process (Chapter 3).

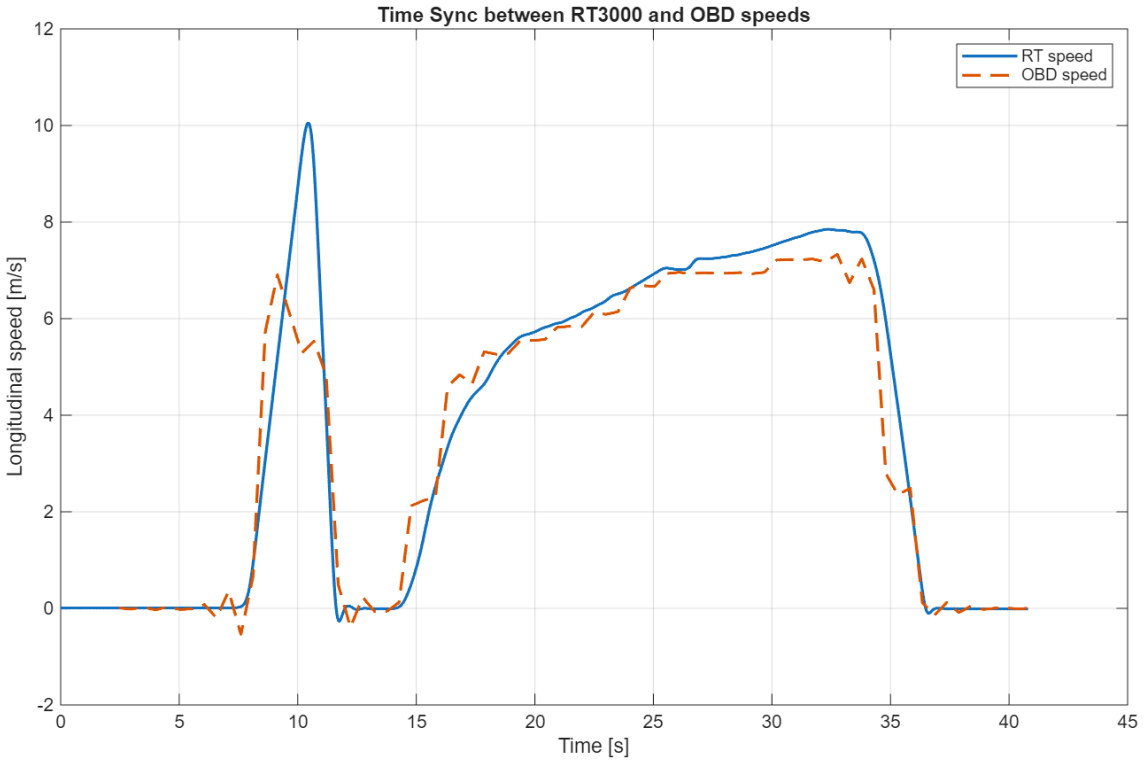



**Figure 5.10:** Time syned OBD II and RT3000 Longitudinal velocity signal

This project also focuses on comparing the vehicle model response to the actual vehicle before testing for steering system response. This is usually done by comparing the model's lateral response (Lateral acceleration and yaw rate) with the vehicle's behavior (sensor measurements). Since the RT3000 signals are translated to the steering wheel center by the software, the accelerations should be translated to the COG for comaprison with the model response. This step is now necessary for the yaw rate because the angular rates will be the same at any point in the vehicle body unlike accelerations.

Therefore beyond temporal alignment, a spatial translation of the acceleration data was mandatory because the RT3000 IMU was positioned at the steering wheel center rather than the vehicle's true Center of Gravity (COG). The physical lever arm between the sensor and the loaded COG was established using approximate assumed offsets of $\Delta x = 0.784$ m forward, $\Delta y = 0.368$ m left, and $\Delta z = 0.515$ m upward. While these measurements serve as assumptions due to the complexities of precisely locating the loaded COG (a driver with two rear passengers), they provide a necessary foundation for mapping the sensor frame back to the body origin.

To calculate the true lateral acceleration at the COG, a vectorized two-step rigid-body translation was applied to the filtered signals.

The first step removes the kinematic spinning effects caused by the vehicle's yaw dynamics, using the filtered yaw rate ($r_f$) and yaw acceleration ($\dot{r_f}$):

$$a_y^{kinematic} = a_y^{sensor} - \dot{r_f}\Delta x + {r_f}^2\Delta y$$

The second step eliminates the dynamic height effect introduced by the sensor's vertical placement above the COG, incorporating the roll acceleration ($\dot{p}$):

$$a_y^{COG} = a_y^{kinematic} - \dot{p}\Delta z$$

In theoretical rigid-body translations, a gravity correction term $g\sin(\phi)$ is typically subtracted to account for the sensor tilting with the vehicle's roll angle. However, during the initial post-processing phase, implementing this correction induced a persistent steady-state offset in the lateral acceleration signal while the vehicle was static. This anomaly was attributed to minor IMU mounting misalignments and initial ground slope, which resulted in a non-zero static roll reading. The following figure (5.11) shows the plot of lateral acceleration at the steering wheel center and the approximated COG.

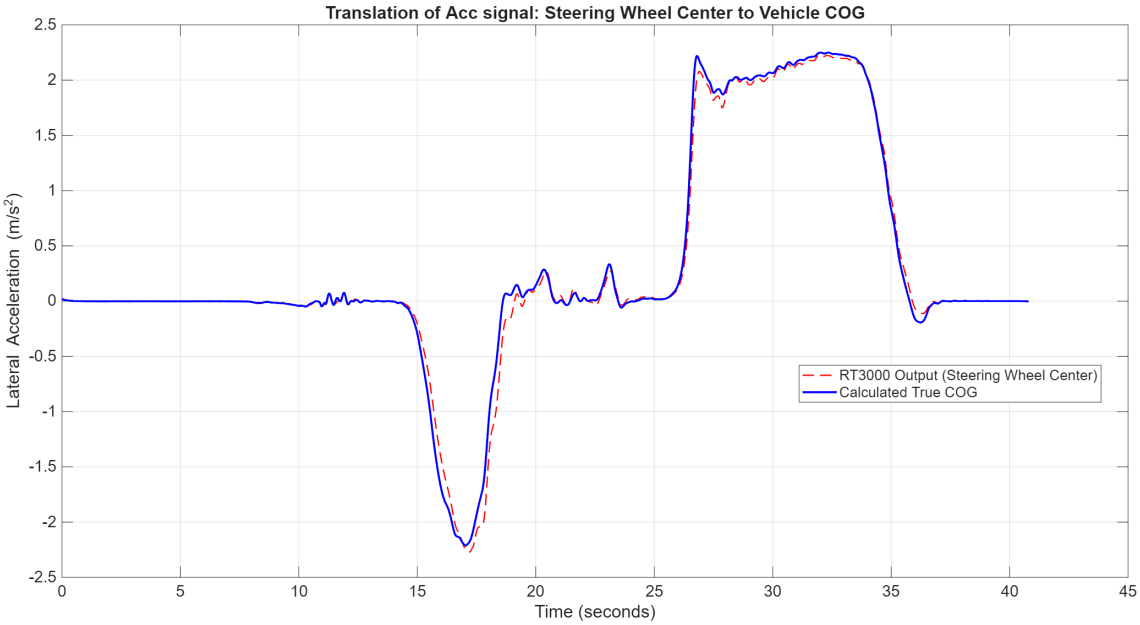



**Figure 5.11:** Plot of Lateral acceleration measured by sensor and Lateral acceleration translated to vehicle CoG

## 5.2 Model refinement using old steering model

During the vehicle testing phase, restricted access to the vehicle's CAN bus prevented the measurement of steering torque signals, such as the driver input torque or the net torsion bar torque which is sent to the simulator steering wheel. Consequently, the estimated steering wheel angle (explained in Chapter 3) was utilized as the primary input to the steering subsystem in the vehicle model.

This measurement limitation presented a challenge for the simulator implementation. In the driving simulator, the Sensodrive motor attached to the steering wheel must generate a force feedback torque—effectively replicating the torsion bar torque—so the driver perceives a realistic haptic response. Without empirical torque data from the test vehicle to serve as a ground truth, tuning the simulator's steering feedback required an alternative baseline.

### 5.2.1 Tuning with HPAS model

To overcome this, a previously developed Hydraulic Power Assist Steering (HPAS) model by vti (Volvo S40) was decided to be used as a tuning reference. The process of utilizing an HPAS model to tune a modern Electric Power Assist Steering (EPAS) system might initially seem disparate, the fundamental mechanical coupling and base haptic characteristics of the two systems do not vary drastically [23]. The primary differences lie in the shape of the assist torque map and the addition of active driver assistance functions in EPAS. The underlying mechanical impedance, governed by the stiffness and damping of the steering column and torsion bar remains functionally comparable.

Therefore, the validated HPAS model was utilized to tune the baseline stiffness and damping parameters of the reference model and this gave room for objective evaluation as followed in [23] considering there is no test vehicle (a completely new system developed) equipped with the new steering architecture, so using a old model as benchmark. The following figure shows the torsion bar torque versus the steering wheel angle plot of both HPAS and tuned EPAS. The torsion bar torque of EPAS was deliberately tuned to provide lesser resisting peak torque after suggestions from test participants and experience of driving the test vehicle.

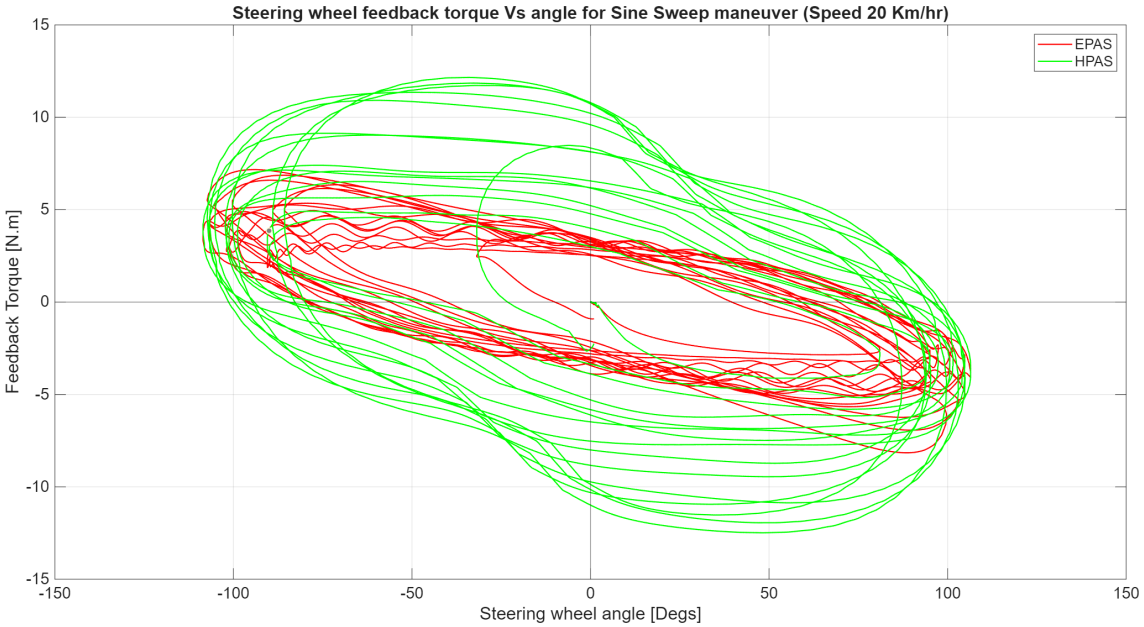



**Figure 5.12:** Plot of SWT Vs SWA of both HPAS and EPAS after tuning for Sine Sweep maneuver performed at 20 Km/hr

This established the possiblity to reproduce a physically realistic behavior of the steering system. By aligning these foundational parameters, a realistic torsion bar torque profile was generated and sent to the Sensodrive motor, ensuring the driver experienced plausible steering feel in the simulator despite the absence of direct torque measurements from the test vehicle.

# 6

# Results

This chapter presents the results and validation of the conducted work, divided into three main sections. The first section analyzes the response of the vehicle model equipped with the newly developed steering system during standard experimental maneuvers. The second section focuses on the validation of the steering-wheel angle estimation method, including simulator-based experiments and an analysis of system tradeoffs. Finally, the third section presents the outcomes of subjective assessments, wherein volunteer drivers compared the performance and feel of the old and new vehicle models.

## 6.1 Model response to Experimental input

To prevent an excessive compilation of plots and to focus on the most relevant data, the analysis in this section is concentrated on two primary maneuvers : the Double Lane Change (DLC) and the Slalom. Both of them executed at a constant longitudinal velocity of 40 km/h. Furthermore, because these two specific maneuvers were replicated during the driving simulator subjective assessments. So, prioritizing them establishes a direct continuity between the objective sensor measurements and the subjective test participant feedback which is vital for further refinement of the subsystem.

### 6.1.1 Slalom

Although the primary scope of this thesis is modeling the Electric Power Assisted Steering (EPAS) system, it was first necessary to validate the foundational lateral dynamics of the vehicle model before integrating the vehicle model into the driving simulator and performing subjective assessments. If the core vehicle model fails to replicate close to actual vehicle yaw and lateral acceleration responses, any further steering feedback tuning would be flawed.

Firstly, the lateral response of the vehicle model and the sensor measurements were compared,

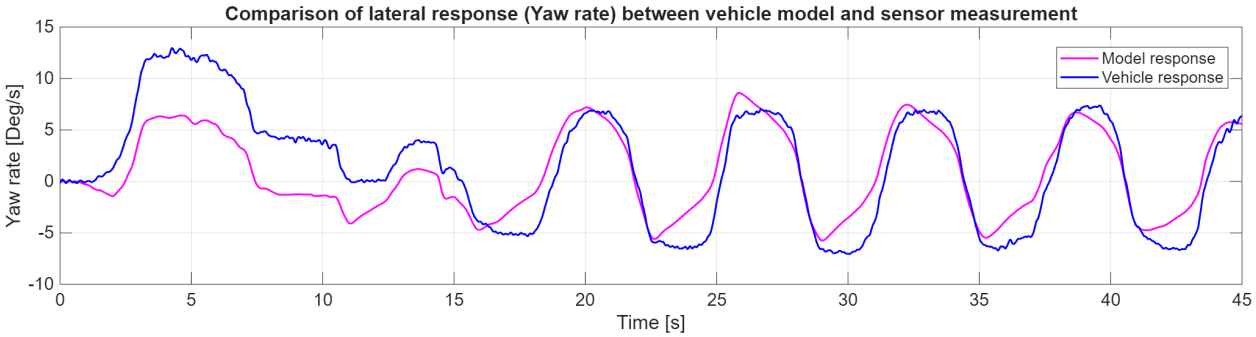



**Figure 6.1:** Yaw rate (Vehicle Vs Model response)

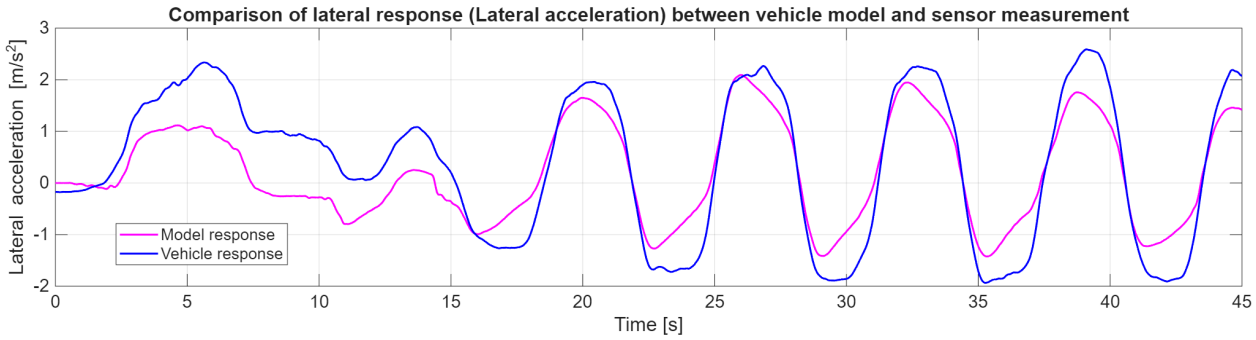



**Figure 6.2:** Lateral acceleration (Vehicle Vs Model response)

Since this thesis work mainly focused on one subsystem and the lateral response of the vehicle model is governed by the combination of other subsystems (Suspension, tires), it is expected that the variables compared will not exactly match in magnitude, phase and gradient. So, a metric to compare the signals (model and real) and give a score for their correspondence will be needed.

For this comparison to objectively quantify how well the model's variables matched the physical vehicle's sensor data (measured via RT3000), the ISO/TS 18571 standard was employed.

This standard for comparing signals was originally developed to provide reproducible correlation metrics for vehicle safety applications, this mathematical standard calculates a deterministic score between an experimental reference signal and a computational simulation curve. In our case its the measured signal and the model output.

The overall ISO rating ($R$) is calculated as a weighted sum of four distinct submetrics, each evaluating a different geometrical characteristic of the signals:

- **Corridor Score ($E_Z$):** This metric evaluates the general bounds of the signal by generating dynamic inner and outer corridors around the reference curve.
- **Phase Score ($E_P$):** This score quantifies the horizontal (temporal) shift between the two curves, effectively measuring the temporal delay or lag in the simulator's dynamic response compared to the real vehicle.

- **Magnitude Score ($E_M$):** Utilizing Dynamic Time Warping (DTW), this metric assesses the discrepancy in the absolute peak amplitudes of the signals after correcting for phase shift.

- **Slope Score ($E_S$):** The most mathematically stringent metric, the slope score evaluates the first derivative (the rate of change) of the signals, ensuring the transient sharpness of the simulator's response precisely matches the real vehicle.

Following the ISO/TS 18571 standardized thresholds, an overall score ($R$) $\geq 0.94$ is classified as "Excellent," a score between 0.80 and 0.94 is "Good," a score between 0.58 and 0.80 is "Fair," and anything below 0.58 is considered "Poor".

| Variable | ISO Ratings | | | | |
|---|---|---|---|---|---|
| | Corridor | Phase | Magnitude | Slope | Overall |
| Yaw rate | 0.5400 | 0.9749 | 0.7070 | 0.6440 | **0.6812 (Fair)** |
| Lateral acceleration | 0.4555 | 0.9868 | 0.6721 | 0.7366 | **0.6613 (Fair)** |

**Table 6.1:** ISO scores to analyze correspondence of model and vehicle response

The objective validation (Table 6.1) reveals that the fundamental lateral dynamics model performs adequately, though with some identifiable limitations. The model achieved an overall ISO rating of 0.6812 ("Fair") for Yaw Rate and 0.6613 ("Fair") for Lateral Acceleration. The phase scores ($E_P$) were consistently excellent (approaching 0.98), confirming that the model suffers from virtually no temporal lag. The primary reductions in the overall ratings stem from the magnitude and slope scores, indicating that vehicle model needs to be tuned further (Suspension) to replicate the actual vehicle response for maneuvers involving continuous load transfer and Steering angle input like Slalom scenario.

With the lateral dynamics characterized, the next part of the validation is the steering wheel feedback torque. To show the response of both the steering systems to driver input, a plot comparing steering wheel feedback torque versus steering wheel angle was generated (Figure 6.4). Also, a plot of the feedback torque versus time (Figure 6.3) was also generated to inspect the profile with the steering angle input.

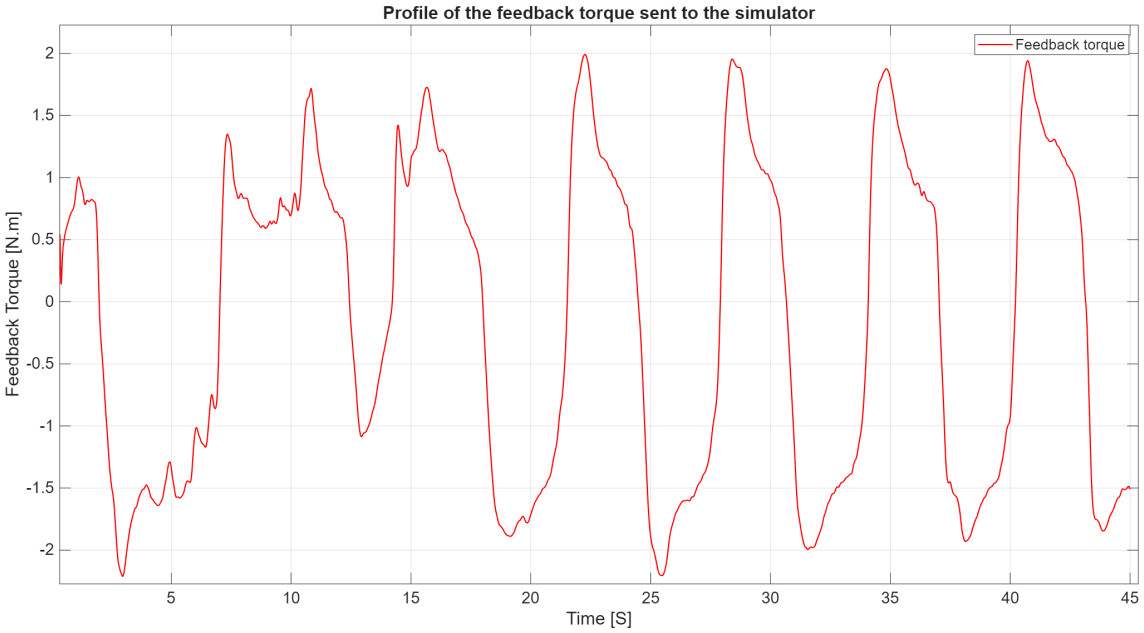



**Figure 6.3:** Feedback torque profile as a function of time

During the initial subjective assessment trials, volunteer drivers and vti engineers reported that the new EPAS model felt overly stiff. Consequently, the EPAS tuning parameters (mainly the reference model stiffness and the assist contribution) were retuned to provide a lighter and smooth response.
This is visually evident in the torque-angle plot, the resulting EPAS hysteresis loop (red trace) operates with a noticeably less steeper slope and a reduced resistive feedback compared to the HPAS model (green trace). This perfectly correlates with the engineering directive to provide a less stiff and more realistic steering resistance profile.

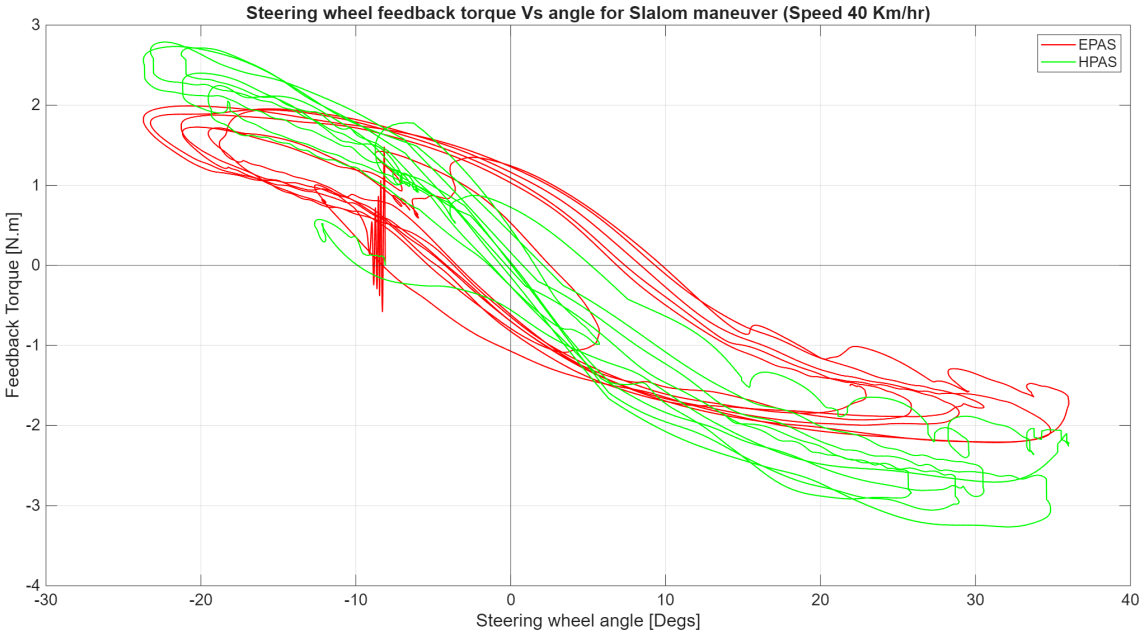



**Figure 6.4:** Feedback torque (SWT) Vs Steering wheel angle (SWA) input

### 6.1.2 Double Lane Change

This is the next maneuver of interest for objective comparison. First, the lateral response was inspected, the following figures shows the yaw rate and lateral acceleration response of both the model and the vehicle.

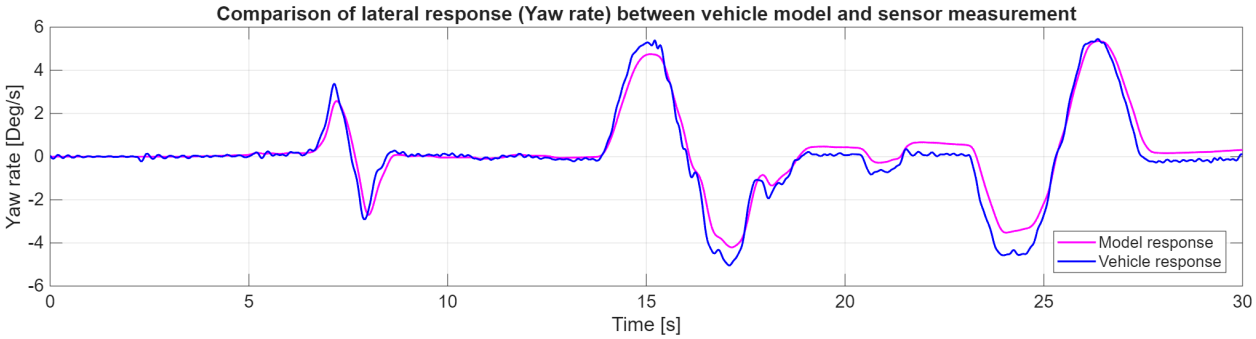



**Figure 6.5:** Yaw rate (Vehicle Vs Model response)

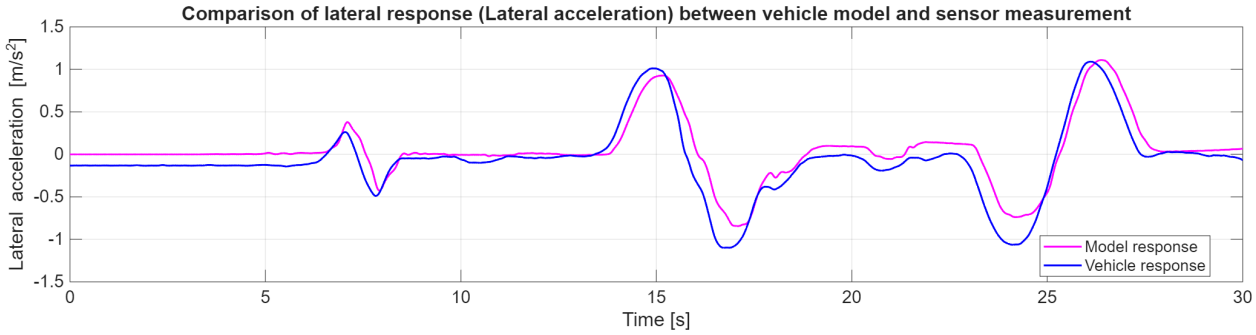



**Figure 6.6:** Lateral acceleration (Vehicle Vs Model response)

| Variable | ISO Ratings | | | | |
|---|---|---|---|---|---|
| | Corridor | Phase | Magnitude | Slope | Overall |
| Yaw rate | 0.8839 | 0.9867 | 0.8115 | 0.7611 | **0.8654 (Good)** |
| Lateral acceleration | 0.7150 | 0.9678 | 0.5987 | 0.7849 | **0.7563 (Fair)** |

**Table 6.2:** ISO scores to analyze correspondence of model and vehicle response

For the DLC maneuver (Table 6.2), the model demonstrated an improved correlation compared to the Slalom since it involved lesser effects from other subsystems, achieving an overall ISO rating of 0.8654 ("Good") for Yaw Rate and 0.7563 ("Fair") for Lateral Acceleration.
Similar to the Slalom results, the phase scores remained near-perfect. The higher yaw rate correlation in the DLC indicates that the model is slightly effective in replicating the actual vehicle response for singular evasive maneuvers than it is for continuous oscillatory maneuvers.

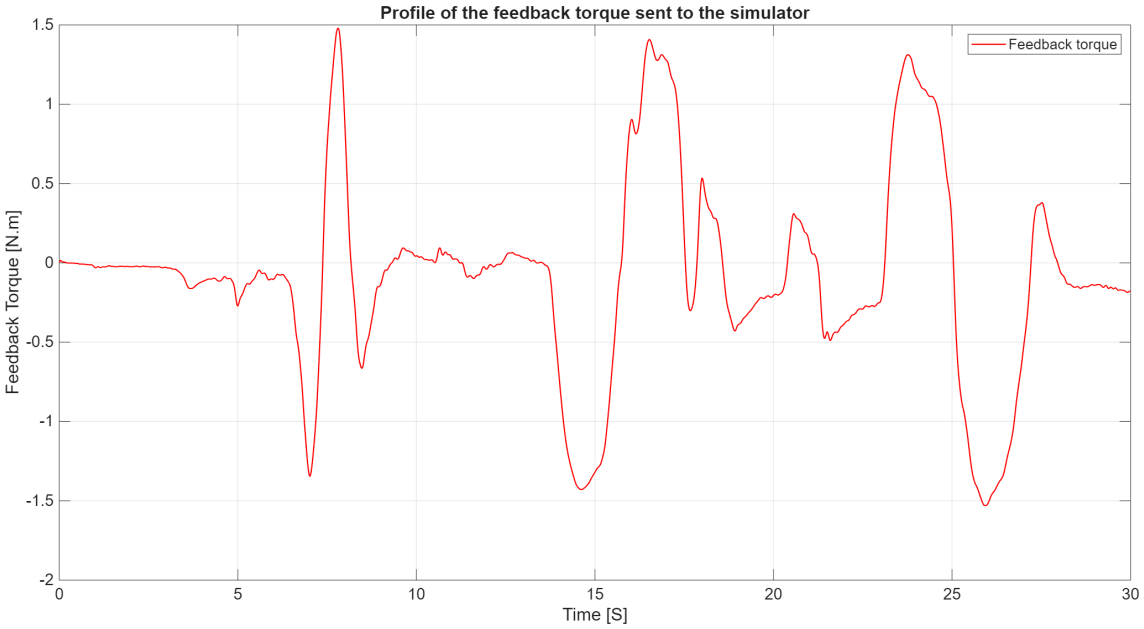



**Figure 6.7:** Feedback torque profile as a function of time

The steering wheel feedback validation (Figure 6.8) exhibits a similar dynamic shift to the Slalom. The EPAS loop (red trace) once again demonstrates a reduced peak torque amplitude and a shallower gradient when compared against the stiffer HPAS system (green trace), confirming that the EPAS stiffness refinements have successfully translated across multiple dynamic scenarios.

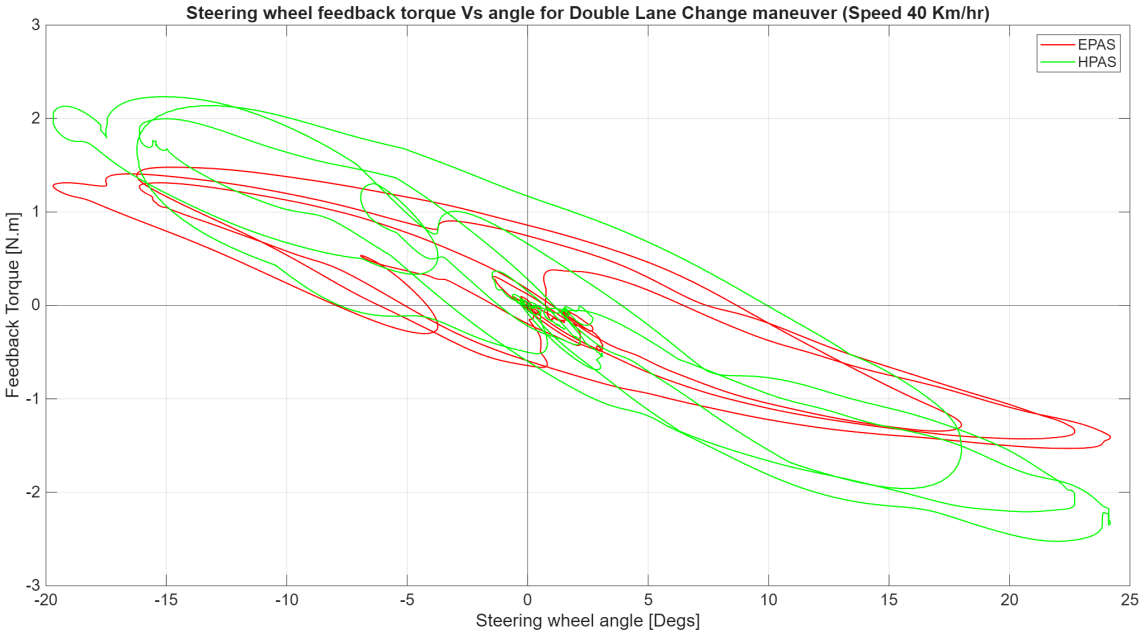



**Figure 6.8:** Feedback torque (SWT) Vs Steering wheel angle (SWA) input

### 6.1.3 Steer and Release

The steer and release maneuver served to characterize and validate the steering system's return behavior. The steering wheel angle estimate was used to study the return profile since during that instant its basically the steering system and wheels doing the job of bringing back the steering wheel to the center. The following figure shows the steering wheel angle estimate from the maneuver, wherein after steering to the desired angle (180 degs), the driver lets go of the steering wheel ($\mathbf{T}_{\text{driver}} = 0$).

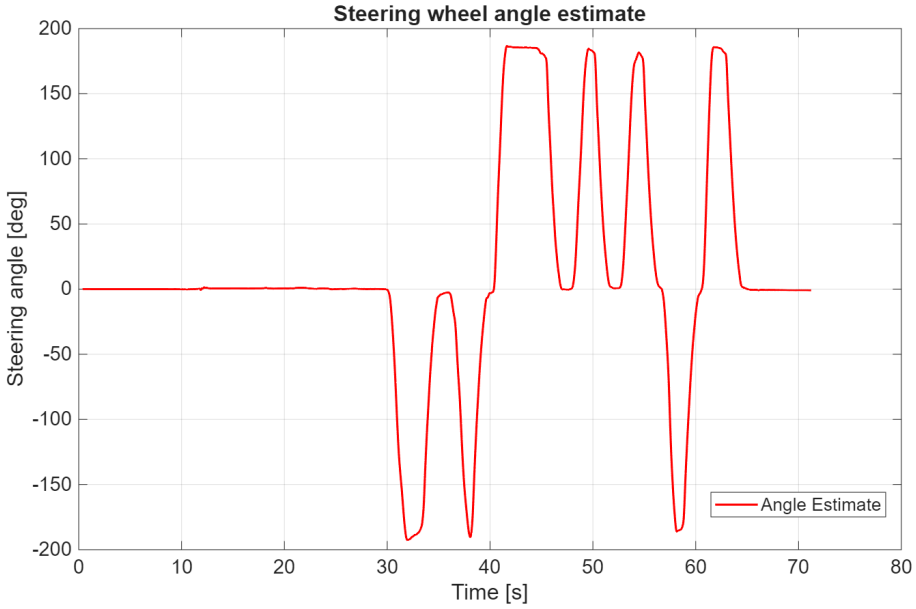
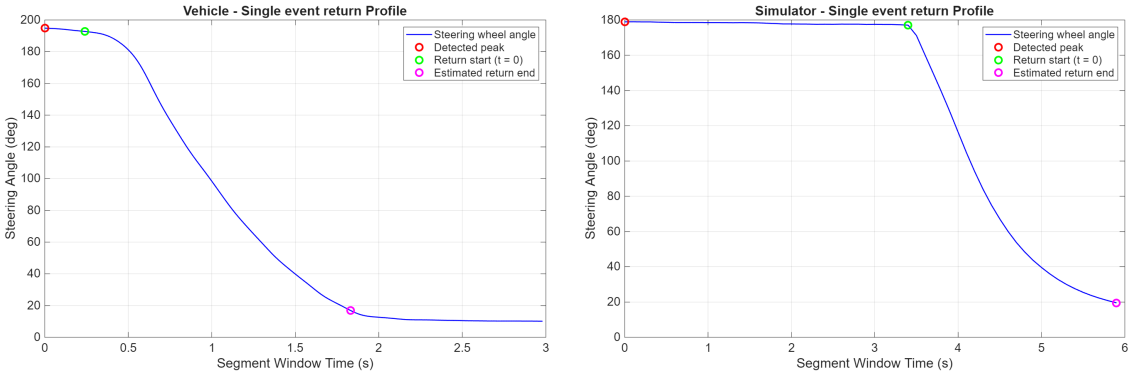



**Figure 6.9:** Steering wheel angle estimate for Steer and release maneuver performed at 20 Km/hr

The return profile of the steering wheel angle is of main interest since it was used to calibrate the amount of contribution from tires, whether is has to return fast or slow and also how fast or slow (slope).




**(a)** Vehicle return event **(b)** Simulator return event

**Figure 6.10:** Single return event identified from both vehicle and simualtor logs

To verify this, the same maneuver was reproduced in the simulator and the steering

wheel angle was logged from the simulator. With access to both the angle of the simulator (influence of the vehicle model) and the real vehicle, the steering system was tuned to replicate the return behavior of the real vehicle when there is no driver intervention. The following figure shows the return profile of the steering wheel angle from the simulator and the estimate.

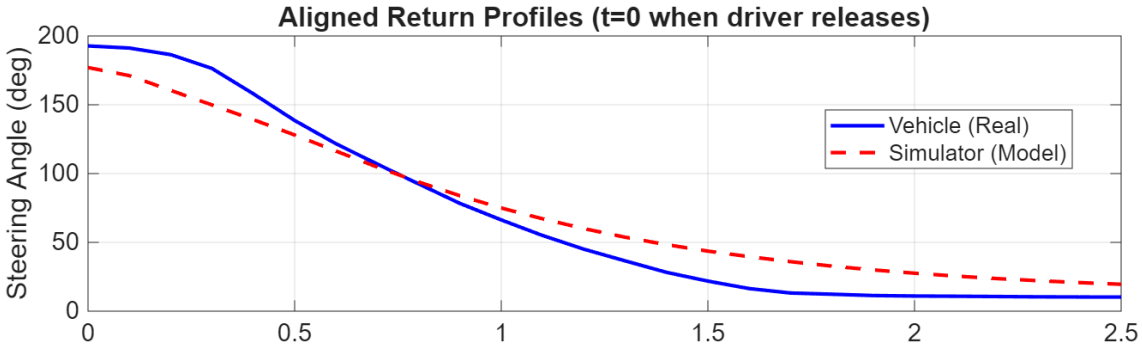



**Figure 6.11:** Return profile of steering wheel angle after tuning the model

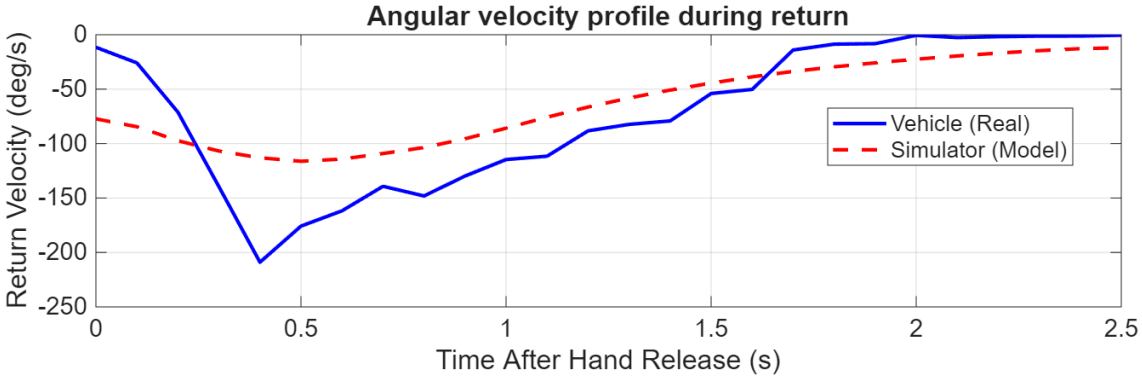



**Figure 6.12:** Angular velocity profile during the return event after tuning

The same comparison was done for the same maneuver performed at 40 Km/hr which can be found in the Appendix.
The other steering functions designed were tuned by trial and error and response from participants, while the steering system return behavior was tuned to replicate the actual vehicle and was validated objectively.

## 6.2 Validation of Steering wheel angle estimate

After the angle estimation process for every vehicle maneuver performed during the testing period, the final angle estimate was not validated with any source of ground truth data. Initial validation relied on expected kinematic behavior; for instance, step-steer and sine-sweep maneuvers instructed at 90° and steer-and-release maneuvers instructed at 180° yielded IMU-estimated angles well within the expected theoretical ranges. However, this exploratory approach is insufficient for a complete analysis of the functionality of the method. The angle estimation process which

consists of filter design, sensor bias, and numerical integration is highly sensitive to preprocessing parameters and hardware clock drift which cant be examined with this heuristic approach of validation.

Therefore, it was decided to validate at least some part of the estimation algorithm, which is the angle estimation when the vehicle is static (with vehicle movement captured by the Muse IMU). This will serve as a step to further explore the robustness and validity of the estimation algorithm when a ground truth data from the vehicle CAN bus is available in the future. This validation step was executed in the driving simulator since there was the option to log the steering angle input. The entire experimentation performed and the observations and tradeoffs are discusses further allowing the algorithm's performance to be objectively quantified before eventual checking against the vehicle CAN data. .

### 6.2.1 Experiment in SIM IV

To replicate the physical vehicle setup as closely as possible, the Muse IMU was mounted to the SIM IV steering wheel at a similar offset radius and tilt angle as it was mounted in the vehicle. After that, a set of maneuvers were performed, like a slalom maneuver with increasing frequency (look at the first few seconds in fig 6.13), a maneuver with 90°, 180°, 270° and 360° angle inputs with initial and final impulse inputs for time synchronization and interpolation into same array size for further comparison. The simulator logged the steering wheel angle and angular rate at 100 Hz, serving as the absolute ground truth reference. Simultaneously, the IMU logged the 6-axis kinematic data, which was post-processed through the identical complementary filter algorithm (without the vehicle motion compensation) used for the angle estimation with the vehicle test data. To avoid confusion, just the slalom maneuver is discussed.

A critical challenge in multi-sensor data logging is the absence of a synchronized master clock. The IMU and the simulator systems were turned on manually to log, resulting in a substantial initial time offset (approximately 5.85 seconds). Furthermore, although both systems nominally reported a 100 Hz sampling rate, consumer-grade IMU hardware is subject to internal crystal oscillator drift. The following image shows the plot of the steering wheel angle from the simulator and the estimation algorithm after removing the sensor startup delay.

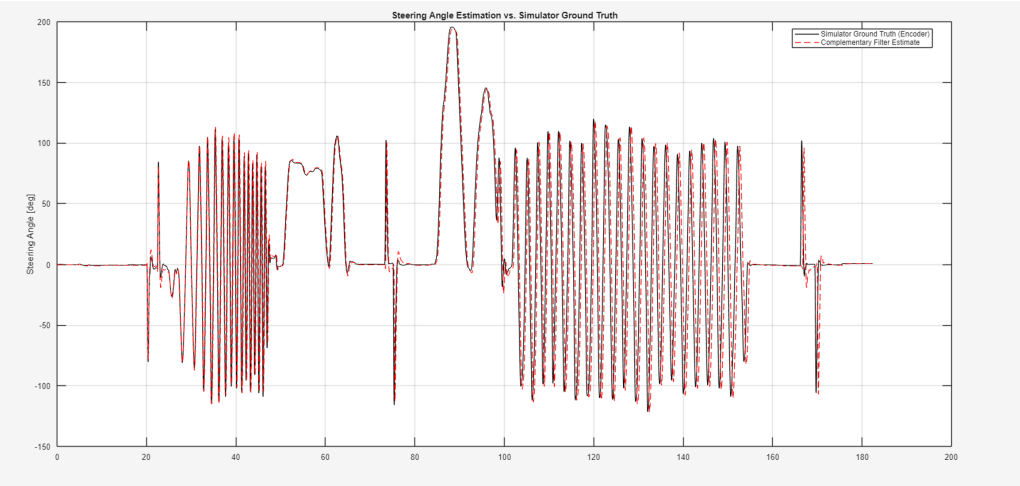



**Figure 6.13:** Plot of steering wheel angle from angle estimate and simulator after initial startup delay sync

To make this hardware clock drift easy to understand, consider two stopwatches that both tick exactly once per second (1 Hz). If one stopwatch relies on a cheaper and slightly slower quartz mechanism, its screen might display exactly 180.00 seconds when 180.49 seconds have actually elapsed in the real world. Similarly, although the IMU software blindly tags each data packet with a mathematically perfect 0.01-second increment in the data log, the actual physical time elapsed between these samples is slightly different. Over the 146.0-second validation interval, a purely kinematic time-alignment revealed a relative hardware clock drift.

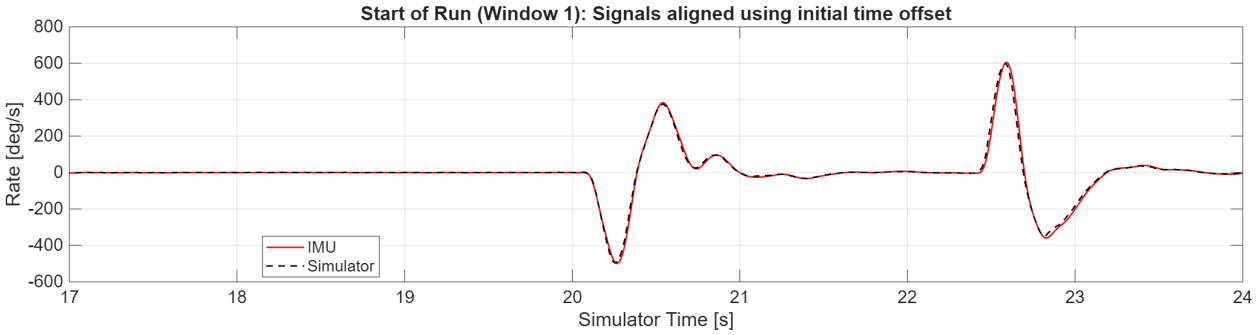



**Figure 6.14:** Initial impulse event used for sync

As shown in the drift analysis plots, if only a static initial time offset is applied, the IMU signal progressively loses phase alignment with the simulator reference, culminating in a nearly half-second phase delay by the end of the run, and this drift in time is also subject to how long the maneuver was performed; the other test case was performed for around 6 mins and the drift was around 1 second.

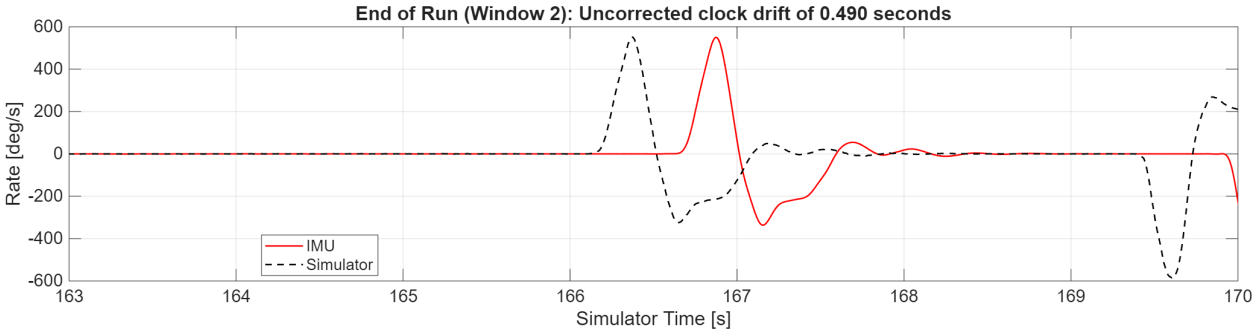



**Figure 6.15:** Final impulse event to show hardware clock drift

To rectify this discrepancy, a mathematical time correction (an affine mapping, $t_{mapped} = a \cdot t_{imu} + b$) was applied. By cross-correlating sharp steering movements (impulse inputs at the start and end) serving as signal flags, physical time anchors were established. This linear equation mathematically stretched the IMU's raw timeline to align perfectly with the simulator's clock which is considered to be accurate, converting the IMU's nominal timestamps into true physical timestamps and effectively eliminating the hardware drift. The following figure shows the aligned plots,

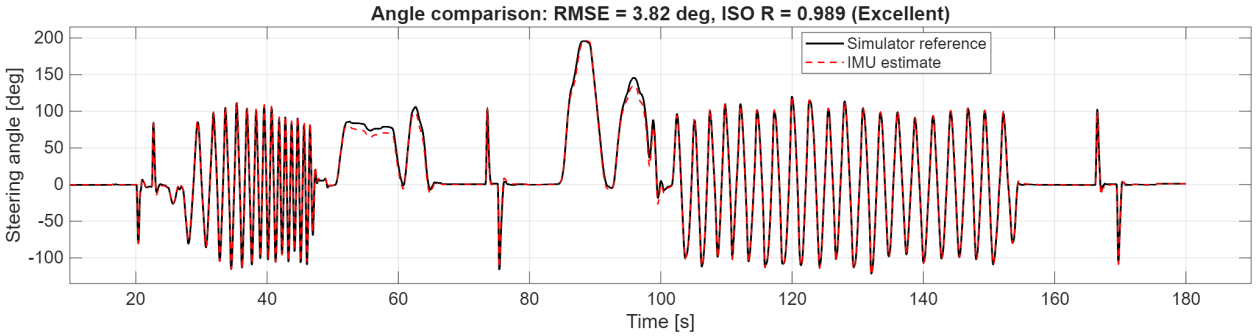



**Figure 6.16:** Steering wheel angle profiles after time correlation

Finally, to objectively quantify the correlation between the IMU estimate and the simulator ground truth, the previously used ISO/TS 18571 standard was again followed. This standard mandates a strict rule for comparison: evaluated signals must share an identical number of samples and a strictly constant sampling interval ($\Delta t$).

This prerequisite of identical number of samples posed another challenge. While the affine time mapping step successfully corrected the timestamps (for the slalom maneuver, shifting the IMU timestamp of 146.00 s to its true physical time of 146.49 s with reference to the simulator time log), it does not change the number of samples the array. To avoid any confusion, 146 secs is the approximate duration between the impulse inputs which is of interest. Because the IMU clock ran slower, it inherently collected fewer values (36448) over the test duration than the simulator did (38430). Therefore, a direct point-by-point subtraction between the arrays was impossible which is essential for the scores.

To fulfill the ISO standard's prerequisites, the drift-corrected IMU data was resampled. Using piecewise cubic Hermite interpolation (PCHIP), a continuous curve was drawn through the newly time-aligned IMU data and re-evaluated at the exact uniform 100 Hz time steps used by the simulator. This final step ensured both signals shared a perfectly matching time grid and identical array lengths, allowing to proceed to the objective scoring.

### 6.2.2 Validation and Tradeoffs

The following scores show that the complementary filter approach for angle estimation tracks the simulator ground truth pretty accurately. The overall Root Mean Square Error (RMSE) across the 180-second maneuver sequence is 3.82°, with a Mean Absolute Error (MAE) of 2.44°. The maximum absolute error (14.6°) occurs momentarily during the sharpest step-steer transitions, likely due to slight physical compliance in the IMU mount or minor phase lag inherent to the complementary filter's low-pass characteristics or the choice of the filter parameters.

The objective ISO/TS 18571 metrics further validate the robustness of the algorithm. The comparison yielded an overall rating of $R = 0.989$, classifying the correlation as "Excellent" against the standard's threshold of 0.94. The sub-metrics break down as follows:

- **Corridor Score (Z = 0.999):** The IMU estimate almost entirely remains within the tight inner corridor bounds relative to the ground truth.
- **Phase Score (EP = 1.000):** Thanks to the affine clock correction preprocessing, the phase alignment is perfect, meaning the complementary filter introduces no significant temporal delay during dynamic steering.
- **Magnitude (EM = 0.974) and Slope (ES = 0.971):** The algorithm accurately captures both the peak amplitudes of the steering maneuvers and the transient angular rates (derivatives).

While the simulator provides a reliable baseline for mathematical validation, certain tradeoffs must be acknowledged when extrapolating these results to physical vehicle testing. The SIM IV steering wheel does not perfectly replicate the road vibrations, cabin roll/pitch dynamics (motion was turned off), or harsh shock events (such as hitting a kerb) present in a real vehicle. Because the complementary filter relies on the accelerometer to bound the gyro integration, the absence of aggressive translational noise in the simulator likely represents a best-case scenario. When CAN bus ground truth becomes available in the future, it is expected that the RMSE may increase slightly due to real-world vehicle body motion and the rotations of the reference IMU (RT3000) which was used as the reference to compute accelerometer based angle. On the whole, this simulator baseline confirms that the core kinematics and math model of the estimation algorithm are fundamentally sound for the static case, while the robustness and functionality of the algorithm during vehicle motion is yet to be validated and explored further.

## 6.3 Subjective Assessments

### 6.3.1 Experiment Design

The subjective assessment of the developed steering model was conducted in Sim IV driving simulator at vti, Göteborg. Unlike studies that compare simulator performance with field experiments, the evaluation in this thesis was carried out entirely in the driving simulator and the motion of the simulator was turned off during the test. The objective was to assess the steering feel and driver perception of the developed steering subsystem (part of the new EV model) by comparing it with the existing Hydraulic Power Steering (HPAS) model currently implemented in the simulator.

Each participant was subjected to the two different vehicle models during the experiment. The first model represented a fully electric vehicle equipped with the developed EPAS system, while the second represented an internal combustion engine vehicle equipped with the existing HPAS system. To eliminate learning effects and participant bias, the order in which the steering models presented was randomized, and the participants were not informed which vehicle model they were driving.

Before the formal evaluation, each participant completed a trial session in the simulator. During this session, the participants were free to drive in both urban and highway environments to become accustomed to the simulator dynamics and the steering characteristics. They were encouraged to perform different steering maneuvers until they felt comfortable with the simulator.

After that, the participants proceeded to the dedicated test track scenario. The evaluation consisted of two standardized steering manoeuvres: a Double Lane Change (DLC) test and a Slalom test. The test tracks were designed according to the corresponding ISO standards, with the cones positioned to satisfy the prescribed geometrical dimensions of each manoeuvre. To reduce any bias caused by the order of the manoeuvres, the sequence of the Double Lane Change and Slalom tests was randomized for each participant. Furthermore, each manoeuvre was performed at two target vehicle speeds: 30 km/h and 50 km/h, allowing the steering behaviour to be evaluated under both low- and moderate-speed driving conditions.

Following the completion of each steering manoeuvre, the participants completed a structured questionnaire to assess the steering characteristics of the vehicle. The questionnaire included several attributes related to steering feel, steering feedback (assist torque and self aligning behavior), steering effort, on-centre behavior, vehicle controllability and overall driver confidence. Each attribute was evaluated using a seven-point Likert scale. Participants completed the questionnaire immediately after each test to ensure that their ratings accurately reflected their driving experience.

The subjective assessment was designed to determine how effectively the developed R-EPAS model reproduces the steering characteristics expected from a modern electric vehicle and how it compares with the existing HPAS model currently used in the

simulator. The collected responses were analysed by comparing the average ratings for each question get deduce an overall conclusion on the developed model's realism.

### 6.3.2 Participants rating and feedback

A total of 17 participants, ranging in age from 24 to 60 years, took part in the study. Among them, one participant was pilot driver who's response and feedback was used to tailor the questions and the test procedure better for the other participants. Consequently, the pilot driver's questionnaire responses were not included in the final statistical analysis.

During the subjective evaluation, two participants discontinued the experiment due to simulator sickness and were therefore unable to complete the procedure to fill the questionnaire. Their incomplete responses were excluded from the final analysis. As a result, the subjective evaluation presented in this chapter is based on the responses of the remaining participants (14) who successfully completed the entire experimental procedure.

The collective responses to the introductory questions are presented in the following section, followed by the participants' ratings and feedback on the steering performance of the two vehicle models evaluated in the simulator.

#### 6.3.2.1 Driver Background and Experience

The first section of the questionnaire focused on the participants' driving background and experience. This information was collected to better understand the characteristics of the participant group and to ensure that the subjective evaluation represented drivers with varying levels of driving experience and familiarity with driving simulator.

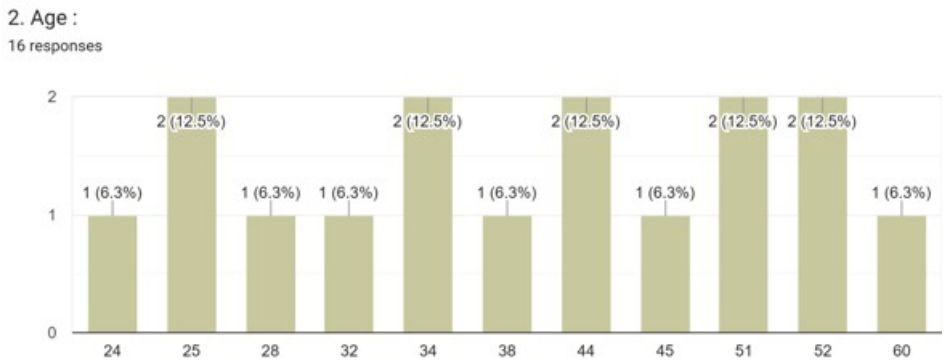



**Figure 6.17:** Chart of participants age

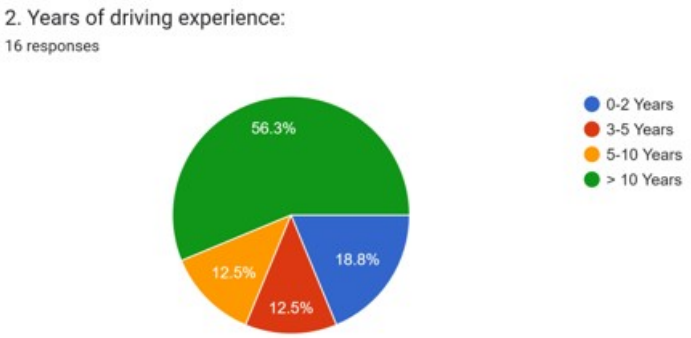



**Figure 6.18:** Pie chart showing driving experience of participants

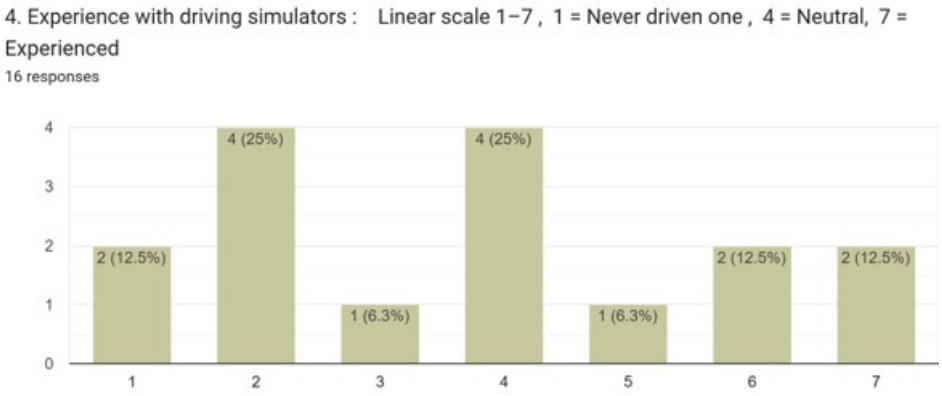



**Figure 6.19:** Chart showing participants experience with driving simulator

#### 6.3.2.2 Subjective comparison of steering systems

The second section of the questionnaire focused on the subjective comparison of the two steering systems. The objective was to identify if participants were able to differentiate between the two systems and also identify the effect of rack inertia in the EPS system.

The two vehicle models were identified simply as System 1 and System 2 throughout the experiment. Furthermore, the order in which the two steering systems were presented was randomized for each participant to minimize learning effects and bias.

After completing the prescribed driving manoeuvres with each steering system, the participants evaluated both systems using a structured questionnaire consisting of 11 questions. These questions covered different aspects of steering performance, including steering feel, steering effort, steering response, on-centre behaviour, controllability and the effect of inertia (asking if they felt like moving a heavy mass which is expected due to the simplicity of the model). Each question was rated

using a seven-point Likert scale, where a higher score indicated a more favourable evaluation of the steering characteristic being assessed.

The mean ratings and corresponding standard deviations for all eleven evaluation criteria are presented in the following figures and tables. These results provide a comprehensive comparison of the subjective performance of the two steering systems.

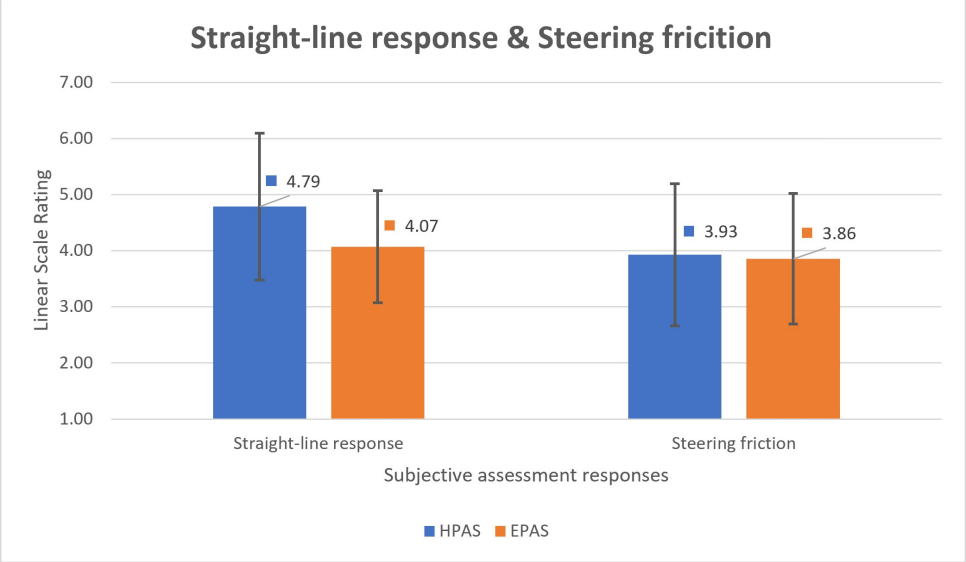



**Figure 6.20:** Straight-line response & Steering friction

Figure 6.20 shows the participants ratings for straight-line response and steering friction. The mean rating for straight-line response was 4.79 for HPAS and 4.07 for EPAS, showing a moderate preference towards the HPAS system in this aspect. For steering friction, the mean ratings were 3.93 for HPAS and 3.86 for EPAS, indicating a very small difference between the two systems. This suggests that the participants perceived the friction characteristics of the two steering systems as relatively similar. The standard deviation, represented by the error bars, shows the spread of individual responses and indicates that the perception of steering characteristics varied among the participants.

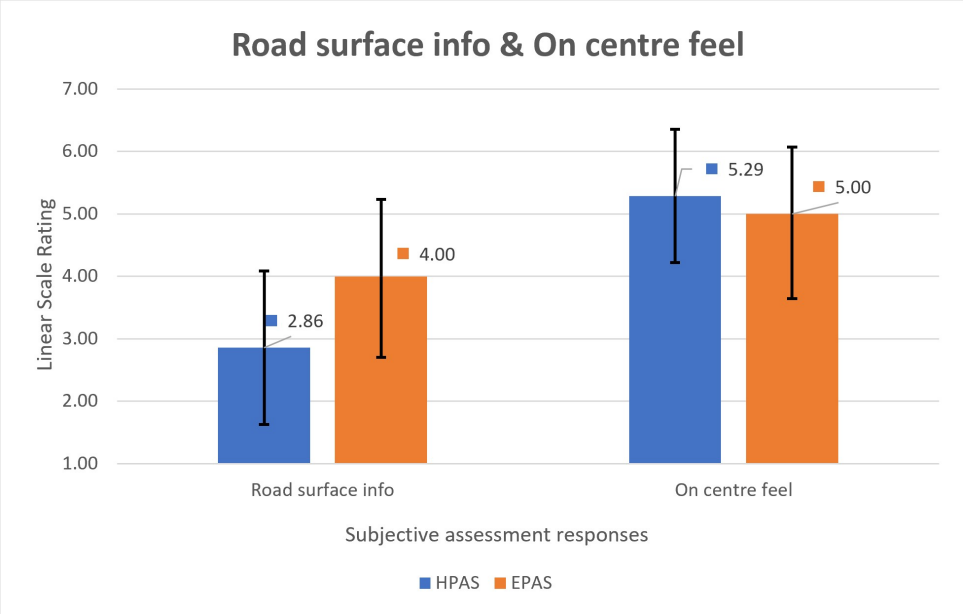



**Figure 6.21:** Road surface info & On-center behavior

Figure 6.21 presents the result of participants evaluation in terms of road surface information and on-centre feel. EPAS received a considerably higher mean rating for road surface information 4.00 compared with HPAS 2.86, suggesting that participants perceived more information from the road through the EPAS system which was unexpected since the heavy mass of the rack acts as a low pass filter absorbing the high frequency vibrations. The reason for the vibrations could also be because of the delay in the controller compensating reference which thereby induces ripples in the feedback torque apart from the road surface information.

For on-centre feel, where a rating of 4 means the steering felt natural and stable, HPAS achieved a mean rating of 5.29, while EPAS received 5.00. Although HPAS was rated slightly higher, the relatively close mean values indicate that the on-centre characteristics of the two systems were perceived as broadly similar and acceptable.

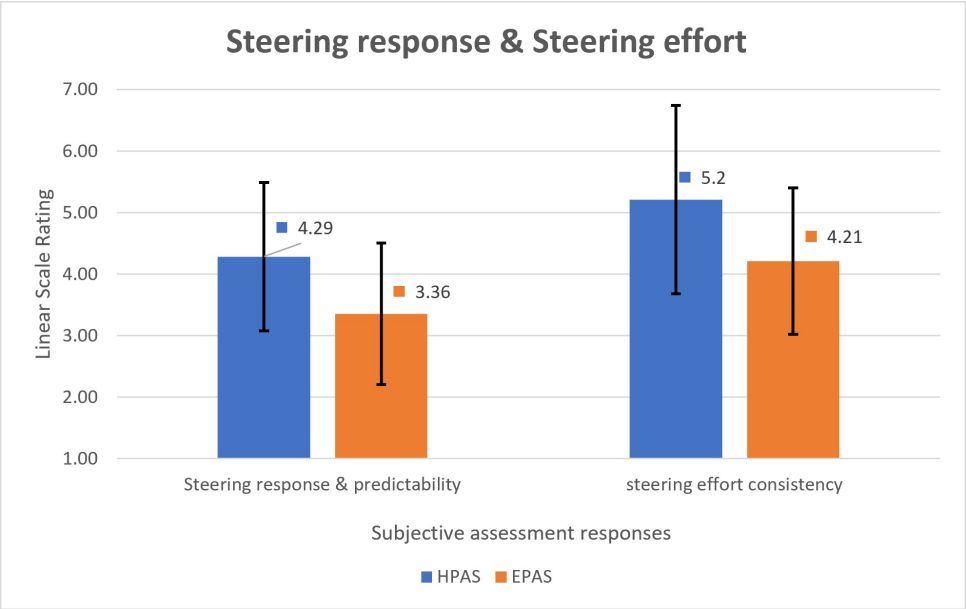



**Figure 6.22:** Steering response & Steering effort

Figure 6.22 presents the participants evaluation of steering response and predictability and steering effort consistency for the two systems. For steering response and predictability, where a rating of 4 means the system is fully controllable, HPAS received a mean rating of 4.29, while EPAS received a mean rating of 3.36. This indicates that the participants felt that both the systems provided controllable response. For steering effort consistency, HPAS achieved a mean rating of 5.20, compared with 4.21 for EPAS. The results therefore suggest that the HPAS system was perceived as more consistent in terms of steering effort.

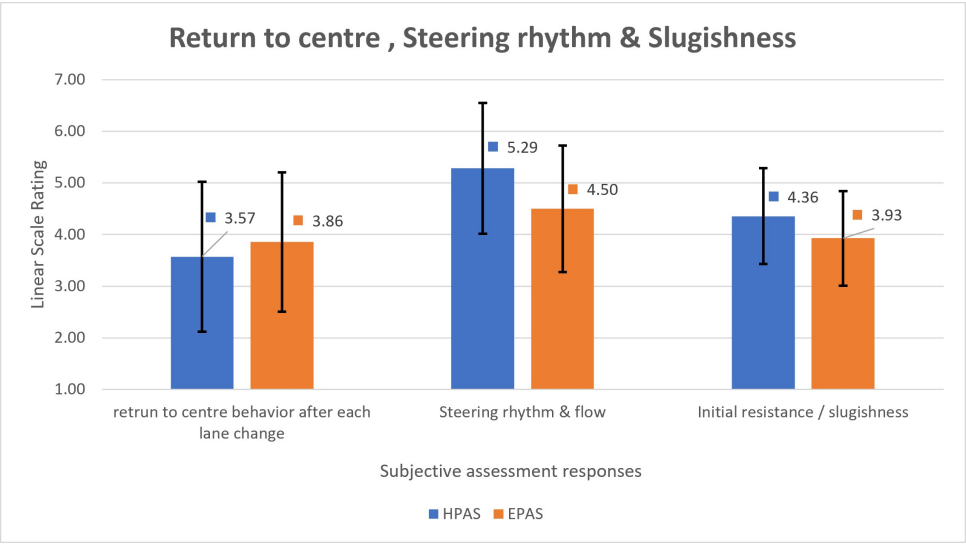



**Figure 6.23:** Return to center behavior, Steering rhythm & flow and Initial resistance (high inertia effect)

Figure 6.23 shows the participants evaluation of return-to-centre behaviour after a

lane change, steering rhythm and flow. For return-to-centre behaviour, where a rating of 4 indicated natural return profile, HPAS received a mean rating of 3.57, while EPAS obtained 3.86, indicating both had a natural return behavior, not stiff or not too slow. The steering rhythm and flow showed a more noticeable difference, with HPAS rated 5.29 compared with 4.50 for EPAS, meaning participants felt HPAS was more rhythmic but this could also be because of the perception of the vehicle body motion during fast switches where the old model is less responsive compared to the new vehicle model.

For initial resistance or sluggishness, where a lower rating means that the steering wheel felt heavy before initial moion, HPAS received 4.36, whereas EPAS was rated 3.93. This result is inconclusive since most of the participants felt that both models performed similar except a few who were able to distinguish the heaviness of the EPS model.

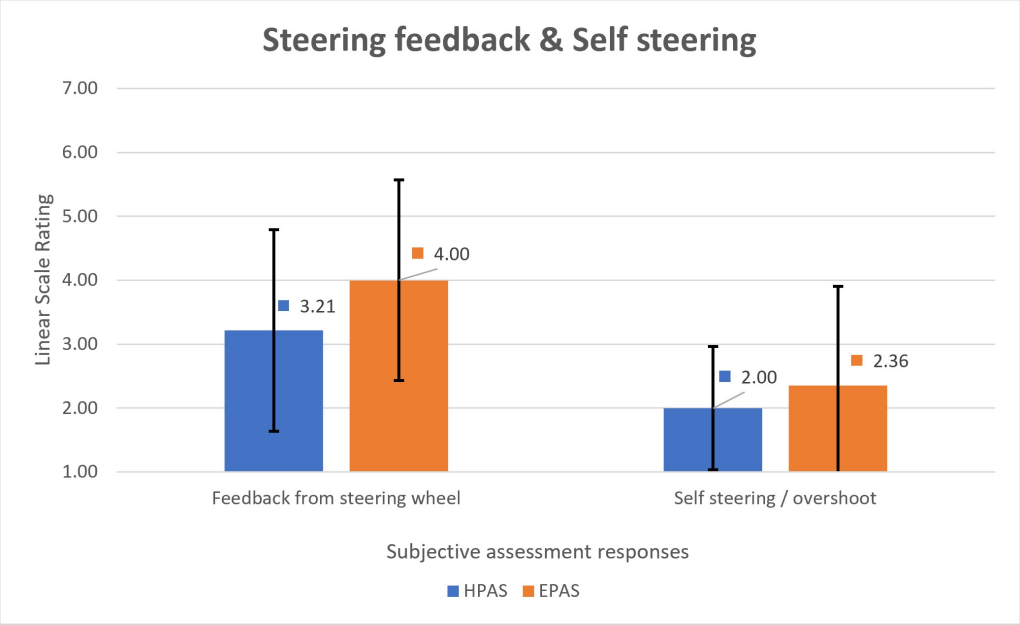



**Figure 6.24:** Steering feedback & Overshoot (steering moving without input)

Figure 6.24 presents the results participants evaluation for steering-wheel feedback (torsion bar torque) and self-steering and overshoot behaviour due to the effect of high rack inertia in EPAS. The EPAS system received a mean rating of 4.00 for steering feedback, compared with 3.21 for HPAS, both indicating near neutral rating.

For self-steering/overshoot, where a lowest rating means that the driver didnt feel the overshoot or inertial effect of the steering wheel moving on its own, HPAS obtained a mean rating of 2.00, while EPAS received 2.36. The difference is relatively small, and very few participants were able to feel the heaviness of the new steering system, meaning that a common driver couldnt really tell the systems apart based on the physics. This effect of EPAS can be explored further with professional test

drivers, then the result would be even more conclusive.

#### 6.3.2.3 Distribution of Subjective Evaluation Outcome

Figure 6.25 presents the overall distribution of outcomes from the subjective evaluation conducted in the driving simulator, where participants were asked to rate which steering model would they prefer over another.

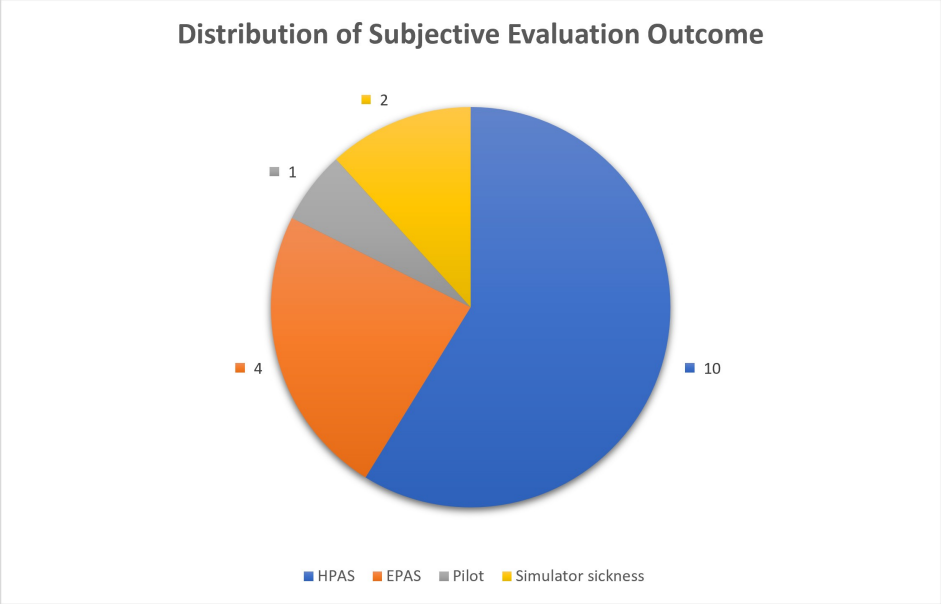



**Figure 6.25:** Distribution of Subjective Evaluation Outcome

The results show that most participants (10) had a more favorable impression of the HPAS system, while 4 participants preferred the EPAS system. This indicates that, under the tested simulator conditions, a larger number of participants perceived the HPAS characteristics as more convenient, predictable, or responsive. However, the preference for EPAS among several participants also indicates that the developed EPAS model provided acceptable steering characteristics for some drivers. One pilot driver who participated also preferred EPAS, but that response was excluded from the main results.

The results should not be interpreted as a direct indication that HPAS is superior to EPAS, since subjective steering perception is affected by individual preferences, and the fidelity of the developed model in this thesis. The higher preference for HPAS nevertheless indicates that the developed EPAS model requires further refinement to achieve steering characteristics closer to those of a real electric vehicle which wasn't fully achievable in this work. Access to the steering CAN of the test vehicle (Volvo EC40) would allow further refinement of the steering functions and scope to objectively compare the feedback torque profile and fully validate the functional steering model built during this thesis.

# 7

# Conclusion

## 7.1 Summary & Project Outcomes

The main outcome of the thesis is the modeling and implementation of a Rack - Electric Power Assisted Steering system (R-EPAS) model for electric vehicle model for use in the driving simulator (SIM IV). The developed model will be replacing the exciting Hydraulic Power Assisted Steering system(HPAS) model and provides the framework for investigating the steering characteristics of an electric vehicle model in the simulator environment and also testing additional assist functions if developed in the future in the simulator before integrating into a test vehicle.

A mathematical model of R-EPAS system was developed in MATLAB/Simulink, including torsion bar, steering column pinion, motor pinion, Lugre friction model (built but not implemented in the simulator), rack dynamics, road induced forces and electric motor dynamics (RL - circuit). A virtual rack approach was also implemented to represent the desired rack behavior and provide a basis for the control of the real rack (high inertia). The motor force was generated using a combination of basic assist, active damping, and feedback control, while the plant was controlled using a PID controller.

Non-linear assist characteristics (Boost curves) was developed to provide more realistic steering torque response. The assist curve was designed based on the characteristics described in the literature and adapted for the developed R-EPAS model. The control strategy was then tuned through simulation to obtain stable rack tracking and an appropriate steering response.

The model was further integrated with the existing electric vehicle model and tested through the Sim IV driving simulator. This allowed the steering behavior to be evaluated under different driving conditions and provided a connection between the mathematical model and the driver's subjective perception. The developed model was compared with the existing HPAS model to investigate differences in steering feel and overall steering behavior.

A technique to estimate the steering wheel angle input from a two IMU setup (external sensors) was developed and partially validated. This will serve as a approach that can be adapted later during further testing if done without relying on OEMs by just mounting external sensors.

Finally, a subjective evaluation was conducted on the driving simulator with participants comparing the HPAS steering system with the internal combustion engine and the EPAS steering systems with the electric vehicle. The results showed that both systems provided distinguishable steering characteristics, although a larger number of participants preferred the HPAS system under the tested conditions. The evaluation also identified areas of the EPAS model that require further refinement, particularly in terms of steering response, steering effort, and overall steering feel.

Overall the thesis demonstrates that an R-EPAS system can be sucessfully modelled and implemented in the SIM IV driving simulator. The model provides the foundation for further development of electric steering system, ADAS functions, ESC and demonstrates the usefulness of combining mathematical modelling, simulation, real-vehicle measurements, and subjective driver evaluation when developing and assessing steering feel.

## 7.2 Limitations

Although a functional R-EPAS model was successfully implemented, the study encountered several technical limitations.

First, the development of a high-fidelity steering model requires precise physical parameters (e.g., rack, torsion bar, column, and motor compliances) as well as proprietary OEM maps for assist and damping profiles. Lacking direct access to these test-vehicle-specific variables, the project relied on approximations and previous literature. For example, fundamental characteristics of the boost curve—such as the deadband limits, assist profile slopes as a function of torsion bar torque, and torque saturation points—had to be estimated. This constraint extended across multiple subsystem blocks, each requiring specific parameters that were ultimately unavailable for the physical test vehicle.

Second, the vehicle's overall lateral behavior is highly dependent on coupled subsystems, specifically the suspension and tires. The complexity of the existing Magic Formula tire model was beyond the scope of modification for this project. Additionally, a lack of specialized measurement equipment restricted the ability to adjust the suspension subsystem. Consequently, the simulated lateral dynamics variables used for assessment—specifically yaw rate and lateral acceleration—did not perfectly match the physical sensor measurements.

Third, the current controller design presents stability and robustness limitations. The feedback mechanism employs a fixed-gain PID controller designed around a simplified second-order linear system, whereas the actual steering plant is non-linear. The use of fixed parameters limits the model's global stability across various operating regions, causing noticeable issues during extreme handling limits and at high vehicle speeds (exceeding 100 km/h). Furthermore, tuning difficulties regarding pa-

rameter optimization led to the deactivation of the active return function in the final implementation. As a result, the model relies entirely on the natural tire-aligning torques generated by the wheel subsystem for self-centering.

Finally, restricted access to the test vehicle's CAN bus prevented the direct measurement of ground-truth steering torque and internal steering ECU signals. Because of this data acquisition constraint, the steering wheel angle had to be estimated using an externally mounted IMU. Furthermore, the simulator's torque feedback was tuned using the legacy HPAS model as a baseline rather than utilizing empirical EPAS torque maps, which would have yielded a model with much higher fidelity.

An additional limitation was in the testing procedure. The experiments were conducted at the StoraHolm driving school track, which lacks the standardized infrastructure of a dedicated automotive proving ground. Meaning, although the selected maneuvers were inspired by ISO standards, strict adherence to ISO testing procedures was not possible. The absence of precise reference lines, cone layouts, and distance markers prevented the execution of formally standardized trajectories. Thereby, the tests were performed with no proper markings and distance references which means that an objective comparison between the real vehicle and the model integrated into the simulator cannot be performed. This is because it is nearly impossible to replicate the maneuver in the exact same way as performed by the driver during testing.

## 7.3 Future Work

Future work or continuation should prioritize acquiring direct access to the test vehicle's CAN bus to extract steering signals to further improve the model performance. Additionally, further vehicle tests should be conducted on a dedicated automotive proving ground equipped with standardized reference markings. This would enable the execution of formal ISO standard maneuvers and provide the precise empirical data which will be helpful in comparing the model and the real vehicle behavior from the sensor measurements and simulator logs, thereby making the validation even stronger.

To address the limitations of the current controller design, future iterations of the model should transition away from a fixed-gain PID controller design. Implementing advanced control strategies, such as gain scheduling or an observer-based feedforward control design, would reduce the load on the feedback controller. This approach would significantly enhance the system's global stability and robustness, particularly across highly non-linear operating regions and at vehicle speeds exceeding 100 km/h. Furthermore, the active return function should be revisited; incorporating precise speed and driver-torque dependencies into the return logic would restore the system's natural self-centering behavior without relying solely on tire-aligning torques. Previous research work shows that the steering system will show differences in behavior, when altering the controller operation (different combinations of steering

functions active), that are significantly different. This means that the controller affects the character of the model greatly and needs a lot more focus.

Furthermore, the subjective evaluations conducted during this study provided critical insights into driver perception, highlighting areas for refinement. With this and some form of ground truth data, the model should be validated again. For that, a secondary series of simulator-based subjective assessments should be executed. This iterative evaluation loop will help determine whether the perceived disparity in steering feel between the legacy HPAS baseline and the new EPAS system has been successfully minimized and at the same time check model behavior with actual vehicle. Ultimately, while current results validate the functional architecture of the R-EPAS model, this continuous tuning process remains essential to achieving a truly realistic steering feel.

Finally, the developed R-EPAS model provides a strong foundation for simulator study and room to add driver assistance functions on top of it. Future work should also have a stage for the angle estimation algorithm developed, this will make the method quite standard for use in further experiments when there is no access to get signals from the vehicle.

# Bibliography


[1] M. Harrer and P. Pfeffer, Eds., *Steering Handbook*. Cham, Switzerland: Springer, 2017.

[2] B. Jacobson *et al.*, *Vehicle Motion Engineering*. Gothenburg, Sweden: Chalmers University of Technology, 2024.

[3] R. N. Jazar, *Vehicle Dynamics: Theory and Application*, 2nd ed. New York, NY, USA: Springer, 2014.

[4] K. J. Åström and R. M. Murray, *Feedback Systems: An Introduction for Scientists and Engineers*, v2.11b ed. Princeton, NJ, USA: Princeton University Press, 2012..

[5] Swedish National Road and Transport Research Institute (VTI). (2026). *Driving Simulators – Sim IV*. [Link]

[6] OXTS RT3000 V4 and NAVsuite. (2026). *Product site*. [Link] *About the software*. [Link]

[7] MuSe V3 wireless IMU and MuSe V3 viewer. (2026). *Product site*. [Link] *Logging software*. [Link]

[8] Variants of EPS - Bosch Mobility. (2026). *Reference site*. [Link]

[9] O. Nordström and S. Nordmark, "Test procedures for the evaluation of the lateral dynamics of commercial vehicle combinations," *Automobil-Industrie*, vol. 23, no. 2, pp. 63–69, Jun. 1978.

[10] Anders Karlsson, *Test Procedures and Evaluation Tools for Passenger Vehicle Dynamics*. Published, 2014.

[11] J. Gao and Z. Wang, "Modelling of Fully Electric Vehicle For Driving Simulator," Master's thesis, Dept. Mech. and Maritime Sci., Chalmers Univ. of Technol., Gothenburg, Sweden, 2024.

[12] M. Hjort, S. Kharrazi, O. Eriksson, and M. Hjälmdahl, "Limit handling in a driving simulator," VTI, Linköping, Sweden, VTI rapport 861A, 2015.

[13] E. Obialero, "A Refined Vehicle Dynamic Model for Driving Simulators," Master's thesis, Dept. Appl. Mech., Chalmers Univ. of Technol., Gothenburg, Sweden, 2013.

[14] J. Gómez Fernández, "A Vehicle Dynamics Model for Driving Simulators," Master's thesis, Dept. Appl. Mech., Chalmers Univ. of Technol., Gothenburg, Sweden, 2012.

[15] A. Gröndahl, "Functional Modelling and Simulation of an Electric Power Assisted Steering: Development of an advanced engineering tool," Master's thesis, Dept. Mech. and Maritime Sci., Chalmers Univ. of Technol., Gothenburg, Sweden, 2018.

[16] U. Khan and A. Bianchi, "Steering system development using test rig and driving simulators," Master's thesis, Dept. Vehicle Eng., KTH Royal Inst. of Technol., Stockholm, Sweden, 2019.

[17] Y.-B. Jia, "Rotation in the Space," COMS 4770/5770 Notes, Sep. 2024.

[18] S. Nordmark, *VTI Driving Simulator: Mathematical Model of a Four-Wheeled Vehicle for Simulation in Real Time*, VTI Report 267A, Swedish Road and Traffic Research Institute, Linköping, Sweden, 1984.

[19] C. Zhan, N. Xu, and Z. Ma, "Research on Modeling and Control Strategy of Electric Power Steering," *Applied Mechanics and Materials*, vols. 97-98, pp 677-680, 2011.

[20] J.-H. Kim and J.-B. Song, "Control logic for an electric power steering system using assist motor," *Mechatronics*, vol. 12, no. 4, pp. 447–459, May 2002.

[21] C. Certosini, F. Vinattieri, R. Capitani, and C. Annicchiarico, "Development of a real-time steering system model for driving simulators," *Proc. IMechE Part D: J. Automobile Engineering*, pp. 1–13, 2018.

[22] J. H. Choi, K. Nam, and S. Oh, "Steering feel improvement by mathematical modeling of the Electric Power Steering system," *Mechatronics*, vol. 78, 102629, 2021.

[23] S. Ancha, A. Baviskar, J. R. Wagner, and D. M. Dawson, "Ground vehicle steering systems: modelling, control, and analysis of hydraulic, electric and steer-by-wire configurations," *Int. J. Vehicle Design*, vol. 44, nos. 1/2, pp. 188–208, 2007.

[24] L. Bruck, B. Haycock, and A. Emadi, "A Review of Driving Simulation Technology and Applications," *IEEE Open Journal of Vehicular Technology*, vol. 2, pp. 1–21, 2021.

[25] N. Mohajer, H. Abdi, K. Nelson, and S. Nahavandi, "Vehicle motion simulators, a key step towards road vehicle dynamics improvement," *Vehicle System Dynamics*, vol. 53, no. 7, pp. 1022–1045, 2015.

[26] M. K. Salaani, G. Heydinger, and P. Grygier, "Modeling and Implementation of Steering System Feedback for the National Advanced Driving Simulator," *SAE Transactions*, vol. 111, sec. 6, pp. 1767–1775, 2002.

[27] C. Canudas de Wit, H. Olsson, K. J. Åström, and P. Lischinsky, "A New Model for Control of Systems with Friction," *IEEE Transactions on Automatic Control*, vol. 40, no. 3, pp. 419–425, Mar. 1995.

[28] B. Kim and Y. Baek, "Sensor-Based Extraction Approaches of In-Vehicle Information for Driver Behavior Analysis," *Sensors*, vol. 20, no. 18, 5197, 2020.

[29] J. F. Dols, V. Girbés-Juan, Á. Luna, and J. Catalán, "Data Acquisition System for the Characterization of Biomechanical and Ergonomic Thresholds in Driving Vehicles," *Sustainability*, vol. 12, no. 17, 7013, 2020.

[30] M. Moussa, A. Moussa, and N. El-Sheimy, "Steering Angle Assisted Vehicular Navigation Using Portable Devices in GNSS-Denied Environments," *Sensors*, vol. 19, no. 7, 1618, 2019.

[31] T. A. Nguyen, "Mathematical modeling and characteristics of automotive electric power steering systems: A state-of-the-art literature review," *Ain Shams Engineering Journal*, vol. 16, no. 9, 103516, Sep. 2025.

[32] T. Chugh, W. Chen, M. Klomp, and S. Ran, "Design and control of model based steering feel reference in an electric power assisted steering system," in *The Dynamics of Vehicles on Roads and Tracks (IAVSD)*, vol. 1, pp. 43–49, 2018.

[33] R. Rodrigues da Silva, A. M. de Almeida Pinto, M. M. Dias Santos, and E. L. Silva Teixeira, "A Model Based Control Strategy for an Electric Power Assisted Steering," *SAE Technical Paper 2017-36-0281*, 2017.

[34] C.-H. Hu, "Modeling and Simulation of Automotive Electric Power Steering System," in *Second International Symposium on Intelligent Information Technology Application*, 2008, pp. 436–440.

[35] Z. Qun and H. Juhua, "Modeling and simulation of the Electric Power Steering System," in *2009 Pacific-Asia Conference on Circuits, Communications and System*, 2009, pp. 236–239.

[36] G. L. Gil Gómez, C. Andersson Eurenius, J. Donnay Cortiñas, E. Bakker, M. Nybacka, L. Drugge, and B. Jacobson, "Validation of a Moving Base Driving Simulator for Subjective Assessments of Steering Feel and Handling," in *Proceedings of the 14th International Symposium on Advanced Vehicle Control (AVEC'16)*, Munich, Germany, Sep. 2016.

[37] B. Huber and R. Drews, "How to use objective measurement data for Vehicle Dynamics Testing," *SAE Technical Paper 2009-01-0428*, 2009.

[38] R. R. Hiremath and T. B. Isha, "Modelling and simulation of electric power steering system using permanent magnet synchronous motor," *IOP Conference Series: Materials Science and Engineering*, vol. 561, no. 1, Art. no. 012124, 2019, doi: 10.1088/1757-899X/561/1/012124.

[39] M. Euston, P. Coote, R. Mahony, J. Kim, and T. Hamel, "A complementary filter for attitude estimation of a fixed-wing UAV," in *Proc. 2008 IEEE/RSJ International Conference on Intelligent Robots and Systems (IROS)*, Nice, France, Sept. 22–26, 2008, pp. 340–345, doi: 10.1109/IROS.2008.4650766.

[40] Farid Al-Bender, Vincent Lampaert, and Jan Swevers (2005), "The Generalized Maxwell-Slip Model: A Novel Model for Friction Simulation and Compensation," IEEE Transactions on Automatic Control.

[41] Y. Wen, M. Chu, and H. Sun, "Friction parameters identification and compensation of LuGre model based on genetic algorithms," School of Automation, Beijing University of Posts and Telecommunications, Beijing, China.

# A

# Appendix 1

The Appendix chapter contains the angle estimation results for the test maneuvers for all the speed cases. Note that the U-turn, Parking and Straight drive maneuver cases are not included here and in the next chapter because they were intended for future use.

## A.1 Angle Estimation Results

### A.1.1 Double Lane Change

#### A.1.1.1 Speed - 20 Km/hr

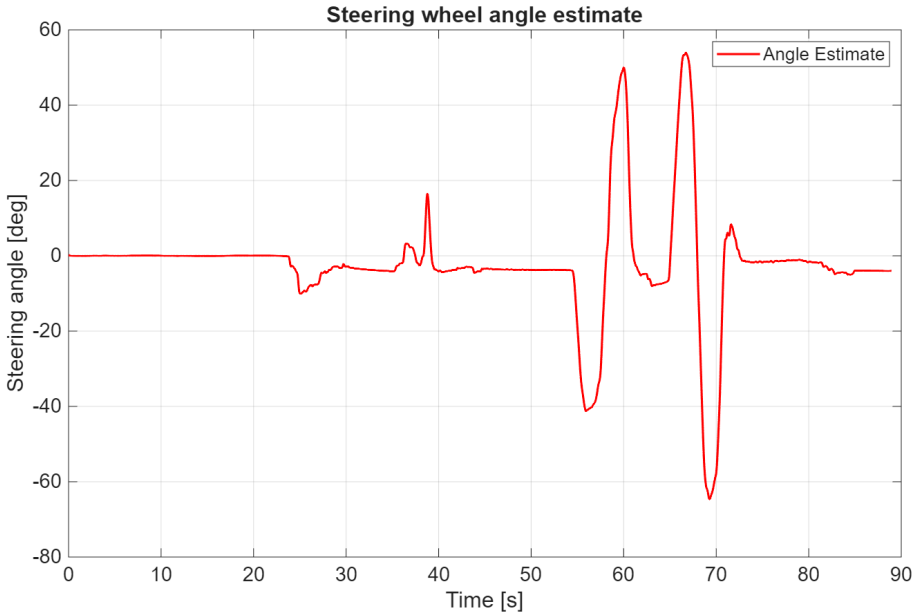



**Figure A.1:** Angle estimate for DLC maneuver performed at 20 Km/hr

### A.1.1.2 Speed - 40 Km/hr

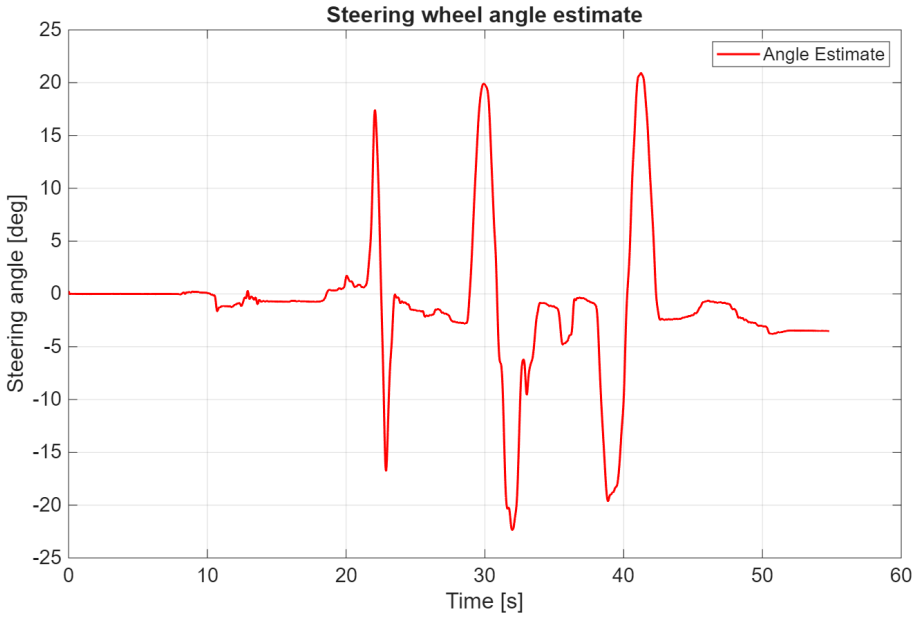



**Figure A.2:** Angle estimate for DLC maneuver performed at 40 Km/hr

### A.1.1.3 Speed - 60 Km/hr

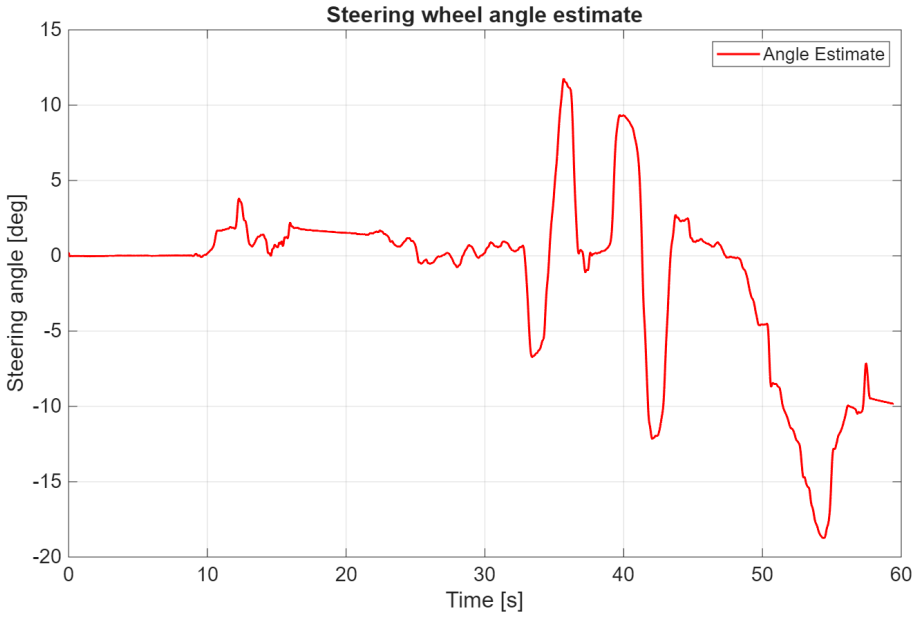



**Figure A.3:** Angle estimate for DLC maneuver performed at 60 Km/hr

#### A.1.1.4 Speed - 80 Km/hr

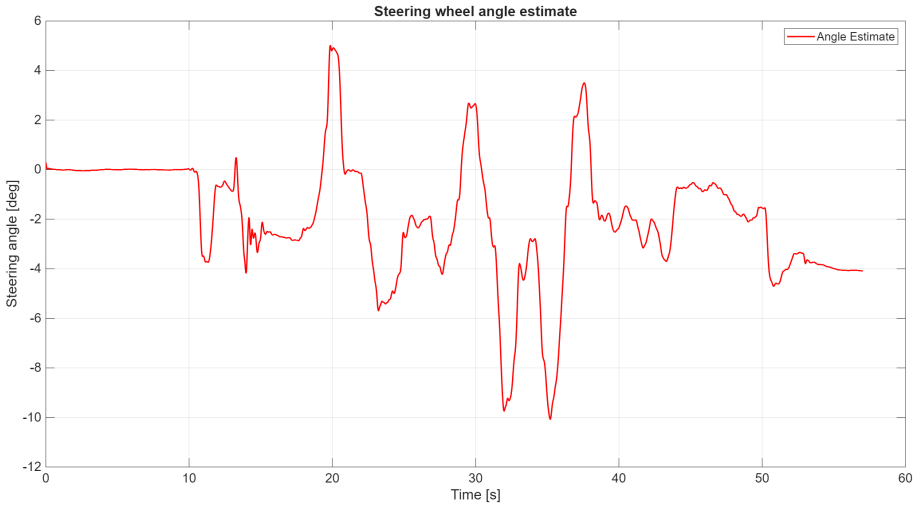



**Figure A.4:** Angle estimate for DLC maneuver performed at 80 Km/hr

### A.1.2 Single Lane Change

#### A.1.2.1 Speed - 20 Km/hr

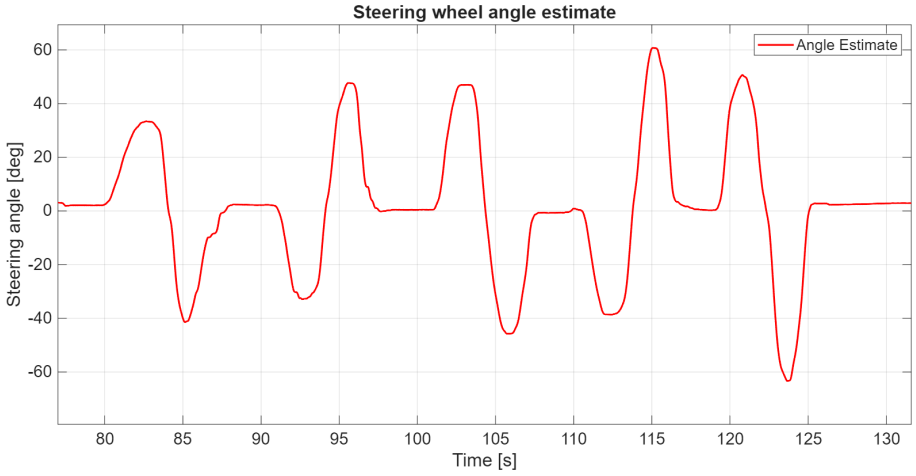



**Figure A.5:** Angle estimate for SLC maneuver performed at 20 Km/hr

### A.1.2.2 Speed - 40 Km/hr

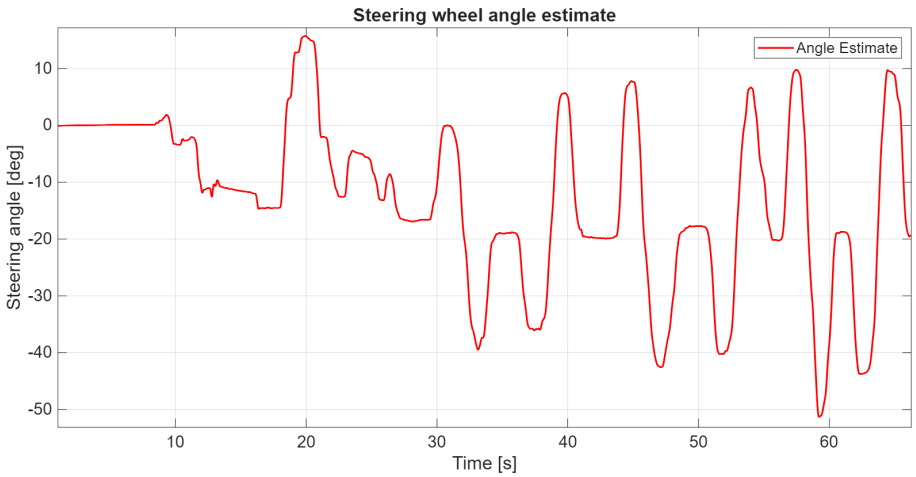



**Figure A.6:** Angle estimate for SLC maneuver performed at 40 Km/hr

### A.1.2.3 Speed - 60 Km/hr

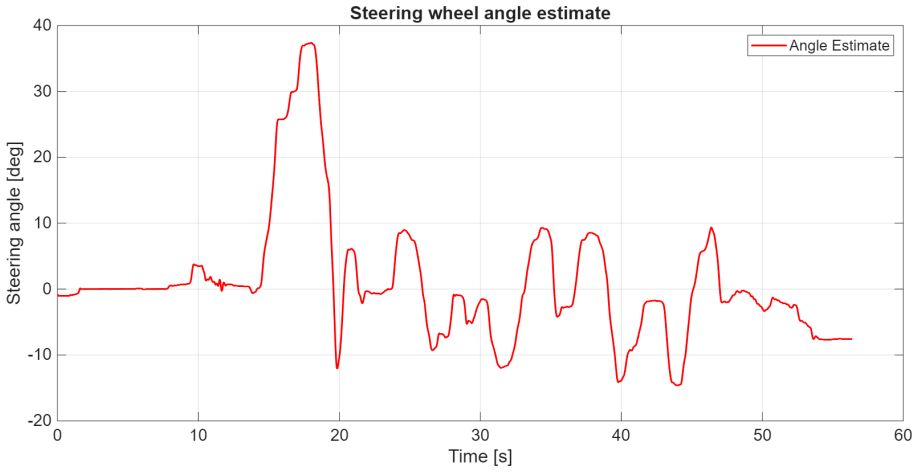



**Figure A.7:** Angle estimate for SLC maneuver performed at 60 Km/hr

#### A.1.2.4 Speed - 80 Km/hr

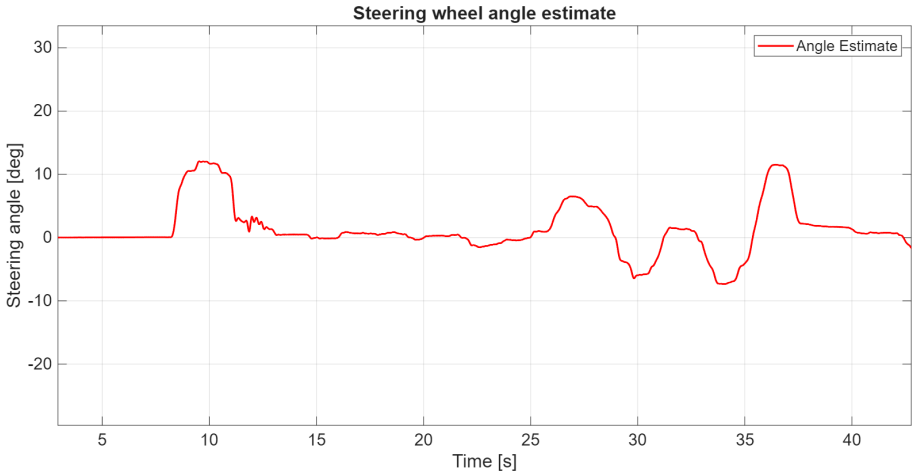



**Figure A.8:** Angle estimate for SLC maneuver performed at 80 Km/hr

### A.1.3 Sine Sweep (90 degs)

#### A.1.3.1 Speed - 20 Km/hr

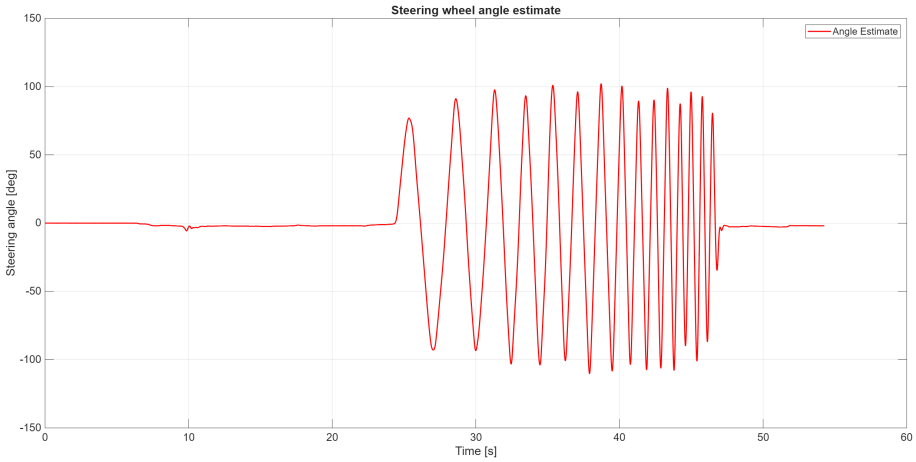



**Figure A.9:** Angle estimate for Sine Sweep (90 degs) maneuver performed at 20 Km/hr

### A.1.3.2 Speed - 40 Km/hr

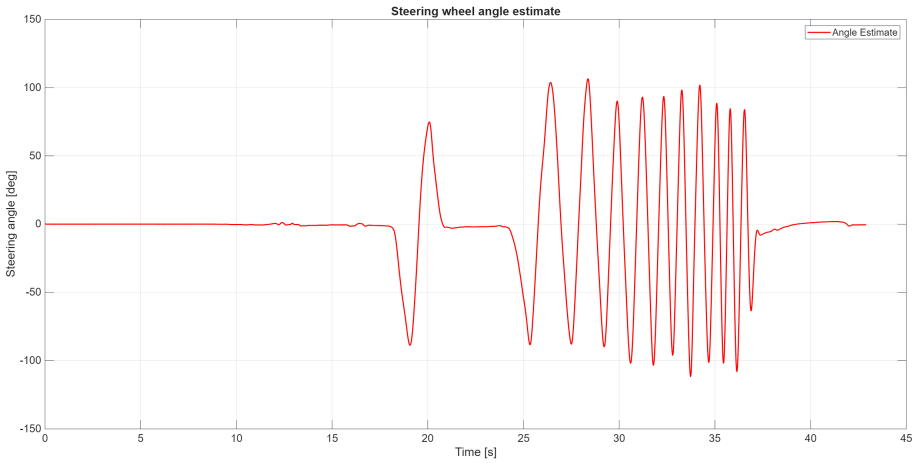



**Figure A.10:** Angle estimate for Sine Sweep (90 degs) maneuver performed at 40 Km/hr

### A.1.3.3 Speed - 60 Km/hr

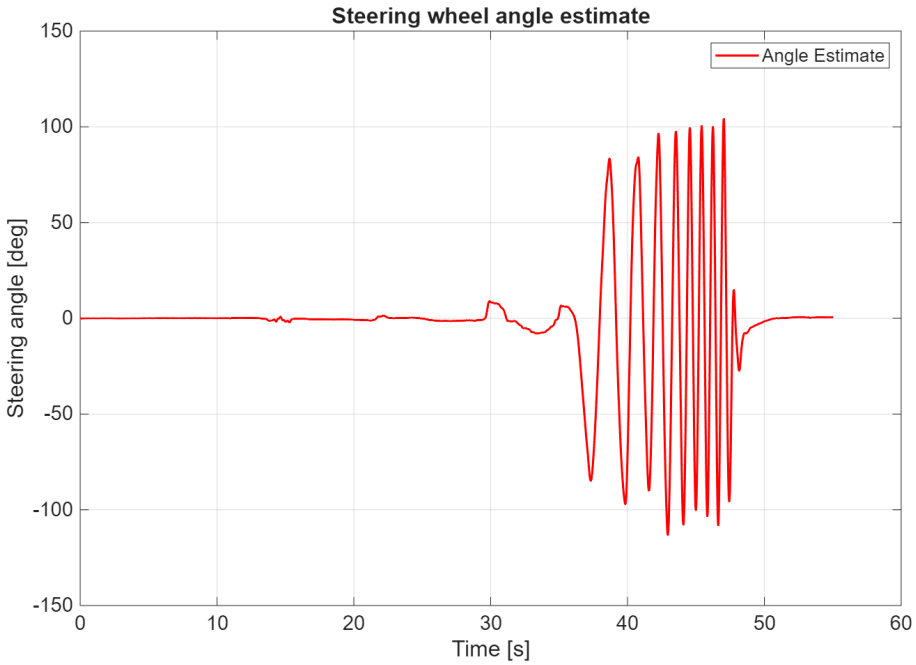



**Figure A.11:** Angle estimate for Sine Sweep (90 degs) maneuver performed at 60 Km/hr

### A.1.4 Slalom

#### A.1.4.1 Speed - 40 Km/hr

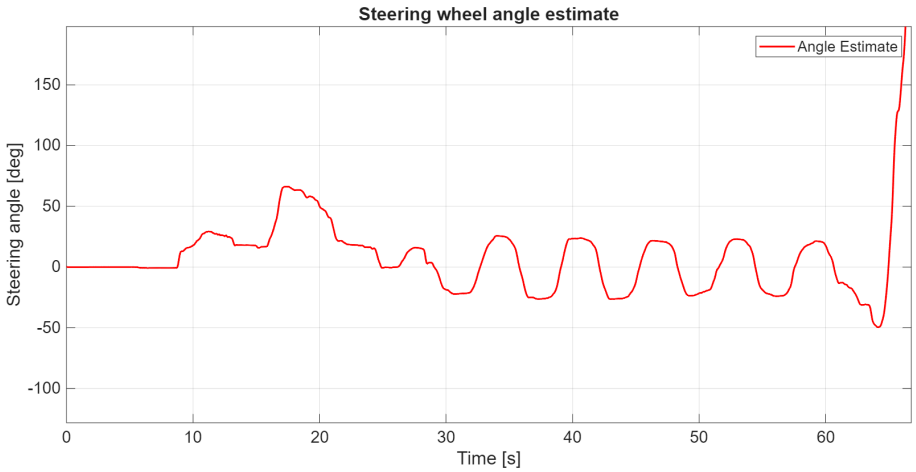



**Figure A.12:** Angle estimate for Slalom maneuver performed at 40 Km/hr

#### A.1.4.2 Speed - 60 Km/hr

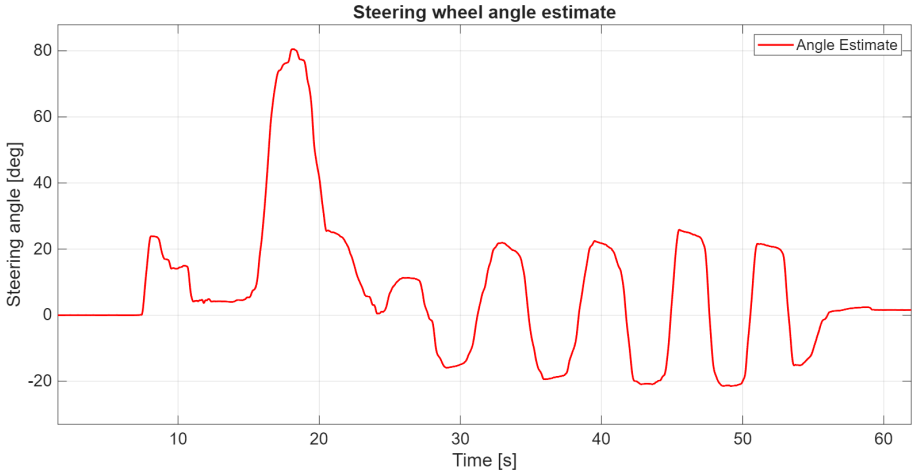



**Figure A.13:** Angle estimate for Slalom maneuver performed at 60 Km/hr

### A.1.4.3 Speed - 80 Km/hr




**Figure A.14:** Angle estimate for Slalom maneuver performed at 80 Km/hr

## A.1.5 Steer and Release (180 Degs)

### A.1.5.1 Speed - 10 Km/hr

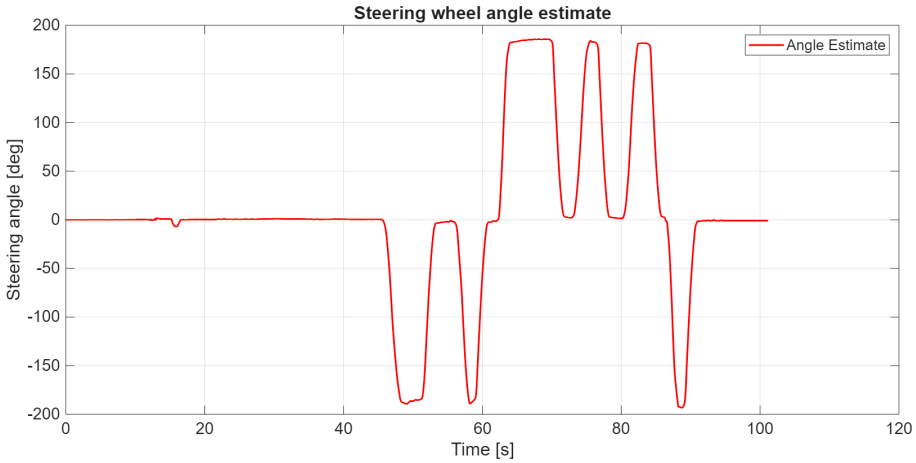



**Figure A.15:** Angle estimate for Steer and Release (180 degs) maneuver performed at 10 Km/hr

### A.1.5.2 Speed - 20 Km/hr

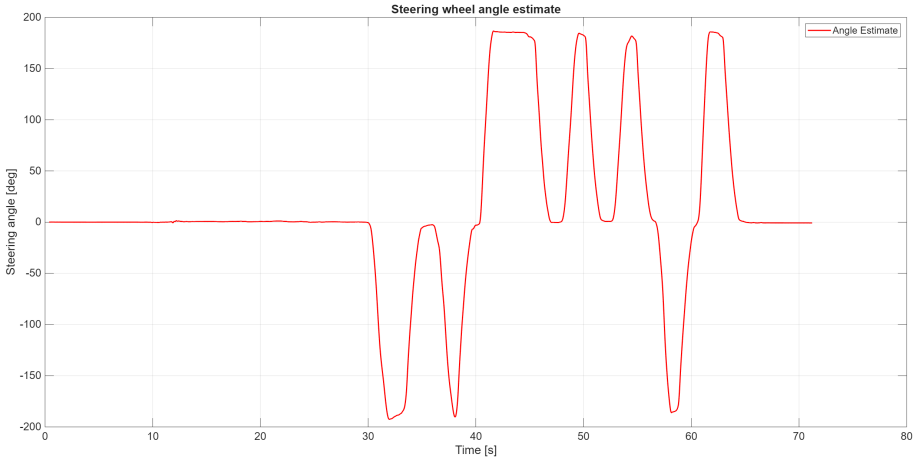



**Figure A.16:** Angle estimate for Steer and Release (180 degs) maneuver performed at 20 Km/hr

### A.1.5.3 Speed - 40 Km/hr

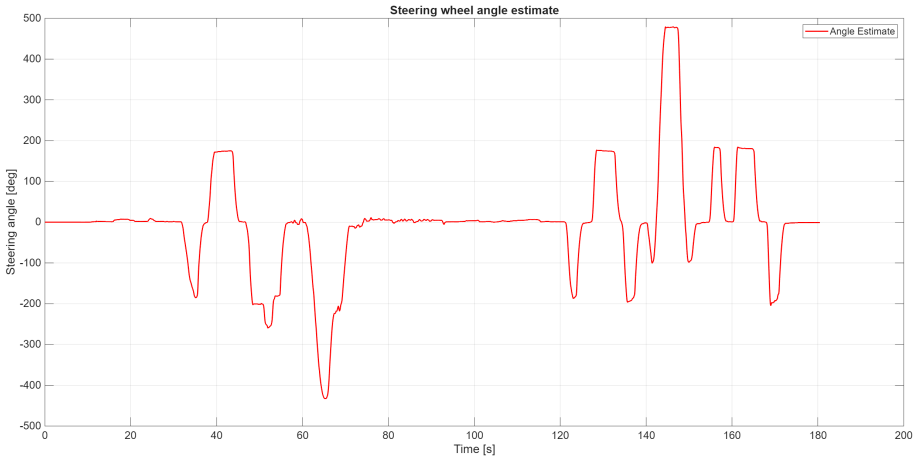



**Figure A.17:** Angle estimate for Steer and Release (180 degs) maneuver performed at 40 Km/hr

### A.1.6 Steady state circle

#### A.1.6.1 Steering wheel angle input - 90 Degs

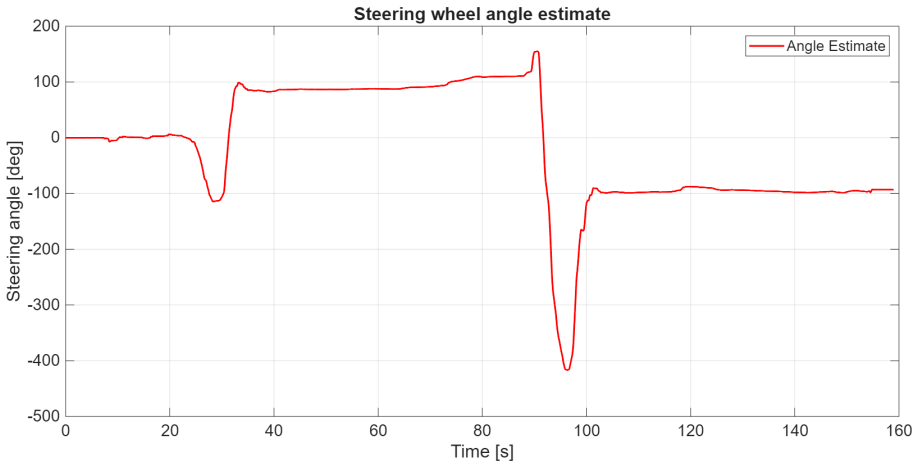



**Figure A.18:** Angle estimate for Steady state circle (90 degs fixed steering angle, speed ramped) maneuver

#### A.1.6.2 Steering wheel angle input - 180 Degs

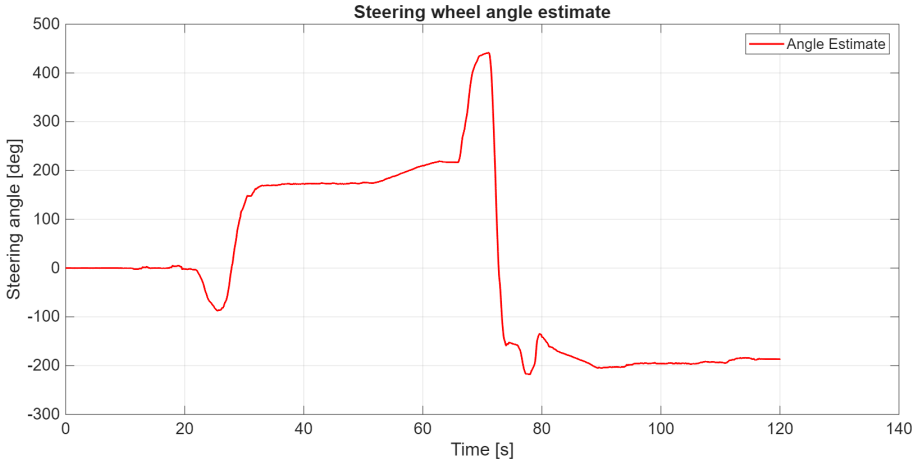



**Figure A.19:** Angle estimate for Steady state circle (180 degs fixed steering angle, speed ramped) maneuver

## A.1.7 Step Steer

### A.1.7.1 Speed - 20 Km/hr

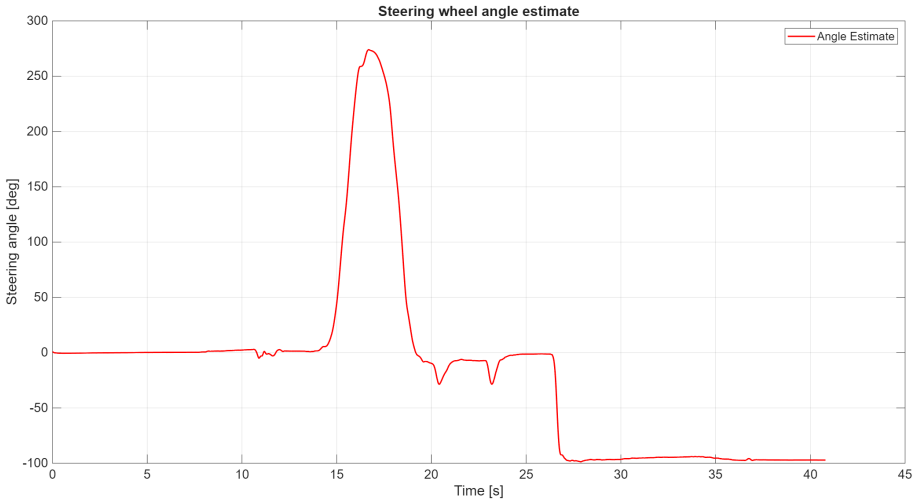



**Figure A.20:** Angle estimate for Step Steer maneuver performed at 20 Km/hr

### A.1.7.2 Speed - 40 Km/hr

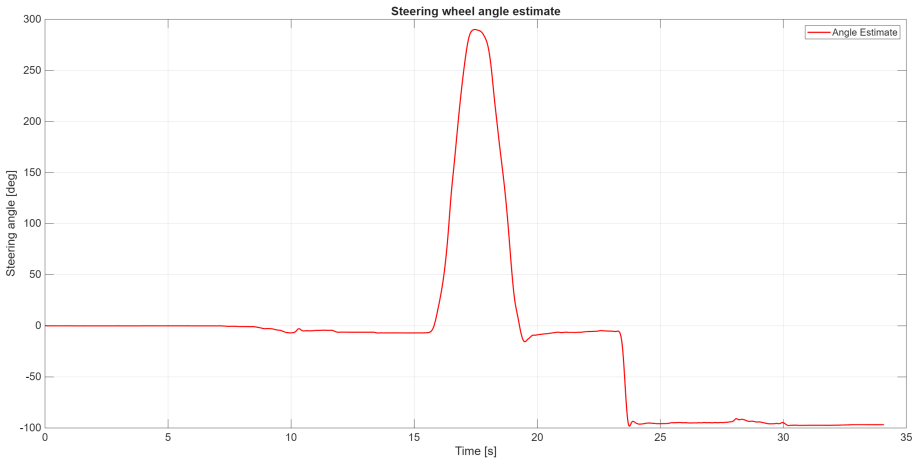



**Figure A.21:** Angle estimate for Step Steer maneuver performed at 40 Km/hr

### A.1.7.3 Speed - 60 Km/hr

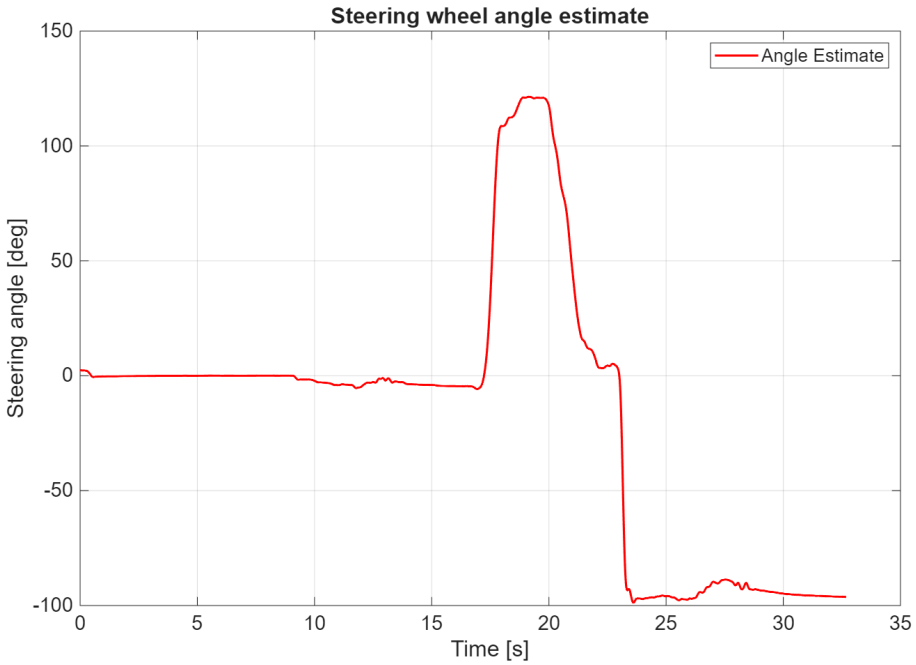



**Figure A.22:** Angle estimate for Step Steer maneuver performed at 60 Km/hr

# B

# Appendix 2

This Appendix chapter contains the model response to experimental inputs for the test maneuvers and their corresponding speed cases.

## B.1 Model Response to Experimental Input

### B.1.1 Double Lane Change

#### B.1.1.1 Speed - 20 km/h

##### B.1.1.1.1 Lateral Response Comparison (Model vs. Vehicle)

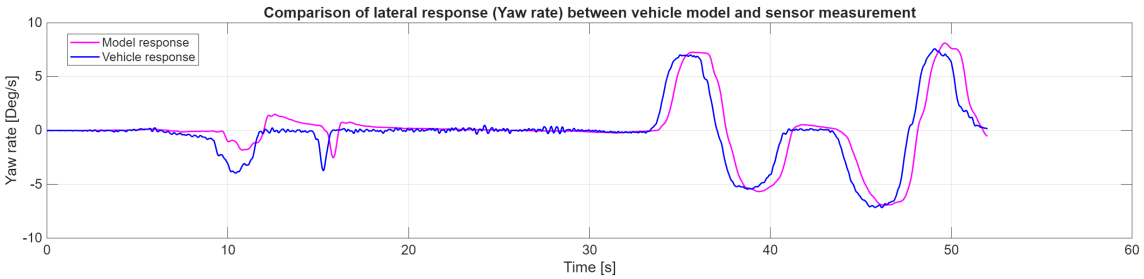



**Figure B.1:** Yaw rate: Vehicle Vs Model response.

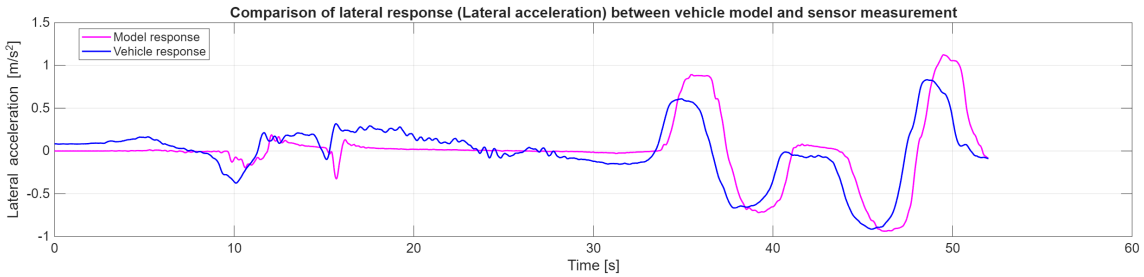



**Figure B.2:** Lateral acceleration: Vehicle Vs Model response.

#### B.1.1.1.2 Steering Response (HPAS vs. EPAS)

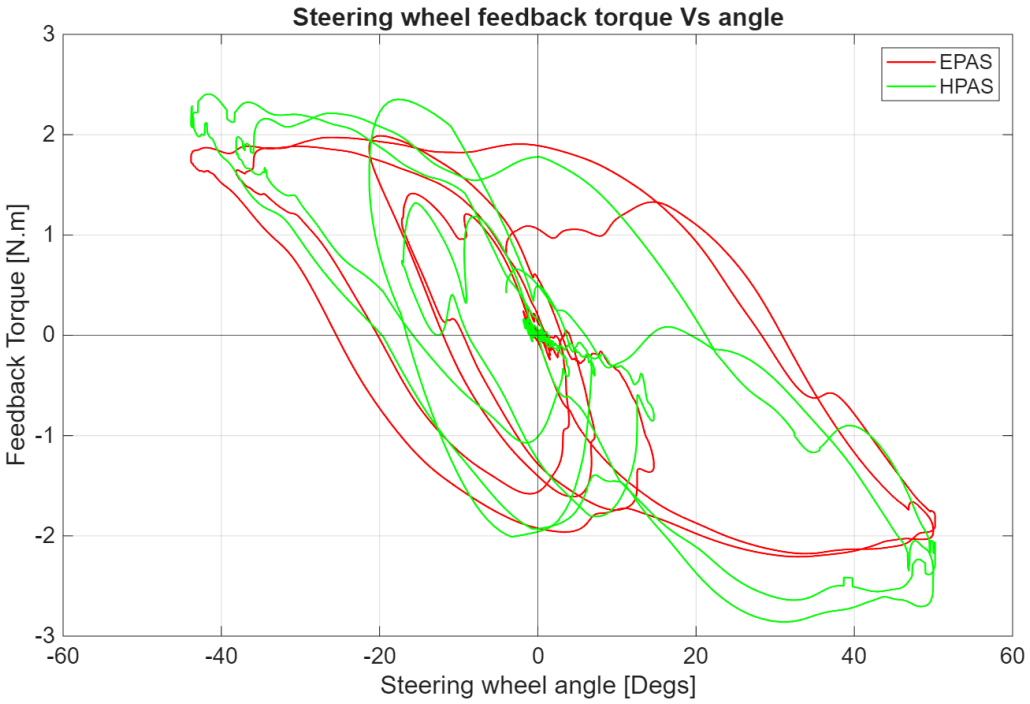



**Figure B.3:** SWT Vs SWA for the Double lane change maneuver

### B.1.1.2 Speed - 60 Km/hr

#### B.1.1.2.1 Lateral Response Comparison (Model vs. Vehicle)

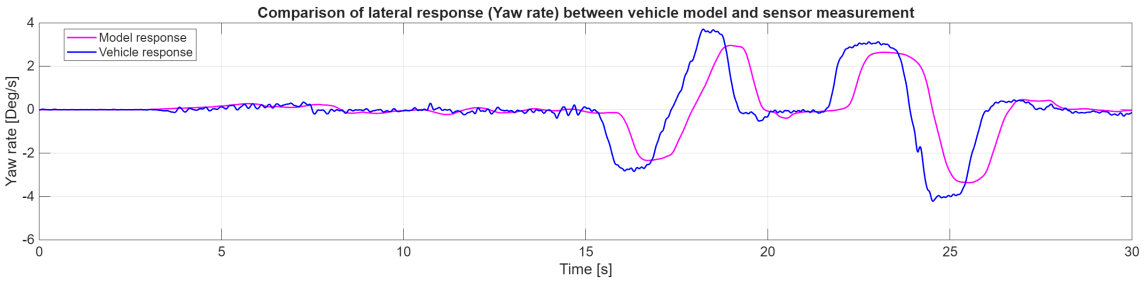



**Figure B.4:** Yaw rate: Vehicle Vs Model response.

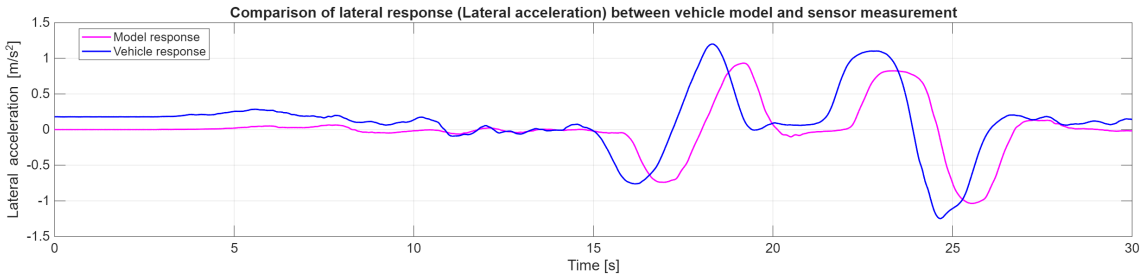



**Figure B.5:** Lateral acceleration: Vehicle Vs Model response.

#### B.1.1.2.2 Steering Response (HPAS vs. EPAS)

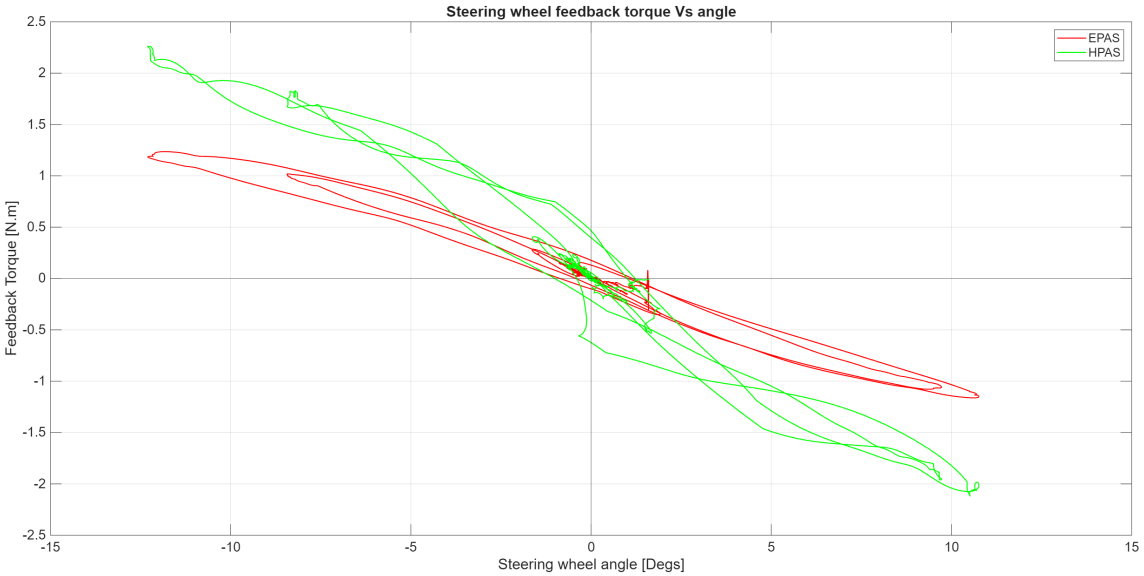



**Figure B.6:** SWT Vs SWA for the Double lane change maneuver

### B.1.1.3 Speed - 80 Km/hr

#### B.1.1.3.1 Lateral Response Comparison (Model vs. Vehicle)

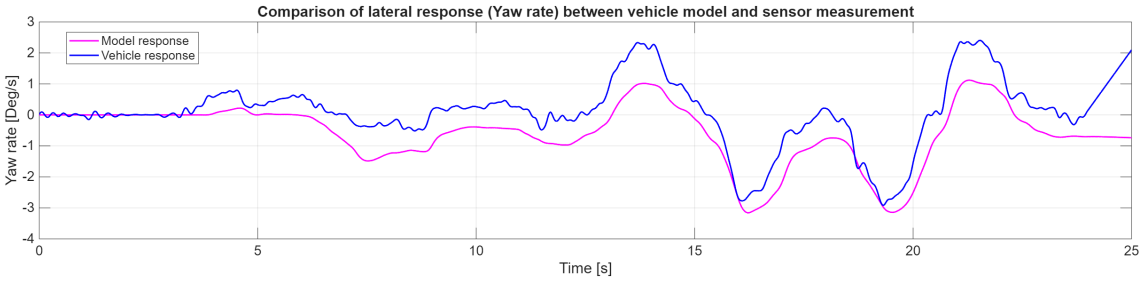



**Figure B.7:** Yaw rate: Vehicle Vs Model response.

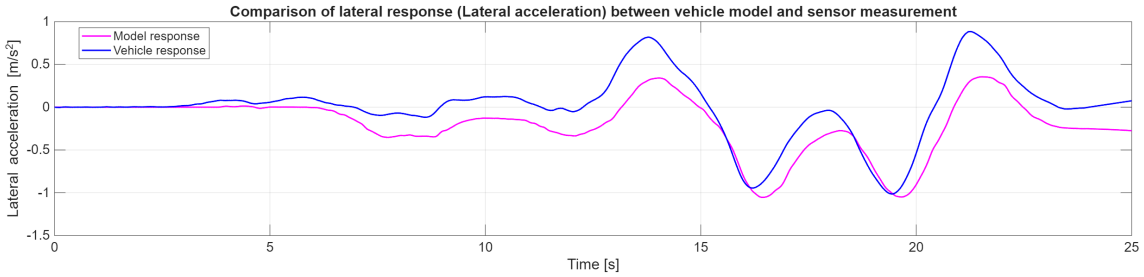



**Figure B.8:** Lateral acceleration: Vehicle Vs Model response.

#### B.1.1.3.2 Steering Response (HPAS vs. EPAS)

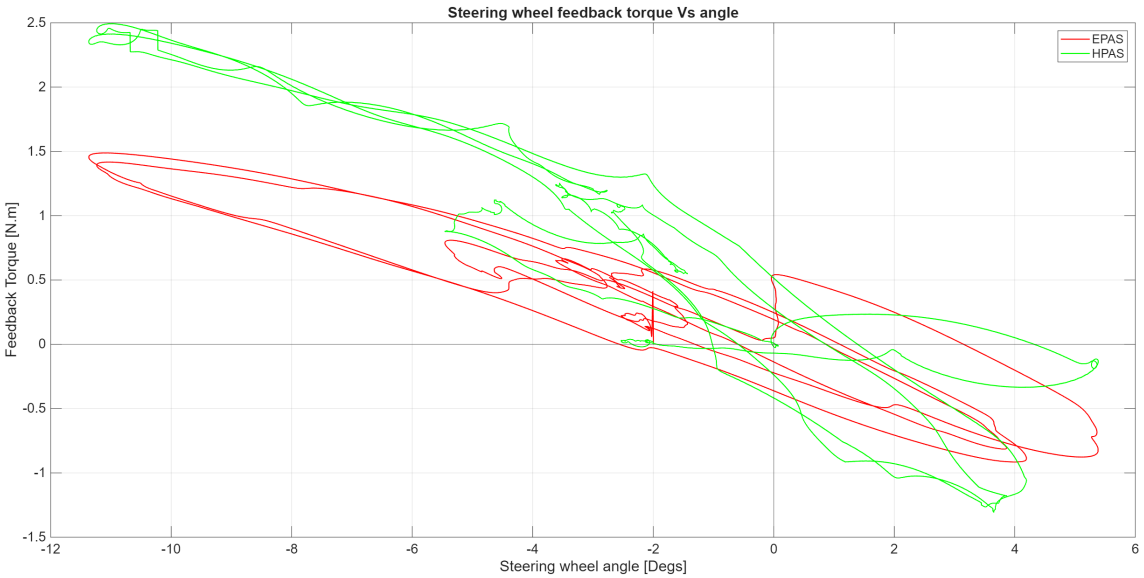



**Figure B.9:** SWT Vs SWA for the Double lane change maneuver

## B.1.2 Single Lane Change

### B.1.2.1 Speed - 20 Km/hr

For this speed condition there was issue with the OBD II log (Throttle pedal position signal), so the case is neglected.

### B.1.2.2 Speed - 40 Km/hr

#### B.1.2.2.1 Lateral Response Comparison (Model vs. Vehicle)

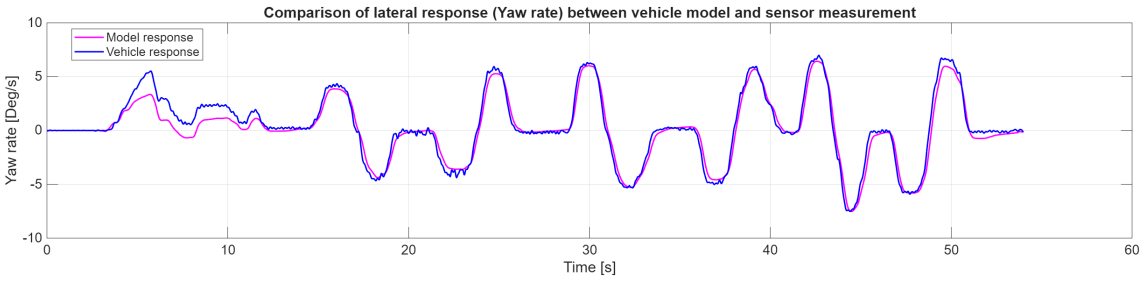



**Figure B.10:** Yaw rate: Vehicle Vs Model response.

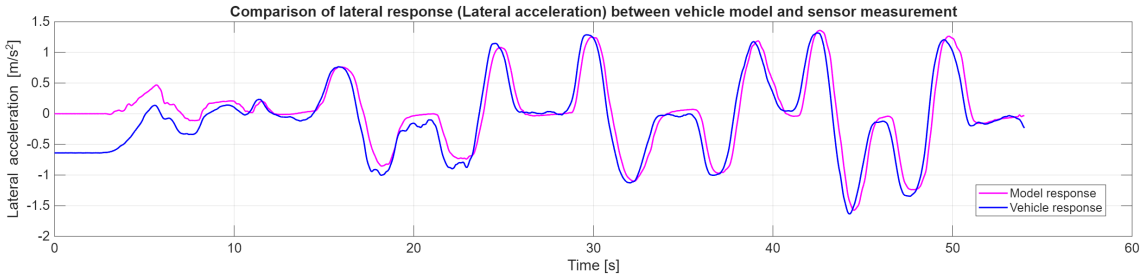



**Figure B.11:** Lateral acceleration: Vehicle Vs Model response.

#### B.1.2.2.2 Steering Response (HPAS vs. EPAS)

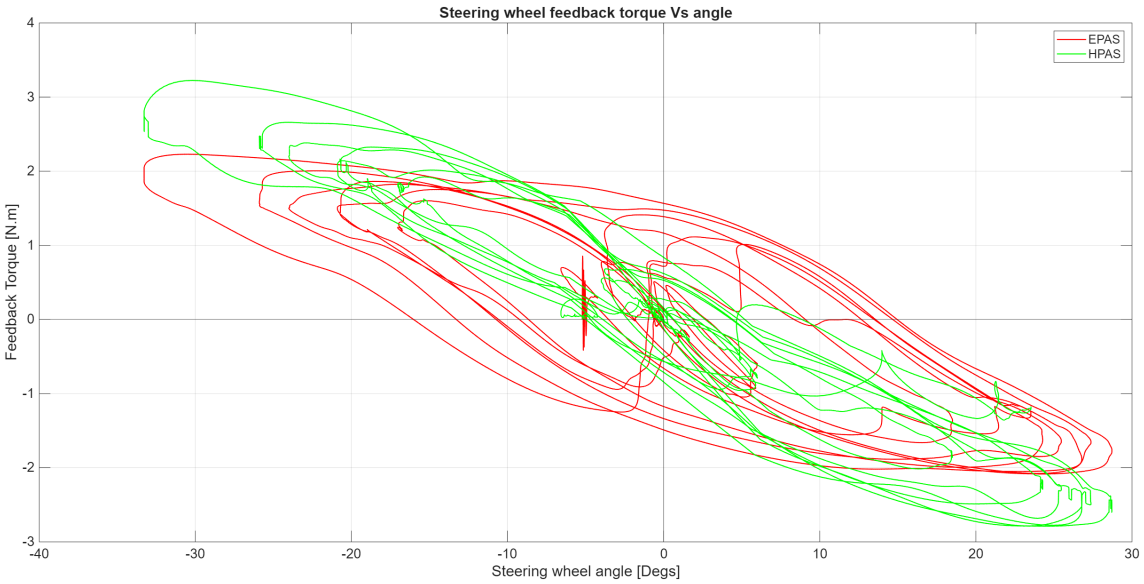



**Figure B.12:** SWT Vs SWA

### B.1.2.3 Speed - 60 Km/hr

#### B.1.2.3.1 Lateral Response Comparison (Model vs. Vehicle)

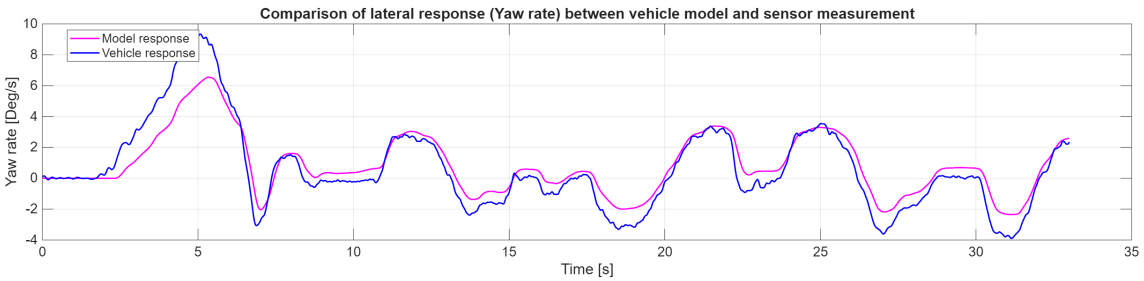



**Figure B.13:** Yaw rate: Vehicle Vs Model response.

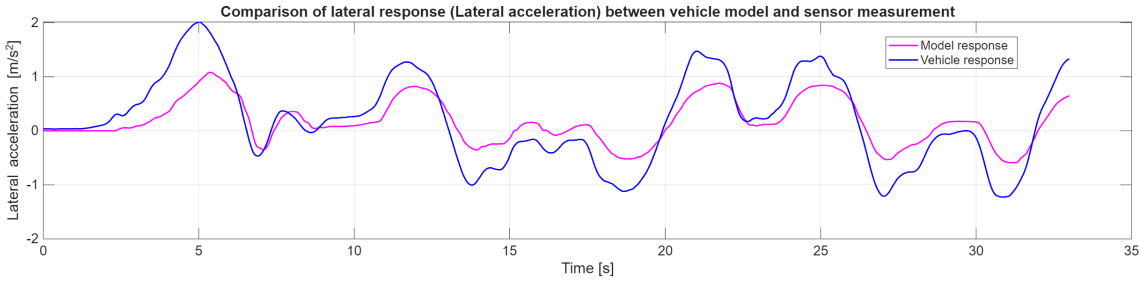



**Figure B.14:** Lateral acceleration: Vehicle Vs Model response.

#### B.1.2.3.2 Steering Response (HPAS vs. EPAS)

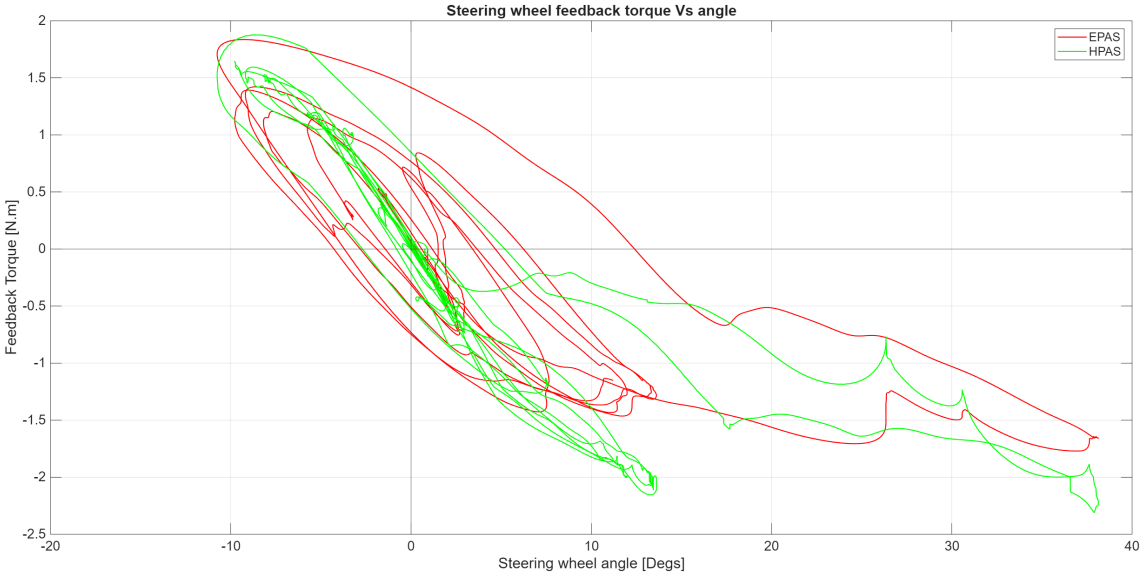



**Figure B.15:** SWT Vs SWA

### B.1.2.4 Speed - 80 Km/hr

For this speed condition there was issue with the OBD II log (Throttle pedal position signal), so the case is neglected.

### B.1.3 Sine Sweep (90 degs)

#### B.1.3.1 Speed - 20 Km/hr

##### B.1.3.1.1 Lateral Response Comparison (Model vs. Vehicle)

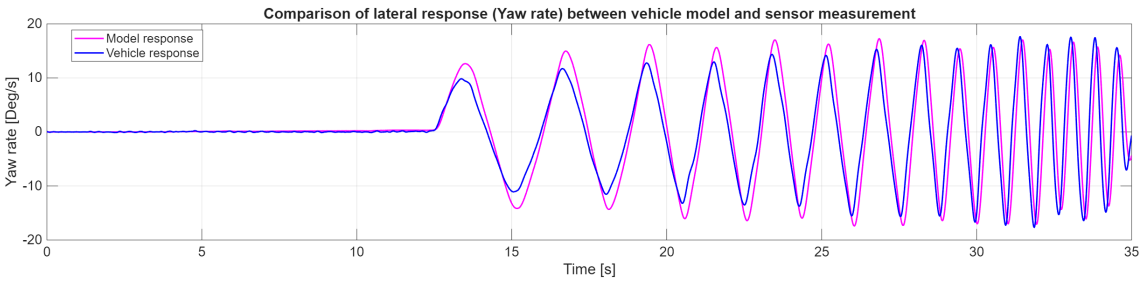



**Figure B.16:** Yaw rate: Vehicle Vs Model response.

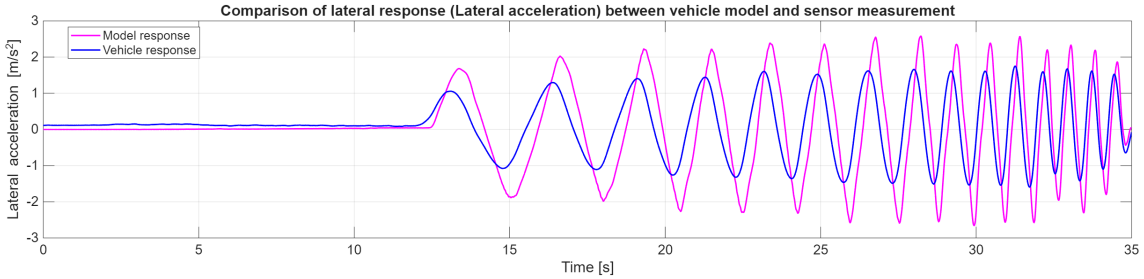



**Figure B.17:** Lateral acceleration: Vehicle Vs Model response.

##### B.1.3.1.2 Steering Response (HPAS vs. EPAS)

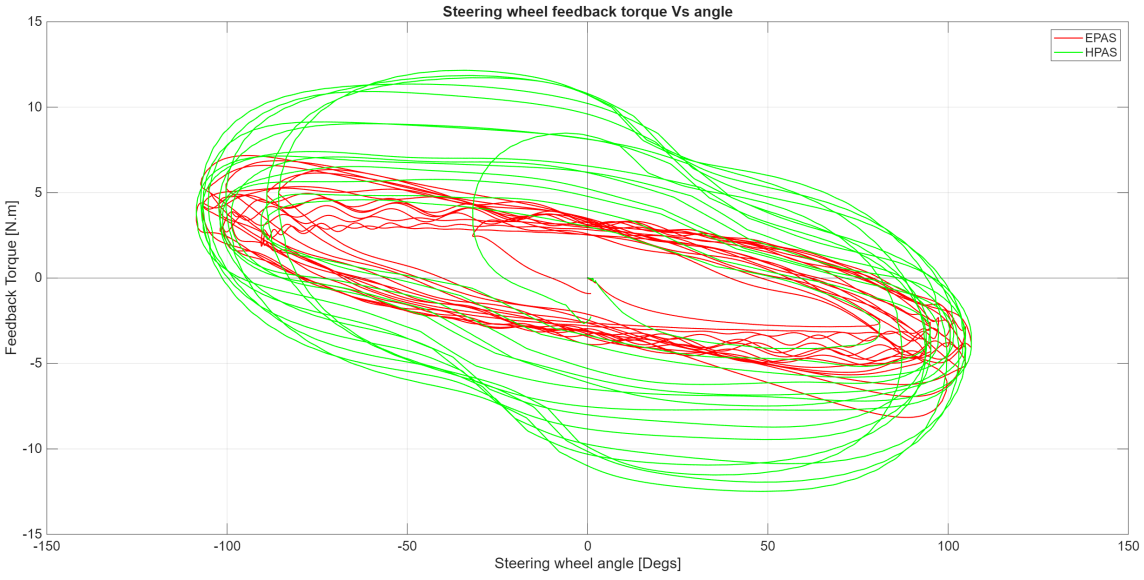



**Figure B.18:** SWT Vs SWA

### B.1.3.2 Speed - 40 Km/hr

#### B.1.3.2.1 Lateral Response Comparison (Model vs. Vehicle)

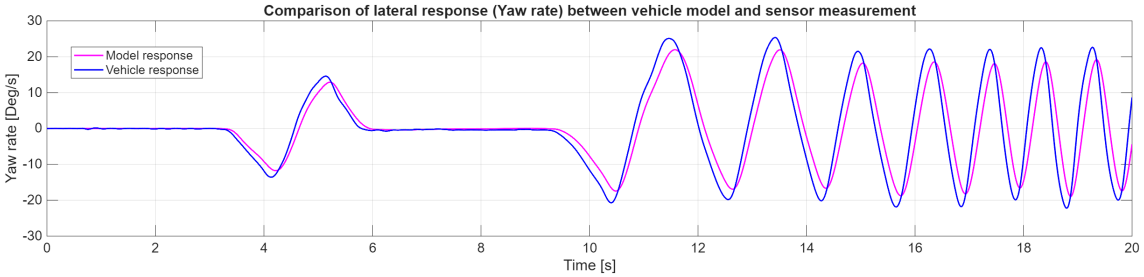



**Figure B.19:** Yaw rate: Vehicle Vs Model response.

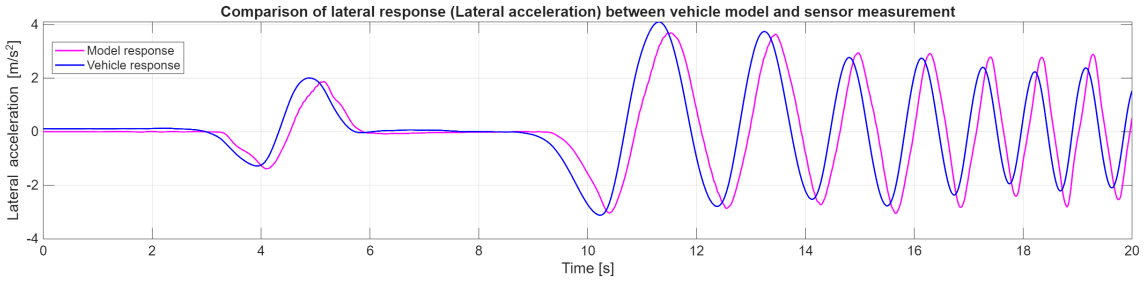



**Figure B.20:** Lateral acceleration: Vehicle Vs Model response.

#### B.1.3.2.2 Steering Response (HPAS vs. EPAS)

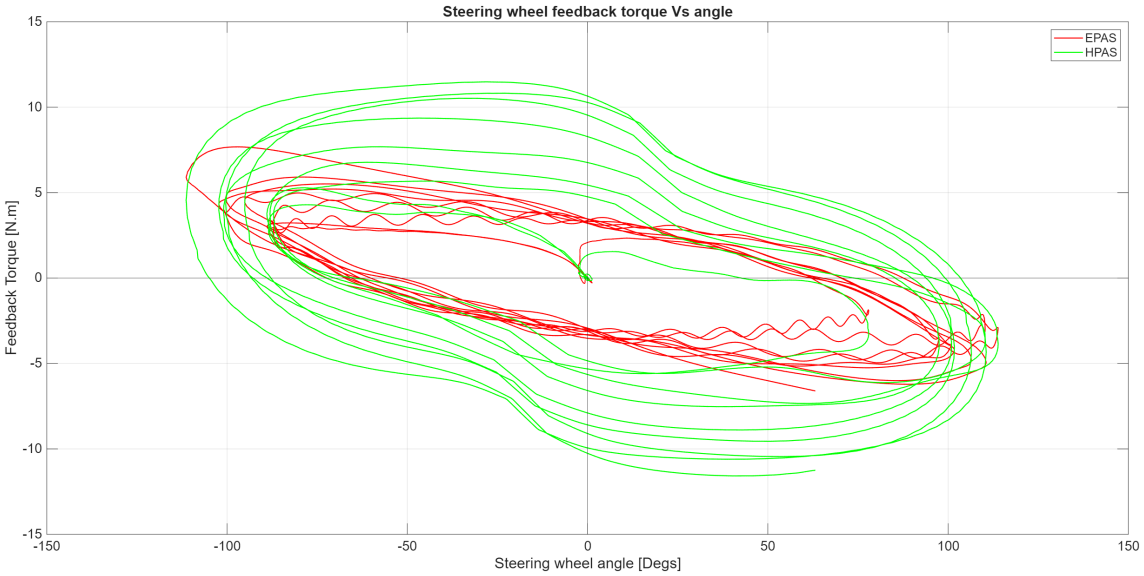



**Figure B.21:** SWT Vs SWA

### B.1.3.3 Speed - 60 Km/hr

#### B.1.3.3.1 Lateral Response Comparison (Model vs. Vehicle)

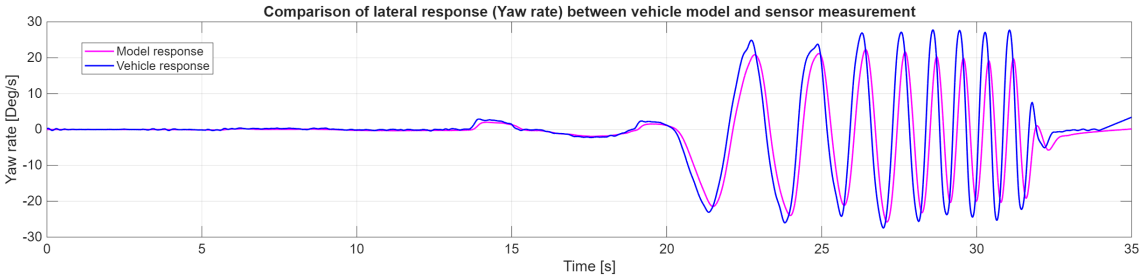



**Figure B.22:** Yaw rate: Vehicle Vs Model response.

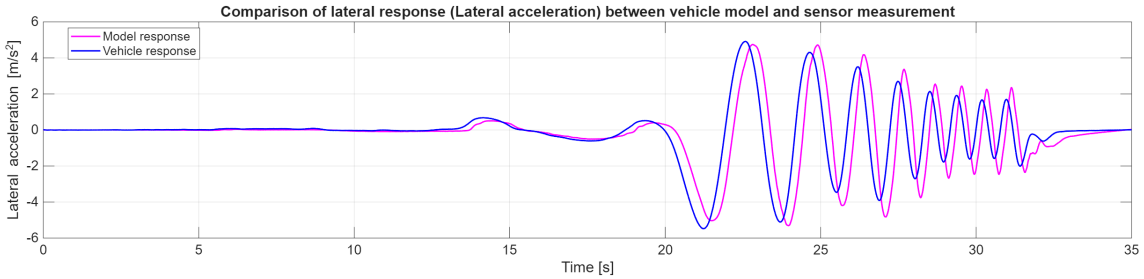



**Figure B.23:** Lateral acceleration: Vehicle Vs Model response.

#### B.1.3.3.2 Steering Response (HPAS vs. EPAS)

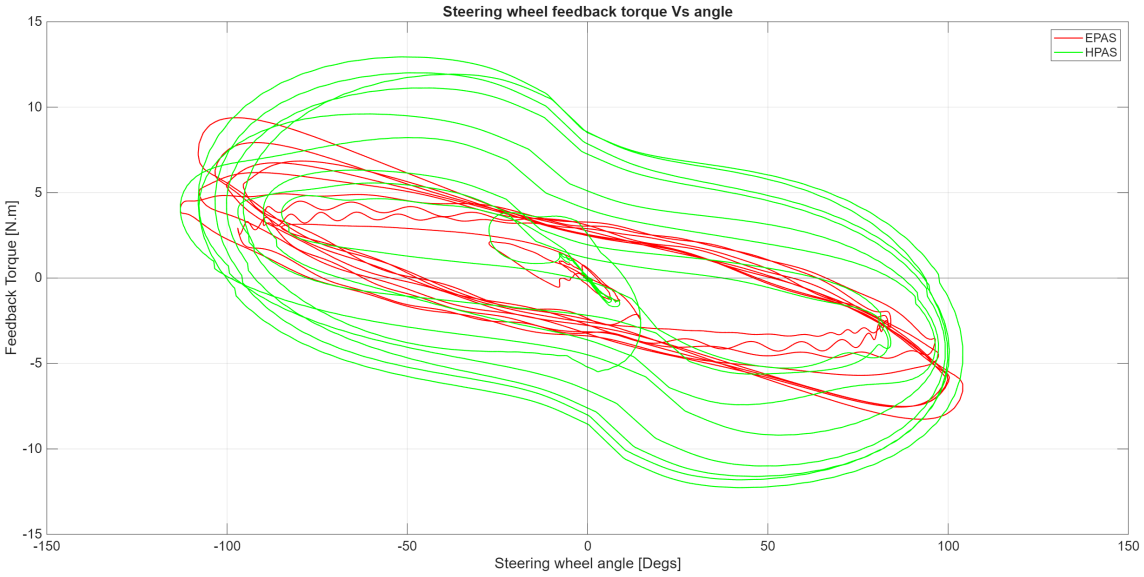



**Figure B.24:** SWT Vs SWA

## B.1.4 Slalom

### B.1.4.1 Speed - 60 Km/hr

#### B.1.4.1.1 Lateral Response Comparison (Model vs. Vehicle)

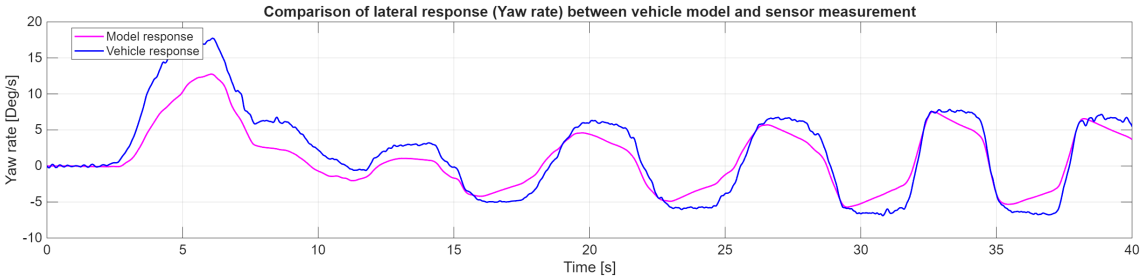



**Figure B.25:** Yaw rate: Vehicle Vs Model response.

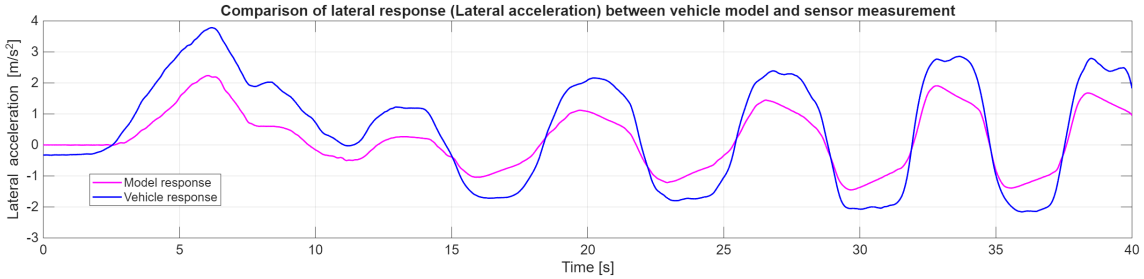



**Figure B.26:** Lateral acceleration: Vehicle Vs Model response.

#### B.1.4.1.2 Steering Response (HPAS vs. EPAS)

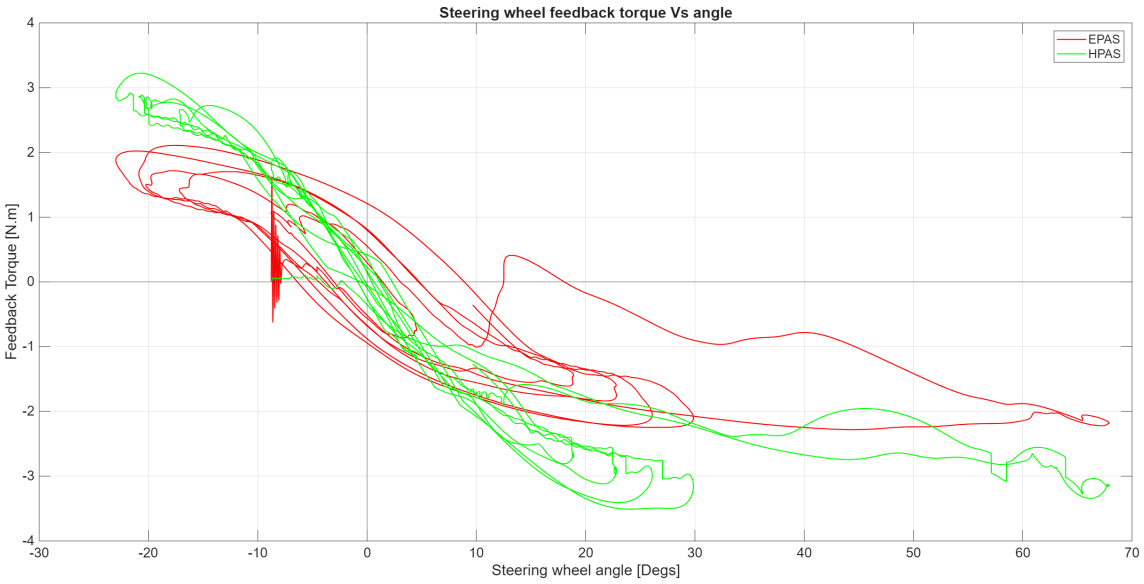



**Figure B.27:** SWT Vs SWA

#### B.1.4.2 Speed - 80 Km/hr

For this speed condition there was issue with the OBD II log (Throttle pedal position signal), so the case is neglected.

### B.1.5 Steer and Release (180 Degs)

This particular test maneuver was not intended for Vehicle model lateral dynamics validation but to tune the steering system (return behavior).

### B.1.6 Steady state circle

#### B.1.6.1 Steering wheel angle input - 90 Degs

##### B.1.6.1.1 Lateral Response Comparison (Model vs. Vehicle)

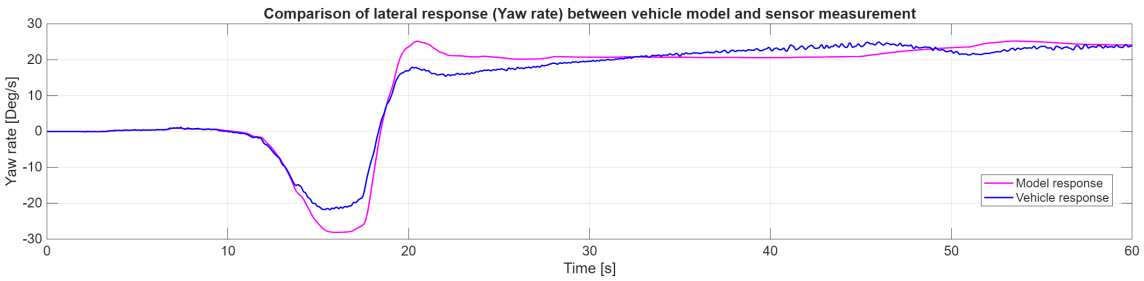



**Figure B.28:** Yaw rate: Vehicle Vs Model response.

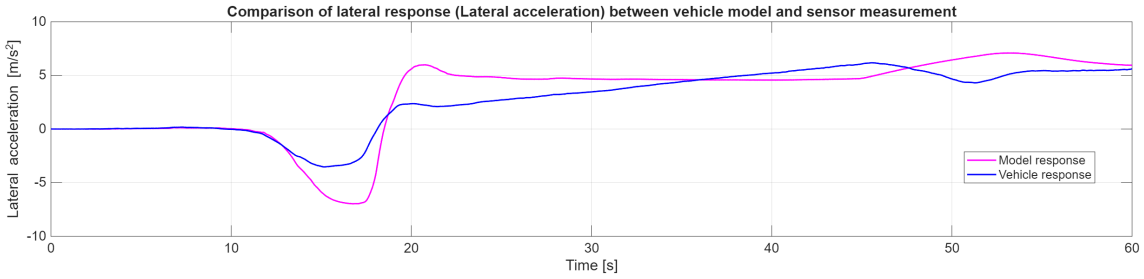



**Figure B.29:** Lateral acceleration: Vehicle Vs Model response.

#### B.1.6.1.2 Steering Response (HPAS vs. EPAS)

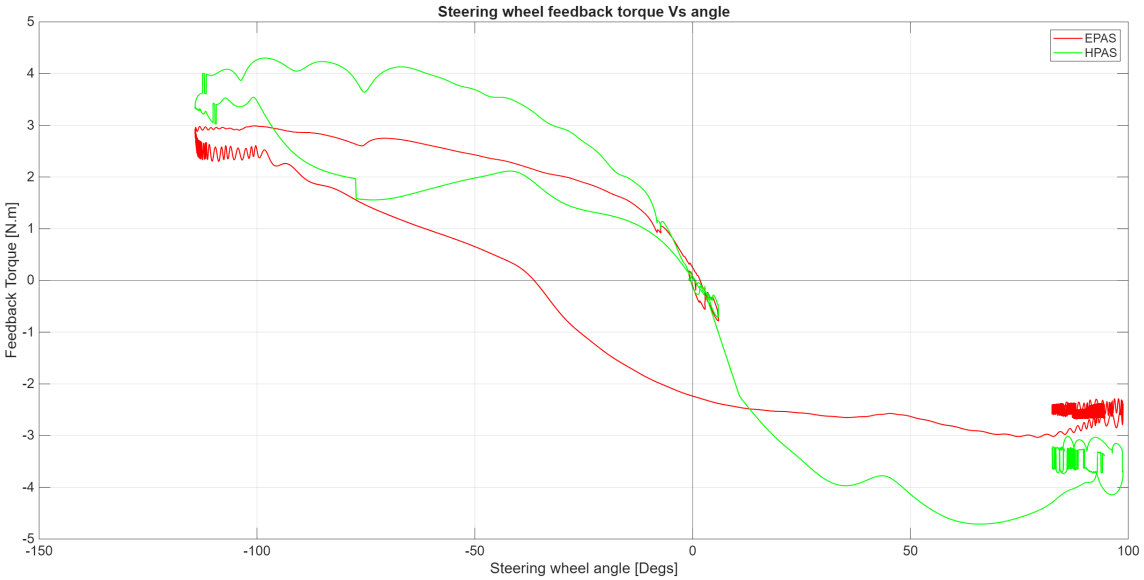



**Figure B.30:** SWT Vs SWA

### B.1.6.2 Steering wheel angle input - 180 Degs

#### B.1.6.2.1 Lateral Response Comparison (Model vs. Vehicle)

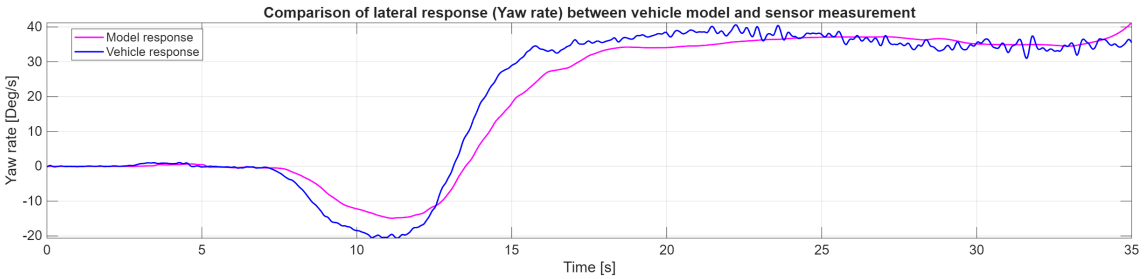



**Figure B.31:** Yaw rate: Vehicle Vs Model response.

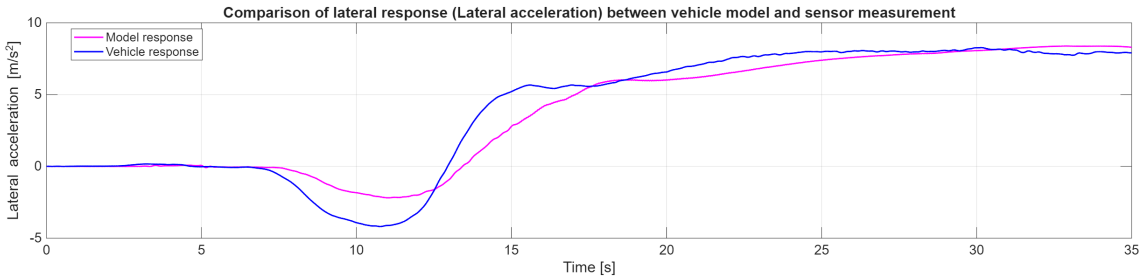



**Figure B.32:** Lateral acceleration: Vehicle Vs Model response.

#### B.1.6.2.2 Steering Response (HPAS vs. EPAS)

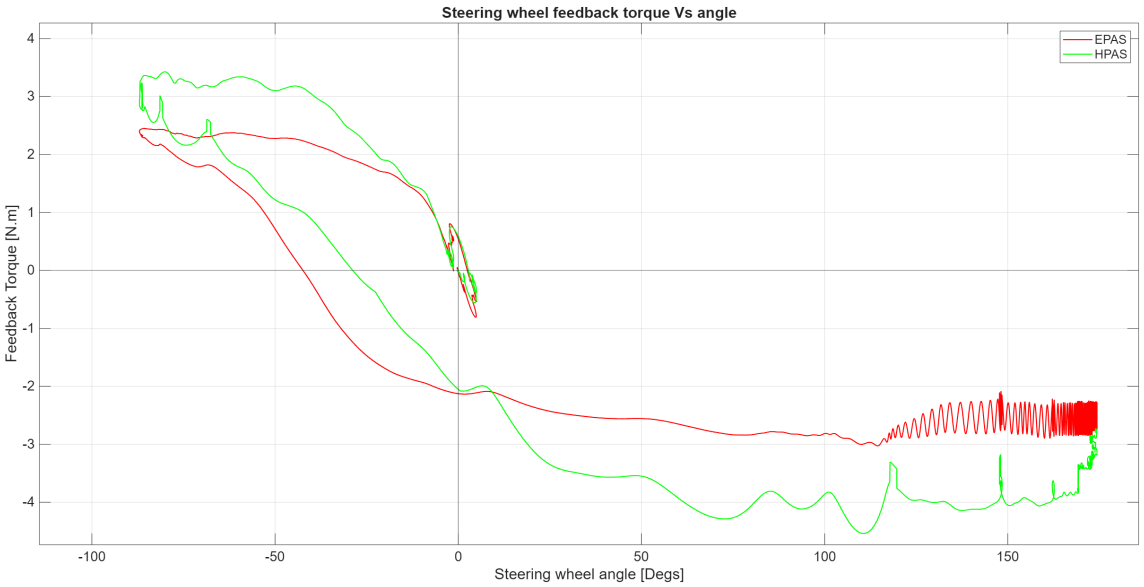



**Figure B.33:** SWT Vs SWA

## B.1.7 Step Steer

### B.1.7.1 Speed - 20 Km/hr

#### B.1.7.1.1 Lateral Response Comparison (Model vs. Vehicle)

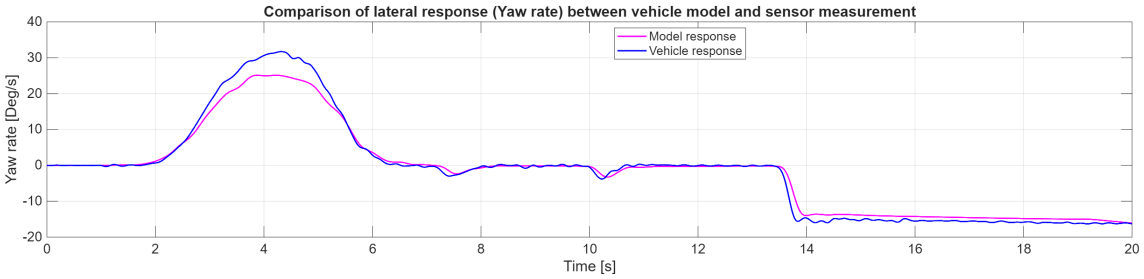



**Figure B.34:** Yaw rate: Vehicle Vs Model response.

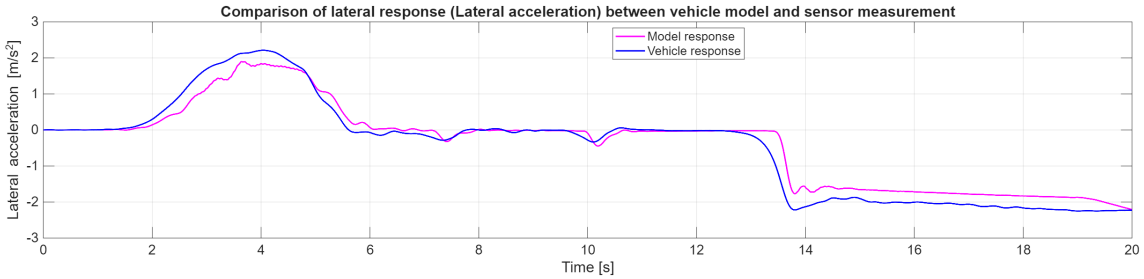



**Figure B.35:** Lateral acceleration: Vehicle Vs Model response.

#### B.1.7.1.2 Steering Response (HPAS vs. EPAS)

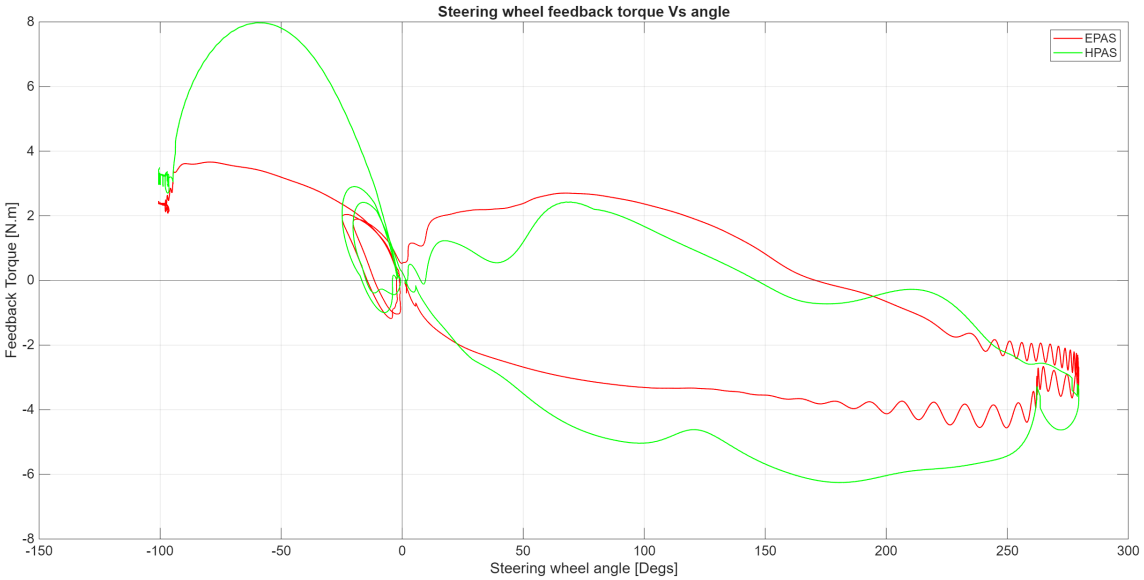



**Figure B.36:** SWT Vs SWA

### B.1.7.2 Speed - 40 Km/hr

#### B.1.7.2.1 Lateral Response Comparison (Model vs. Vehicle)

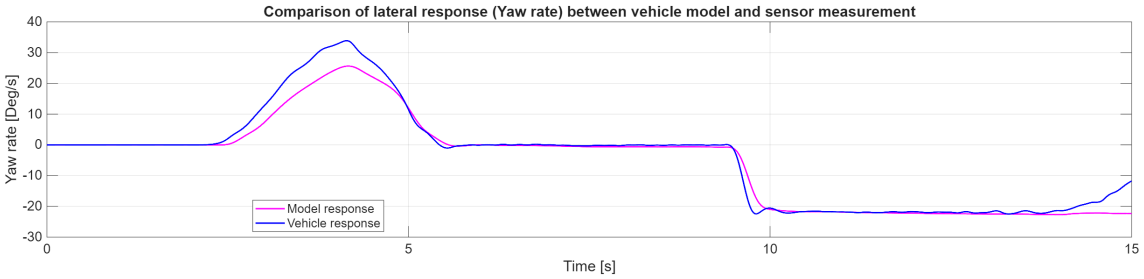



**Figure B.37:** Yaw rate: Vehicle Vs Model response.

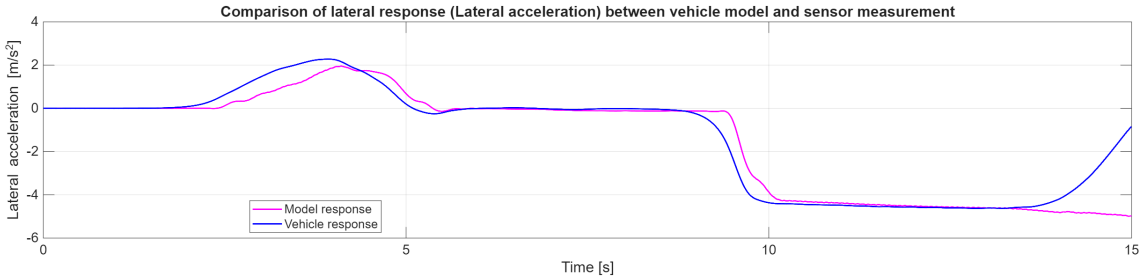



**Figure B.38:** Lateral acceleration: Vehicle Vs Model response.

#### B.1.7.2.2 Steering Response (HPAS vs. EPAS)

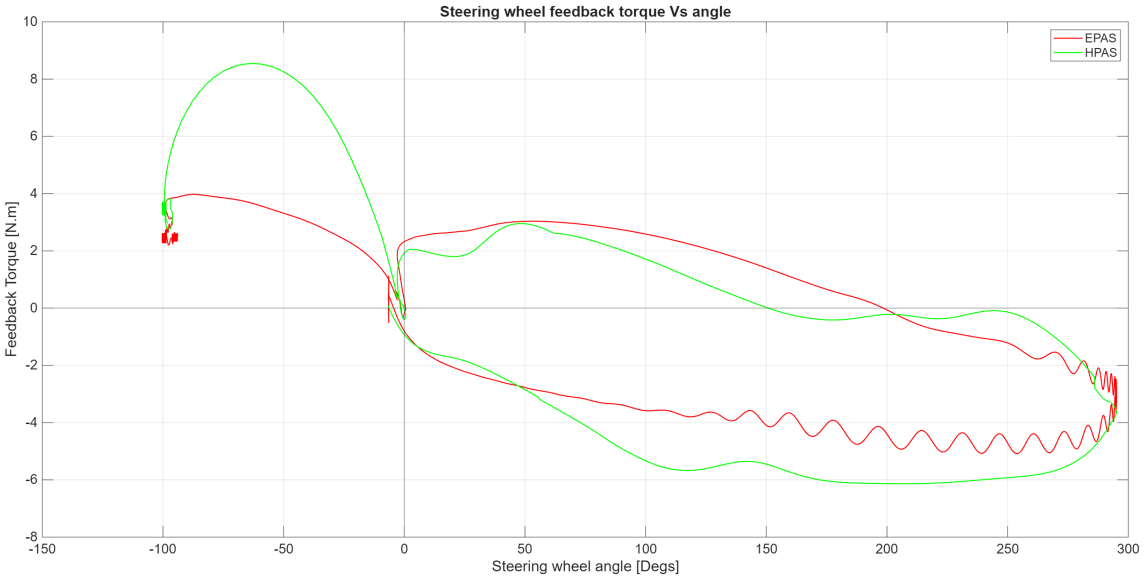



**Figure B.39:** SWT Vs SWA

### B.1.7.3 Speed - 60 Km/hr

For this speed condition there was issue with the OBD II log (Throttle pedal position signal), so the case is neglected.

**DEPARTMENT OF MECHANICS AND MARITIME ENGINEERING**
**CHALMERS UNIVERSITY OF TECHNOLOGY**
Gothenburg, Sweden
www.chalmers.se




CHALMERS
UNIVERSITY OF TECHNOLOGY